Trivalent Chromium Based Conversion Coatings Containing Cobalt on the Zinc Plated Steel

Dissertation

zur Erlangung des akademischen Grades
Doktor der Ingenieurwissenschaften
(Dr.-Ing.)
Vorgelegt der Fakultät für Elektrotechnik und Informationstechnik
der Technischen Universität Ilmenau
von
M.Sc. Sanaz Hesamedini

Gutachter:
Herr Univ.-Prof. Dr. rer. nat. habil. Dr. h.c. Andreas Bund
Technische Universität Ilmenau
Herr Prof. Dr. rer. nat. habil. Uwe Ritter
Technische Universität Ilmenau
Frau Prof. Dr. Sannakaisa Virtanen
Friedrich-Alexander-Universität Erlangen-Nürnberg

Tag der Einreichung: 10.12.2019
Tag der wissenschaftlichen Aussprache: 11.08.2020

urn:nbn:de:gbv:ilm1-2020000368

Acknowledgement

This work would not have been possible without the advice and support of many people. Firstly, I would like to express my gratitude to Prof. Andreas Bund for his support, patience, and guidance throughout this study. I am especially grateful for his confidence and the freedom he gave me to do this work.

I sincerely thank the committee members Prof. Spiess, Prof. Ritter, Prof. Svetlozar Ivanov, and Prof. Müller for their kind attention to this work. In addition, a thank you to Prof. Virtanen for her kind support and being such a role model for all women in science.

I wish to express my gratitude to Dr. Gernot Ecke for his kind support with AES measurements.

I would like to appreciate Dr. Philip Nickel in Atotech Deutschland GmbH for giving me the opportunity to access the ICP-OES device and his kind support.

I extend my sincere thanks to all members of the Department of Electrochemistry and Electroplating and the Institute of Micro- and Nanotechnologies of Technische Universität Ilmenau for their support and kindness. Appreciation is due to Dr. Ralf Peipmann, Mathias Fritz, Dr. Henry Romanus, Dr. Michael Stich, Mario Kurniawan, Steffan Link, Dr. Wassima El Mofid, Diana Rossberg, Karin Keller, Marianne Lerp, Anneliese Täglich for the kind support and helpful discussions throughout this work.

Many thanks to Dr. Werner Richtering and Ercan Karapinar in Atotech Deutschland GmbH for their kind support.

Acknowledgment is also given to Atotech Deutschland GmbH and Technische Universität Ilmenau for financial support in the form of two studentships.

I would especially like to express my gratitude to Dr. Ali Khajehesamedini and Dr. Thomas Müllerleile for generously sharing their expertise and for their helpful suggestions whenever I had problems during the journey of doing my PhD.

Nobody has been more important to me in the pursuit of this goal than the members of my family. I am grateful to my beloved parents for their patience and support throughout my life and especially during this time. I am indebted to my best companions, my beloved siblings, Farnaz and Ali, for their presence and emotional support.

Zusammenfassung

Im Zuge neuer EU-Direktiven wurde die Verwendung von Cr(VI)-Verbindungen stark reglementiert. In der Oberflächentechnik wurde daraufhin sechswertiges Chrom durch sicherere und gleichzeitig effektive Passivierungen auf Cr(III)-Basis ersetzt. Der Korrosionsschutz von Cr(VI)-Beschichtungen ohne Wärmebehandlung ist im Allgemeinen besser. In bisher durchgeführten Untersuchungen zeigte sich, dass durch Zusatz von Übergangsmetallionen der Korrosionsschutz der Cr(III)-Passivierungsschicht verbessert werden kann. In dieser Arbeit wird der Einfluss der Zusammensetzung von Cr(III)-Passivierung mit Kobaltanteil auf die Bildung und die Struktur von Konversionsschichten auf verzinkten Substraten untersucht. Auf den verzinkten Stahl wurden Modelllösungen mit zwei verschiedenen Komplexbildnern, nämlich Fluorid und Oxalat, mit und ohne Kobalt aufgetragen. Rasterelektronenmikroskopie (REM) und Rasterkraftmikroskopie zeigten Oberflächenmorphologien mit mikrostrukturellen Defekten. In Anwesenheit von Kobalt wurden die Schichten gleichmäßiger. Die elementare Zusammensetzung der Schichten wurde mit der Augerelektronenspektroskopie (AES) untersucht. Die Mengen an Cr und Co in den Beschichtungen wurden mithilfe der optischen Plasma-Emissionsspektroskopie (ICP-OES) bestimmt. Sowohl AES als auch ICP-OES zeigten Co-Gehalte in den Schichten. Mithilfe eines thermodynamischen Modells wurde die Konzentration von Cr(III)-, Zn(II)- und Co(II)-Spezies in der Behandlungslösung im pH-Bereich von 0,0 bis 14,0 und auch der minimale pH-Wert für die Abscheidung der Metallionen in der entsprechenden Lösung berechnet. Die Ergebnisse der Korrosionstests (Polarisationsmessung und elektrochemische Impedanzspektroskopie) legen nahe, dass die Bildung einer dichten Schicht für eine gute Korrosionsbeständigkeit entscheidend ist. Außerdem wurde der Bildungsmechanismus von Cr(VI) in den Schichten untersucht. Die Anwesenheit von Cr(VI) wurde mittels Spektrophotometrie nachgewiesen. Die Morphologie und

Struktur der Filme wurden per REM beobachtet. Die Gesamtwassermenge in den Schichten wurde mittels Karl-Fischer-Titration gemessen. Es zeigte sich, dass die Morphologie des fluoridhaltigen Films mit einer hohen Dichte an Mikroporen die Wahrscheinlichkeit eines Wassereinschlusses erhöht. Dies führte zu einer Oxidation von Cr(III) zu Cr(VI) durch Sauerstoff in Gegenwart von Wasser bei erhöhten Temperaturen.

Abstract

Since hexavalent chromium has been recognized as toxic and carcinogenic, its usage has been restricted. Thereafter, Cr(VI) was substituted by a safer, yet effective, trivalent chromium-based treatment solution. The addition of transition metal ions into the Cr(III)-based treatment solution was proposed to improve the corrosion resistance of the produced passivation film. The present study intends to elucidate the effect of treatment solution composition on the formation and structure of Cr(III)-based conversion coatings containing cobalt. Model solutions with two different complexing agents, viz. fluoride and oxalate, with and without cobalt were applied to the zinc-plated steel. The scanning electron microscopy (SEM) and atomic force microscopy images revealed a morphology with microstructural defects that can be improved to a more uniform and adherent structure by adding cobalt to the passivating bath. The elemental composition of the layer was investigated by Auger electron spectroscopy (AES). Furthermore, the amounts of Cr and Co in the coatings were measured with the aid of inductively coupled plasma optical emission spectroscopy (ICP-OES). AES and ICP-OES both detected cobalt in the layers. Using a thermodynamic model, the concentration of Cr(III), Zn(II), and Co(II) species in the pH ranges of 0.0 to 14.0 and the minimum pH for the deposition of each metal ion species in the relevant treatment solution were calculated. The results of accelerated corrosion tests (polarization measurement and electrochemical impedance spectroscopy) suggested that the formation of a dense layer is crucial for good corrosion resistance of the coating. Furthermore, the formation mechanism of Cr(VI) in the layers formed in Cr(III)-based treatment solutions containing Co, was also studied. The presence of Cr(VI) was detected by means of spectrophotometry. The morphology and structure of the films were observed with SEM. Besides, Karl Fischer titration was used to measure the total amount of water in the layers. It

was shown that the morphology of the fluoride-containing film with a high density of micropores increased the probability of water entrapment. This resulted in the oxidation of Cr(III) to Cr(VI) by oxygen in the presence of water at elevated temperatures.

Contents

List of Figures

List of Tables

List of Abbreviations

AA	Atomic absorption
AES	Auger electron spectroscopy
AFM	Atomic force microscopy
ASTM	American society for testing and materials
CCC	Chromate conversion coating
CHA	Concentric hemispherical analyser
cKFT	Coulometric Karl Fischer titration
CPE	Constant phase element
DI	Deionized
EA	Electro-assisted
EBSD	Electron backscatter diffraction
EDXRF	Energy-dispersive X-ray fluorescence
EDXS	Energy-dispersive X-ray spectroscopy
EEC	Electrochemical equivalent circuit
EIS	Electrochemical impedance spectroscopy
ELV	End-of-live-vehicle
FIB	Focused ion beam
FIB-SEM	Focused ion beam scanning electron microscope
FT-IRAS	Fourier transform infrared reflection absorption spectroscopy
GDOES	Glow discharge optical emission spectroscopy
HER	Hydrogen evolution reaction
ICP	Inductively coupled plasma
ICP-AES	Inductively coupled plasma atomic emission spectroscopy
ICP-OES	Inductively coupled plasma optical emission spectroscopy

IAP	Ion activity product
KFT	Karl Fischer titration
LFSE	Ligand field stabilization energy
LOD	Limit of detection
NAVAIR	US naval air systems command
NR	Neutron reflectivity
NSS	Neutral salt spray
OCP	Open circuit potential
OSHA	Occupational safety and health administration
PP	Potentiodynamic polarization
RBS	Rutherford backscattering spectroscopy
REACH	Registration, evaluation, authorisation, and restriction of chemicals
RS	Raman spectroscopy
SCE	Saturated calomel electrode
SEM	Scanning electron microscopy
SHE	Standard hydrogen electrode
SI	Saturation Index
SKP	Scanning Kelvin probe
TCC	Trivalent chromium conversion
TCP	Trivalent chromium process
TEM	Transmission electron microscopy
TOF-SIMS	Time-of-flight secondary ion mass spectrometry
UV-VIS	Ultraviolet-visible spectrophotometry
XPS	X-ray photoelectron spectroscopy
XRD	X-ray diffraction

1 Introduction

1.1 Motivation and problem definition

Chromate conversion coating (CCC)s have long been used to enhance the corrosion protection of zinc-plated steel [1, 2] and aluminium alloys [3, 4]. Based on the process parameters and composition of the CCC treatment solution, a variety of colours with a good corrosion protection layer can be achieved [5, 6]. The CCC process is considered as relatively easy to set up and maintain [7]. Immersion of the base metal into a chromic acid bath at ambient temperature produces a thin film consisting of a complex mixture of Cr(III) and Cr(VI) compounds [5].

Chromate has strong oxidation properties. Chromate conversion coatings contain residual hexavalent chromium that provide a self-healing effect to the defects in layers [8]. This means that Cr(VI) ions migrate to fill in areas where the coating is damaged and form a protective layer [9]. Unfortunately, Cr(VI) is dangerous to the environment, despite presenting superior corrosion protection [10]. Hexavalent chromium indirectly reacts with human DNA, through a reduction to Cr(V), which eventually causes DNA damage [11]. Numerous epidemiological studies have reported a high incidence of lung cancer and other toxicological effects among people exposed to Cr(VI) by inhalation, ingestion, and skin contact [12].

Due to the fact that hexavalent chromium compounds were recognized as toxic and carcinogenic [13, 14], the End-of-live-vehicle (ELV) directive allowed a maximum of 2 g Cr(VI) per vehicle after July 2003 [15, 16]. The industrial usage of Trivalent chromium conversion (TCC) coatings has been put into practice by European

directives [17–19] since prohibiting hexavalent chromium from being used in surface finishing industries [20].

Moreover, CCCs fail to maintain corrosion protection after annealing above 60°C. In contrast, TCC coatings resist high temperatures up to 150°C and yet maintain until 80% of their corrosion protection [21].

Although the TCC layer acts as a barrier, without heat treatment, the corrosion protection of CCC is generally better [15]. However, studies showed that transition metal ions such as Co(II), Ni(II), and Fe(II) incorporated into TCC treatment solutions induce better corrosion protection [22, 23]. Not only is the corrosion resistance of the coating improved in the presence of cobalt ions [24–27], but also, the layer formed in the cobalt-containing treatment solution has the advantage of better surface appearance [28].

According to some studies [25, 29], cobalt was not detected in the layer formed in the cobalt-containing TCC treatment solution. Furthermore, it is reported that adding a cobalt salt to the TCC treatment solution did not affect the microstructure of the formed layer significantly [24]. Nonetheless, the role of cobalt in the TCC treatment solution has not been understood yet [24, 29].

Cr(III) octahedral complexes are generally very slow to the exchange of water molecules with other ligands [30]. The kinetic inertness results from the type of orbital charge distribution with the electron configuration of $3d^3 4s^0$. Cr(III) has a large range of stability and a very slow ligand displacement and substitution reactions, which allow separation, persistence, and/or isolation of thermodynamically unstable Cr(III) species [31].

To prepare TCC treatment solutions, apart from a Cr(III) salt and additional transition metal ions to increase the corrosion resistance, another component to form a complex with Cr(III), which is kinetically less inert than $[Cr(H_2O)_6]^{3+}$, is needed [24]. In a hexavalent chromium conversion process, the Cr(VI) ion acts as an oxidizing agent, while in the TCC process the role of the oxidation agent is mainly carried out by nitrate [24]. A very limited number of papers dealt with complexants in TCC treatment solutions. Overall, fundamental studies of the TCC

formation mechanism plus the physical and chemical structure of the coating and its correlation with corrosion protection behaviour of the layer are rarely carried out. Besides, the composition of the substrate was shown to influence the mechanism of the film growth [32–34]. Most studies [35–44] investigated proprietary products as the treatment solution on an aluminium substrate, whereas, zinc substrates have been rarely studied and yet are very important for the automotive industry.

Due to the toxicity of Cr(VI), the oxidation process of chromium from the trivalent state to the hexavalent state is a crucial environmental issue. Although the TCC process is generally recognized as an environmentally preferential alternative, some studies reported traces of hexavalent chromium in TCC coatings [45–47]. Furthermore, some investigations suggested that trivalent chromium is oxidized to hexavalent chromium following corrosion tests in a salt spray chamber [48], despite the apparent absence of strong oxidizing agents [46]. The generation of Cr(VI) was attributed to the presence of atmospheric oxygen in the cabinet. Another work [40] reported no presence of Cr(VI) in trivalent conversion coatings, either as deposited or corroded (kept in corrosion environment for 24 h), except in the case that hexavalent chromium was formed as an intermediate or in undetectable amounts. Likewise, another research [42] also considered the transient formation of Cr(VI) in TCC coatings. Whereby, it is suggested that the reduction of oxygen at copper-rich intermetallic sites generates hydrogen peroxide that can oxidize trivalent chromium species. Chromate ions are, however, mainly in the form of mobile CrO_4^{2-} and are strong oxidizing agents under acidic conditions. They eventually diffuse to corroding sites and get reduced to generate $Cr(OH)_3$. Additionally, some investigations proposed that the presence of cobalt in the coating promotes the formation of Cr(VI) species in the layer [45, 47].

Due to the fact that the soluble Cr(VI) in a scratched or abraded films forms a new passivate film with water and zinc [21], hexavalent chromium in the layer provides self-healing effect, as long as the Cr(VI) content in the film is not dehydrated by exposure to temperatures above 50 to 60°C for an extended period of time. Hence, it was suggested that the existence of Cr(VI) species in the cobalt-containing passivation offers better corrosion protection. Therefore, the oxidation of Cr(III) to Cr(VI) in

TCC films causes a dispute in the surface finishing industry to consider these coatings as being compatible with the European directives.

1.2 Research aims and objectives

Despite growing interest in the conversion coatings which meet the health and environmental requirements of the European directives [17–19], published articles on Cr(III)-based conversion coating are mostly done on proprietary products. This work aims at studying the formation and composition of coatings formed in the TCC treatment model solution on the Zn-plated steel.

The objectives of this work can be summarized as follows;

- To elucidate the role of the chemical composition in TCC treatment solutions on the Zn-electroplated steel, the following steps will be followed: Initially, the work concentrates on the physical structure and the chemical composition of TCC layers formed in model solutions with two different complexing agents, viz. fluoride and oxalate. Then, to better understand the role of cobalt in the coating structure, the physical and chemical characterization of the layers formed in the TCC treatment solution with and without cobalt are compared.

- Furthermore, the influence of the TCC bath composition, i.e. type of complexing agent and the addition of Co, on the corrosion properties of the formed layer is investigated.

- Some studies outlined the presence of Cr(VI) species in layers formed in Cr(III)-based treatment solutions, especially the TCC solutions containing cobalt. Therefore, at the end of this work, investigations are carried out (a) to detect the presence of hexavalent chromium in conversion coatings prepared from trivalent chromium solutions with different variables (e.g. composition and heat treatment) either as-prepared or corroded (after being kept in salt spray chamber for 24 h); (b) to explain the probable formation mechanism

of hexavalent chromium-based on influencing factors such as the presence of cobalt or type of complexing agents inside treatment solutions.

1.3 Structure of the thesis

This thesis is divided into eight chapters. An introduction to the work is presented in chapter one. After outlining the problems, the research aim and structure of the work are indicated.

Chapter two reviews the important aspects of TCC coatings. In the beginning, a short summary is given about the zinc plating process. The corrosion performance of the conversion coatings based on Cr(III) is compared with that of Cr(VI). The methods employed to study the coating properties (e.g. composition, morphology, and corrosion resistance) are discussed. Furthermore, the impact of process parameters (e.g. pH, temperature, and immersion time), and passivating bath composition are explained by reviewing published investigations. This chapter is carried out employing a manual search of 68 peer-reviewed articles. With the aid of published papers related to the trivalent chromium conversion coating, five main research questions are answered. In the end, the potential remaining questions about Cr(III)-based treatment solution to be studied in the future are summarized.

In chapter three, the author set outs the experimental approach and processes; the sample preparation; and the used methods and devices of this dissertation.

The experimental part of the work encompasses three main areas: (1) morphological and compositional characterization of TCC layers, (2) evaluating the corrosion protection properties of TCC coatings, and (3) the feasibility of the hexavalent chromium formation in TCC films.

Chapter four deals with the physical characteristics of the Zn substrate. The Zn layer morphology, the substrate of a TCC film, is observed using Scanning electron microscopy (SEM) and Atomic force microscopy (AFM).

In chapter five, the structure of TCC layers formed in different treatment solutions on the Zn-plated surface is studied by Focused ion beam scanning electron microscope (FIB-SEM) and AFM means. Different immersion times and temperatures are applied to study the formation of the TCC film. In particular, the influence of Co in the treatment solution on the formation of the layer is investigated. The chemical composition of the TCC coating is studied using Auger electron spectroscopy (AES) and Inductively coupled plasma optical emission spectroscopy (ICP-OES).

The corrosion behaviour of the TCC layers, after deposition and also when samples are heat-treated, is investigated by salt spray tests, polarization measurements, and electrochemical impedance spectroscopy analysis, which is presented in chapter six.

Finally, the formation of hexavalent chromium in the TCC layers is studied. The results are discussed in chapter seven.

A summary and conclusion are given in chapter eight, where the ideas for future work are suggested.

2 State of Art

2.1 Introduction

Various types of steel as a family of iron-based materials have been put into a broad variety of applications, including infrastructure, industry, transportation, construction, consumer goods, etc. [49]. Steel is highly prone to rust in a wide variety of situations, and over time this phenomenon causes this part to lose efficacy [50]. This degradation process is called corrosion and is defined as a chemical or electrochemical reaction between a material and its surrounding environments that produces a deterioration of the material and its properties [51, 52]. In the neutral condition, the corrosion of steel occurs as the coupled reaction of anodic oxidation (dissolution) of iron and cathodic reduction of oxygen [53]. Furthermore, in the presence of the chemical species the corrosion can be accelerated [53].

Thus, a variety of methods were sought to protect steel against corrosion and give the part a satisfactory service life, (e.g. paint, hot dip galvanized or aluminized, electroplated, thermally sprayed, and clad with a more corrosion resistant material). The type of surface treatment is restricted by size, weight, and handling problems. Moreover, the type of surface treatment is specified by a further requirement for wear resistance, thin-film coating, etc. [54]. Furthermore, time and temperature are also factors that play a role in the selection of a coating. A metallic coating can protect steel against atmospheric corrosion by means of numerous processes including; electroplating, electroless plating, immersion into the liquid metal, physical or chemical vapour deposition, and thermal spraying [55]. Electroplating is defined as the application of a metal coating or other conducting surface using an electrochemical process [56]. Throughout this process, the metal to be coated plays the role of the

cathode in an aqueous electrolyte from which the coating is deposited. Besides, providing corrosion protection, these coatings can also be decorative. A considerable diversity of coatings can be implemented by electroplating, such as zinc, cadmium, chromium, copper, gold, nickel, tin, and silver; as well as alloys, like tin-zinc, zinc-nickel, brass, bronze, gold alloys, and nickel alloys [57]. In zinc electroplating, a layer of zinc is electrolytically deposited on a cleaned steel surface using a zinc salt solution [58]. Zinc has a standard potential that is more negative than that of iron (Zn/Zn^{2+} -0.73 V/SHE and Fe/Fe^{2+} -0.44V/SHE). Thus, it is used for sacrificial cathodic protection of steel against corrosion [31], especially when protection from either atmospheric or indoor corrosion is the main goal [59]. Functional components in the automotive industry are mostly zinc-plated to be protected against corrosion. The zinc plating process is accomplished using a distinctively different type of plating bath. The three most common types of commercial zinc baths include cyanide baths, alkaline non-cyanide baths, and acid chloride baths [31].

2.1.1 Zinc cyanide baths

These types of baths are made of a highly alkaline solution including cyanide ions. Zinc is present in this bath as complexed to cyanide and/or hydroxyl anions (i.e. $Zn(CN)_4{}^{2-}$, $Zn(OH)_4{}^{2-}$, $Zn(OH)_2(CN)_2$). In these baths, sodium is usually the cation. The composition of a bright cyanide zinc bath may vary depending on cyanide content. These types of baths can be classified into four categories: regular cyanide zinc bath, mid-cyanide baths, low-cyanide baths, and micro-cyanide baths [31]. The operating temperature range is 20-40°C, the average current density is 0.6 A dm^{-2} with the cell voltage of 12-25 V for barrel plating; and 2-5 A dm^{-2} with the cell voltage of 3-6 V for rack plating [31]. The cyanide bath composition is stable, resulting in a good (macro) throwing power [1] and covering power [2]. Although these types of baths are easy to control, the necessity to destruct the extremely toxic

[1] Throwing power is the ability to deposit a plating of uniform depth on a surface of irregular shape [60].

[2] Covering power is the extent to which an electrodeposition electrolyte can cover the entire surface of an object being plated and to deposit metal on the surfaces of recesses or deep holes. This term suggests an ability to cover, but not necessarily to build up a uniform coating [61].

cyanide in waste-water treatment processes convinced many plating companies to use different types of plating bath [62].

2.1.2 Alkaline non-cyanide baths

These types of baths were developed in an effort to produce a non-toxic cyanide-free zinc electrolyte. The composition of these baths is mainly zinc, sodium hydroxide, and proprietary additives. The composition characteristics of alkaline non-cyanide zinc baths pertain to two different concentration limits, so-called low chemistry (LC) and high chemistry (HC). Accordingly, for the chosen type of constituent, LC and HC, the zinc and hydroxide concentrations are increased at the same time. The operating temperature ranges from 15-45°C, the cathode current density is 2-4 A dm^{-2} with the cell voltage of 12-18 V for barrel plating, and 0.6 A dm^{-2} with the cell voltage of 3-6 V for rack plating [31]. These types of baths have a limited range of optimum operating zinc concentrations and thus are difficult to control. Burning or pitting, intermittent deposit blistering, zinc anode passivation are the main problems that need to be dealt with.

2.1.3 Acid chloride baths

Since the 1970s, these types of baths have been used in 50% of all zinc baths for the rack and barrel plating in most developed nations [31]. A typical acid chloride bath consists of zinc chloride and organic additives which are mostly proprietary products, i.e. primary brighteners, and carriers (acting as wetting agents to solubilize the primary brighteners) [31, 62]. The operating temperature of these baths ranges from 15-55°C, the pH values are 5-6. The cathodic current density is 0.3-1 A dm^{-2} with the cell voltage of 4-12 V for barrel plating, and 2-5 A dm^{-2}, with the cell voltage of 1-5 V for rack plating [31]. Acid baths have very good brightness and levelling ability (micro-throwing power). They save energy due to the high conductivity of the baths. In comparison with cyanide or alkaline processes, zinc acid baths have 95-98% higher current efficiencies that result in hydrogen embrittlement [59]. However, the high corrosiveness of the acid bath requires special tank materials [62].

2.2 Conversion coatings

The zinc-plated parts usually require further surface treatments to improve corrosion resistance. Conversion coatings have been extensively used to enhance corrosion protection; to activate a surface for a better paint receptivity; and to increase surface hardness and abrasion resistance of the substrate, to which they are applied [61]. Conversion coatings are based on the adsorption of protective metal oxide into the existing oxide film, which, however, may include non-metals in some cases [63]. By removing and replacing the oxide layer of the metallic substrate and via a chemical or an electrochemical process, conversion coatings supply an insulating barrier of low solubility to the substrate [31]. This method slows down the corrosion reactions which might take place on the substrate with the formation of a diffusion-controlled passive layer [63], or release of corrosion inhibiting species [33]. The inhibiting substances in the layer may include metal oxides, corrosion products, organic adsorbents, etc. [63]. Chromate- [14], phosphate- [64], and oxalate- [65] conversion coatings are typical candidates.

CCCs have been widely produced on various metals and their alloys since World War II; notably, on aluminium [66–69], and zinc [6, 61] substrates. These coatings are achieved by immersing the metal component (e.g. Zn-plated steel, Zn, Mg, and Al) into a chromic acid bath and via chemical/electrochemical reactions (Reaction 2.1). Consequently, a passivation film consisting of a complex mixture of the substrate metal (e.g. Zn or Al), Cr(III) and Cr(VI) oxides and hydroxides is formed at the metal surface [5].

$$2\,\mathrm{HCrO_4^-} + 14\,\mathrm{H^+} + (6/\mathrm{n})\mathrm{M} \longrightarrow 2\,\mathrm{Cr^{3+}} + (6/\mathrm{n})\mathrm{M}^{n+} + 8\,\mathrm{H_2O} \qquad (2.1)$$

(M can be Mg, Zn: n=2, Al: n=3) [9]

Despite excellent corrosion protection, chromate compounds were recognized as restricted items due to being toxic and carcinogenic by the ELV [17], Removal of hazardous substances (RoHS) [18], and Waste electrical and electronic equipment (WEEE) [19]. The U.S. department of Occupational safety and health administration

(OSHA) has also issued a compliance directive for occupational exposure to Cr(VI) [70].

Thereafter, because of environmental legislation, much interest has been dedicated to the development of the formulation and application of alternative conversion coatings. Amongst suggested substitute treatment solutions that were investigated, the TCC has been considered a suitable candidate to date. The TCC coatings were first introduced in 1951 [71]; however, their industrial usage has been put into practice, since hexavalent chromium was restricted from being used in the surface finishing industries [17–20]. Since then, there have been many papers published on TCC coatings on different substrates. The following summary intends to review the published results on the corrosion properties, formulation, and properties of the TCC coatings that were applied to the Zn and Al substrates.

2.3 Method of literature review

With the aid of five specific research questions, this section was aimed at searching exhaustively and comprehensively on the literature focused on the TCC coatings. This section sought to systematically search for identifying major works on the characterization, formulation, and development of Cr(III)-based passivating bath; moreover, to identify gaps, issues, and opportunities for further study and research.

2.4 Research questions

The research questions addressed by this study are:

RQ1: To what extent can the corrosion protection of the conversion coating produced in Cr(III)-based bath be compared with that of Cr(VI)?

RQ2: How do substrates affect the TCC coating formation?

RQ3: What is a TCC treatment solution composed of?

RQ4: How do the process parameters of a TCC treatment solution influence the formation of the coating?

RQ5: Which analytical methods have been used to investigate the layers?

2.5 Search process of literature review

To establish a time span, with respect to the ELV directive [17], the starting point was established in the year 2000. This work mostly focuses on the published research papers; patents and proceedings were barely included, since these reports cannot fully answer most of the above-mentioned questions.

2.6 Discussion

In this section, the answers to the research questions are discussed.

RQ1: To what extent can the corrosion protection of the conversion coating produced in a Cr(III)-based bath be compared with that of Cr(VI)?

As mention earlier, CCCs are formed on different kinds of metals and are not thicker than a few microns [72]. The CCC process involves chemical or electrochemical reactions with mixtures of chromic acid and certain other compounds [5]. The thickness of CCCs varies depending on the chemistry and process parameters of the treatment solution.

CCCs promote good adhesion between the metallic substrate and the post-treatment, such as sealing or painting, and also protect defects and cut edges of the metal to some extent [6, 72]. When corrosion occurs at the surface of a chromated part, soluble Cr(VI) species in the layer migrate toward the defective structures (scratched or abraded), and reduce to protective Cr^{3+} compounds ($Cr(OH)_3$). Gharbi et al. [73] defined the self-healing effect as the process in which the chromate ion ($CrO_4{}^{2-}$) leaches into the electrolyte, so-called “active sites”, and a protective chromium oxide

(Cr_2O_3) film is produced through a cathodic reduction reaction (coupled to anodic metal dissolution). Consequently, a new passivating film (red layer in Figure 2.1) which aids in the protection of defects is generated that diminishes the corrosion propagation [21, 27]. This outcome, which has been seen in CCCs, is known as the self-healing effect [6, 13, 72].

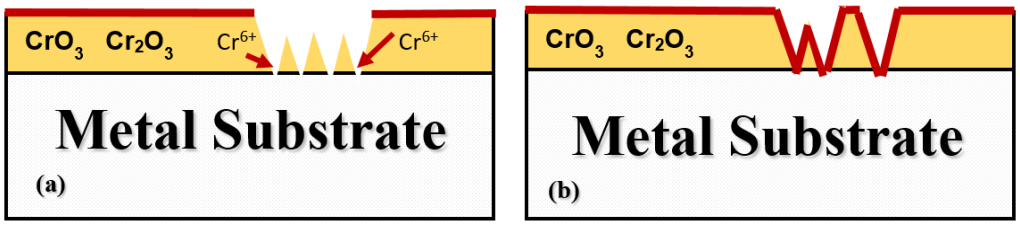

Figure 2.1 Schematic illustrations of the corrosion inhibition associated with Cr(VI) compounds in a CCC (a) when morphological defects (e.g. scratches) occur, (b) when the self-healing properties occur and the barrier film forms, red colour indicate a thin barrier layer, and yellow colour shows the undamaged part of the layer

However, the reduction process of Cr(VI) to Cr(III) causes the dehydration (Reaction 2.2) of the TCC layer which makes the Cr(VI) species immobile [74] and/or insoluble [75]. That is why the supply of Cr^{6+} species decreases with time and consequently, the self-healing effect is restrained [27].

$$Cr_2O_7^{2-}(aq) + 14H^+ + 6e^- \rightleftarrows 2Cr^{3+}(aq) + 7H_2O(l) \qquad E^\circ = +1.33\,V \quad (2.2)$$

Electrochemical impedance spectroscopy (EIS) was used by Grasso et al. to compare the corrosion protection of a CCC and a TCC coating [76]. It was found that the CCC had a better corrosion resistance in chloride solution for short immersion periods, while the TCC coating was more persistent for longer exposure times. This was attributed to the fact that the remaining soluble Cr^{6+} species which might have been reduced to Cr^{3+} compounds were gradually decreased, and consequently, the self-healing effect of CCC was terminated.

The CCC is a gelatinous film composed of hydrated compounds. This layer stabilizes and becomes hydrophobic when exposed to temperatures less than 60°C [21,

77]. However, after heat treatment or prolonged exposure to elevated temperatures, Cr^{6+} ions in the layer are reduced to Cr^{3+} ions due to the total dehydration [21, 77, 78] (Reaction 2.2 and 2.3).

$$2\,CrO_4{}^{2-}\,(aq) + 10\,H^+ + 6\,e^- \rightleftharpoons 2\,Cr(OH)3{\downarrow} + 2\,H_2O\,(l) \tag{2.3}$$

Figure 2.2 shows SEM images at 10,000 times magnification. This figure clearly indicates the effect of heat treatment on the TCC and the CCC coatings. The micro-cracked structure in the CCC became wider after heating at 150°C. As Figure 2.2 shows, the heat treatment (so-called thermal shock in this paper) causes widening and deepening of the cracks and fissures in CCCs and results in early corrosion initiation and propagation of the zinc substrate [15]. Therefore, self-healing properties function as long as water and soluble Cr^{6+} ions are present in the layer. In comparison with CCCs which fail to maintain corrosion protection after annealing, TCC coatings resist high temperatures up to 200°C or more for a prolonged period and still maintain up to 70% of their original protective properties [15, 78].

A study also confirms that the TCC coatings perform well despite not exhibiting self-healing properties [78]. The reason is that the films produced in TCC solutions show more homogenous, much less and smaller cracks. Stable Cr(III) compounds in the layer keep the structure relatively intact even after heat treatment [78]. The TCC layers also act as a barrier [15]. Studies [22, 23] show that adding transition metal ions such as Co(II), Ni(II), and Fe(II) into the treatment solution can improve the corrosion protection of the TCC coatings. It was shown that applying an adequate sealant to the TCC coatings enhanced the corrosion resistance up to the point which was higher than that of unsealed CCCs [25, 80]. A combination of a TCC coating plus a suitable sealant composition results in a more durable resistant film, due to the formation of a thicker protecting barrier layer with corrosion-inhibiting effect. The sealing treatment may contain phosphate, silicon, silanes, silicate, and transition metals in an organic or inorganic matrix, which is applied to TCC coatings at room or elevated temperatures [15, 80]. In a study [81], five commercial treatment solutions, containing Cr(VI) and its substitutes, including and excluding Cr(III), were applied to zinc-plated steel substrates, and their corrosion behaviour was studied using

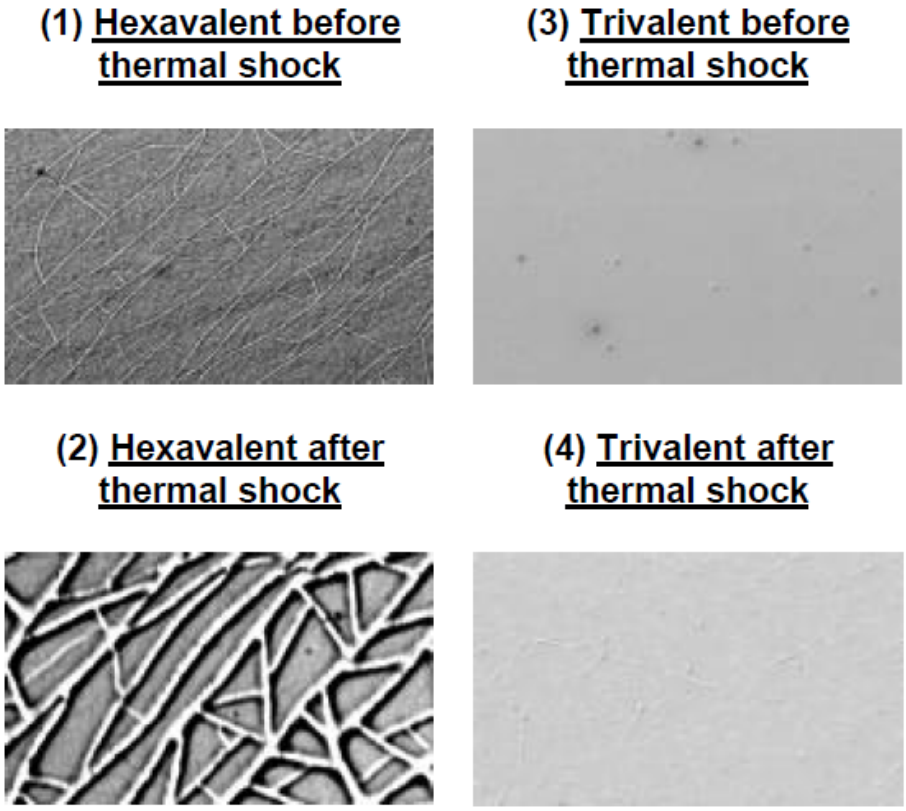

Figure 2.2 SEM images (magnification X10000) of CCC and TCC coatings before and after heat treatment (for 1 hour at 150°C), (1) The CCC with micro-cracked structure, (2) The CCC after heat treatment, it shows that the cracks present in the CCC layer became wider after heat treatment, (3) The TCC coating with less micro-cracked structure compared with CCC, (4) The TCC coating after heat treatment, it is obvious that the TCC coating structure did not change significantly after heat treatment [79]

accelerated corrosion tests (Neutral salt spray (NSS) and humid chamber test) along with electrochemical measurements (cathodic polarization curves and EIS analysis). It was concluded that the Cr(III)-based treatment solution was the best alternative to Cr(VI).

EIS and polarization measurements of the samples treated with a solution containing Cr^{3+} and Co^{2+} showed a higher corrosion resistance compared to the samples treated with a Cr^{6+} solution [27]. The results were attributed to the stability of Cr_2O_3 and the inhibitive action of the Co^{2+} ions, besides the barrier structure that slows down the oxygen transport to the zinc layer. It was suggested that the TCC coatings with a more uniform structure presented a lower corrosion rate and may still support applications in a wide variety of applications [82].

Using an artificial scratch technique, Guo et al. [38] studied active corrosion inhibition[3] of an Al alloy (AA2024-T3) by TCC coatings. To assess the self-healing properties of the TCC coating, a cell containing a corrosive electrolyte was assembled with two parallel Al alloy (AA2024-T3) specimens (one TCC-treated and the other untreated) separated by an O-ring. Even though the TCC-treated and untreated samples were not in contact, Cr species were found on the adjoining untreated specimen. This dissolution and transport of Cr were ascribed to the transient formation of Cr(VI). Furthermore, the polarization resistance of the untreated surface adjacent to the TCC-treated was twice the untreated control sample. This implies that the TCC film supplies active corrosion inhibition to a neighbouring untreated surface. Furthermore, EIS analysis of the artificial scratch cell indicated an excellent corrosion protection for the TCC treated sample due to the barrier protection provided by the dense Zr/Cr oxide structure.

With the aid of polarization measurements carried out in 0.5 mol/L Na_2SO_4, the corrosion resistance of an Al alloy surface was compared with its surface when it was passivated in a TCC treatment solution. The results showed that both the anodic and cathodic currents were considerably decreased for the TCC treated specimens [41].

[3] Active corrosion inhibition is the ability of a material to reduce or avoid corrosion by means of manipulation of the corrosion process [83].

It was suggested that TCC coatings protect the substrate as a barrier rather than an inhibitive layer [22, 38, 46]. A variety of colours can be achieved by TCC coatings; these layers are able to endure heat treatment and the passivating electrolyte is simple to waste-water treatment [21].

RQ2: How do the substrates affect the TCC coating formation?

Metallic substrates, such as Al and Zn, are chemically reactive and form a hydroxide/oxide layer when exposed to water or air. These layers have a detrimental effect on the stability, adhesion, and uniformity of the further coating formation. Applying the treatment solution to a metallic substrate, without any surface pretreatment, with the aim of corrosion protection is not enough. An ideal coating needs to be uniform, well adhering, and pore-free to be able to provide adequate corrosion protection. Surface preparation has a crucial impact on the surface microstructure and thus on the formation of a coherent protective layer [84, 85].

With the aid of SEM images and EIS measurements, Defloriana et al. [86] studied TCC coatings applied to hot-dip galvanised coatings and electro-deposited zinc alloy coatings. When the deposition of the TCC layer on the above-mentioned substrates was compared, it was discovered that the films that were produced on the electrodeposited zinc layers (pure Zn and ZnFe alloy) were more uniform. Consequently, these films showed better corrosion protection and barrier properties. This was attributed to the fact that the surface of the zinc coating obtained by hot dipping was more oxidized and was less convenient for the pretreatment deposition. This resulted in the insufficient surface preparation of the studied hot-dip samples. Additionally, the TCC coatings applied to the electro-deposited pure Zn and ZnFe alloys were also studied. Even though SEM images showed the same film coverage for both types of substrates, Energy-dispersive X-ray spectroscopy (EDXS) found a lower amount of Cr on the ZnFe surface compared to that on the pure Zn surface. A loss of adhesion was observed for the TCC layer formed on the ZnFe substrate; while the TCC layer produced on the pure electro-deposited Zn showed higher stability. This was ascribed to a rather homogeneous surface of the pure Zn in comparison to the ZnFe alloys.

It was reported that a rough surface decreases the probability of a TCC coating to conformally form across the surface [87]. Therefore, the physical structure of the substrate onto which the coating is deposited determines how uniformly the coating precipitates.

In the conversion coating process, the metal substrate provides ions that become part of the protective coating after (electro-) chemical reactions of the substrate with a reactive medium [84]. To improve the adhesion and uniformity of the conversion coating, the substrate must be chemically activated. As a result, the oxide layer formed on the surface is removed and dissolved metal ions are incorporated into the conversion layer and at the interfacial surface. Therefore, the surface chemistry and the substrate pre-treatment influence the mechanism of conversion coating deposition [33]. A typical coating formation process involves cleaning, rinsing, deposition, rinsing, and drying [85]. The cleaning process may include mechanical and chemical treatment [33], provide a uniform grease-free surface [84], improve wetting [85], and adherence [84, 88]. Mechanical pretreatment might include grinding and/or polishing, abrasive finishing followed by rinsing with ethanol or acetone to remove impurities such as oxides or dirt from the parts. The pretreatment solutions may contain alkaline degreasing or etching, alone or combined with acid desmutting or deoxidation, and acid cleaning or activation [33]. Deionized (DI) water might also be used for rinsing. Proper surface cleaning influences the hydrophobic/hydrophilic properties of the surface as well as its corrosion protection [81]. Aluminium (Al alloys), iron (steel) and zinc (galvanized steel) are among the most investigated substrates for CCC [89].

TCC coatings were applied to aluminium [35–44, 90, 91], and zinc-plated steel [78, 85] substrates. Surface pretreatment may vary according to the substrate used. In some cases, cleaning treatment solutions are industrial products [41, 87], and sometimes they are diluted acid solutions. Prior to applying the TCC process, the aluminium substrates were electropolished [91, 92]. Qi et al. [35] reported the surface treatment for Al surface prior to the Cr(III)-based passivating as follows; I) cleaning by acetone, ethanol and DI water, (II) electropolishing in the mixture electrolyte of perchloric acid and ethanol (1/4 volume) at 20 V for 4min below 10°C, (III) cleaning by ethanol and DI water and drying in cool air, (IV) a consecutive HF etching in a

mixture of 1.5 mL HF, 10 mL H_2SO_4 and 90 mL H_2O for 30 seconds to generate the network of metal ridges, (V) cleaning by DI water and drying in a cool air stream. Table 2.1 lists some examples of pretreatment on different substrates, before applying the TCC process.

Table 2.1 Examples of pretreatment processes applied to the different substrates, before applying the TCC coating

Substrate	Pretreatment	Ref.
Steel	Degreased in a sodium silicate-based alkaline solution at room temperature, with a current density of 4 A dm^{-2} for 3min	[27]
Aluminum (99.99%)	Electropolished for 240s in a 20 vol% perchloric acid (60 wt%) and 80 vol% ethanol mixture below 10 °C, using a potential of 20 V applied between the specimen and an aluminum counter electrode, followed by rinsing in DI water and drying in a stream of cool air.	[39]
Zinc plate	Polished with 2000 grit silicon carbide paper, degreased with acetone, cleaned (ultrasonically) in ethanol for 3min, rinsed in distilled water, activated for 2s in 3 wt% nitric acid and rinsed in distilled water.	[35]

To study the influence of substrate structure and composition on the formation of TCC coatings, Wanotayan et al. [93] applied a TCC solution onto the zinc-electroplated steel produced from Zn baths with three different organic additives. The alkaline non-cyanide zincate ($Zn(OH)_4^{2-}$) bath consisted essentially of 10 g/L of Zn and 120 g/L of NaOH with 1 mL/L of the selective additives. The additives used included imidazole and epichlorohydrin for the first bath, a polyquaternary amine salt for the second one, and polyethylenimine for the last. X-ray diffraction (XRD) was used to study the structure of the Zn layer. The corrosion protection of the TCC coated zinc-electroplated steel was analysed with EIS, and the structure of the layer was observed by SEM. Results indicated that the organic additives in the Zn bath have a large effect on the structure of the Zn layer and subsequently the formation of the TCC film. The Zn bath with polyethylenimine produced a better

corrosion protection with the TCC layer, amongst the studied organic additives in the polyamine group. This was attributed to the produced Zn layer structure with these additives, which favoured the formation of a TCC film with a higher chromium content in comparison with the others.

For the case of Al alloys, it was suggested that the TCC film does not cover over all the Cu-rich intermetallic areas [41]. This was ascribed to the high potential difference at Al-Cu in the Al alloy (AA204-T3), which hindered the film deposition at the cathodic sites.

In another research that was mainly done to study the corrosion protection of a TCC coating on an Al alloy substrate in atmospheric sulphuric acid, it was explained that the corrosion of the Al alloy surface initiated at (intermetallic) sites where the TCC coating or the native oxide did not cover (passivated) the surface [94].

RQ3: What is a TCC treatment solution composed of?

Bath formulation: TCC treatment solutions have been commercially available since the early 2000s [95]. The main components of these types of treatment solutions are Cr(III) compounds and oxidizing agent(s) [35, 52]. In the presence of a primary oxidizing agent, such as dissolved oxygen, the surface can oxidize to its higher oxidation state cations, generating hydroxides [52]. Consequently, the existing Cr(III) ions are enabled to react with produced hydroxides to form a protective conversion coating consisting of mixed oxides/hydroxides with the substrate ions and Cr(III), i.e. Al_2O_3 (or ZnO)/Cr_2O_3 and/or $Al(OH)_3$ (or $(Zn(OH)_2)$/$Cr(OH)_3$ [52]. In CCCs, Cr(VI) ions act as an oxidizing agent (Reactions 2.4 and 2.5 [96]), while Cr(III) ions do not have this ability in a TCC treatment solution (Reaction 2.6 [96]).

$$HCrO_4^- + 7H^+ + 3e^- \rightleftarrows Cr^{3+} + 4H_2O(l) \qquad E^\circ = +1.38\,V \qquad (2.4)$$

$$Cr_2O_7^{2-} + 14H^+ + 6e^- \rightleftarrows 2Cr^{3+} + 7H_2O(l) \qquad E^\circ = +1.36\,V \qquad (2.5)$$

$$Cr^{3+} + 3e^- \longrightarrow Cr \qquad E^\circ = -0.74\,V \tag{2.6}$$

Therefore, a TCC treatment solution demands an oxidant. The role of the oxidising agent can be carried out by nitrate, persulfate, hydrogen peroxide, etc. [35]. The chemical composition of a TCC treatment solution might vary depending on the substrate used. Hydrogen peroxide (H_2O_2) is an oxidizing agent which is commonly used for aluminium substrates [95]; while for zinc substrates, nitrate is used [24].

To prepare Cr(III)-based passivation solutions, apart from a Cr(III) salt and additional transition metal ions, another component is needed to form a complex with Cr(III), which is kinetically less inert than $[Cr(H_2O)_6]^{3+}$ [24]. The commercial version of the earliest TCC passivates was based on urea nitrate; a later version was a mixture of sulfamic acid and sodium nitrate to form nitric acid in situ [47]. Cr(III)- nitrate or sulfate are among the most common Cr(III) salts which are used. Moreover, the incorporation of transition metal or rare earth metal ions (e.g. Al, Ni, Fe, Co, Ti, Zr, and Mo) in the form of soluble salts into the TCC treatment solution boosts the corrosion resistance of the layer [22–24, 38].

Cr(III), with the electron configuration of $3d^3\ 4s^0$, has a large range of stability, the trivalent chromium ion has very slow reaction kinetics with regard to ligand exchange reactions [97]. Cr(III) octahedral complexes are generally inert to the exchange of water molecules with other ligands. However, even a small distortion from the six-coordinate geometry by adding a compound which forms a kinetically less inert complex with a Cr^{3+} ion than $[Cr(H_2O)_6]^{3+}$, results in orbital splitting and a more labile (less stable) metal-ligand bond. Principally, adding complexant increases the stability of the Cr(III) in the bath over a wider pH range. It was reported that a film formed by a treatment solution containing Cr^{3+} ions in the form of $[Cr(H_2O)_6]^{3+}$ was rather thick and porous with large micro-cracks. However, when Cr^{3+} ions were complexed with a dicarboxylic acid, the dissolution of zinc substrate as well as Cr(III) deposition on the surface was decreased, and a thinner TCC film with a smooth surface and a superior appearance and a better corrosion protection was formed [24]. The first generation of TCC treatment solutions was based on stable Cr(III) complexes. They produced a relatively thin film (20 to 30

nm) with limited corrosion protection. The second generation of TCC treatment solutions was elaborated to provide a thicker layer. Through this, the formed film thickness was increased up to 300-350 nm by means of adding accelerators, modified complexing agents, a higher concentration of compositions, and a higher operating temperature of the passivating bath [15]. The third generation of TCC treatment solutions relied on the incorporation of the protective Cr(III) oxides (probably also hydroxides), inhibiting agents, such as silicon oxide (SiO_2), used in the form of nano-sized particles. Auger depth profiling analysis detected Si both at the surface and throughout the coating. It was suggested that the SiO_2 particles were strongly bound into the conversion layer [98]. The fourth generation of the TCC treatment solutions is a combination of transition metals and nano-sized particles (as inhibiting agents) [99].

Moreover, the Cr(III) aquo complex has three electrons in the t2g orbital of the d-shell, resulting in substantial Ligand field stabilization energy (LFSE), thus undergoing ligand substitution reactions more slowly [100]. As was mentioned earlier, Cr^{3+} ions in a Cr(III)-based passivating bath should form a kinetically less inert complex than $[Cr(H_2O)_6]^{3+}$. Because Cr(III) ligand exchange is slow, to prepare the treatment solution after mixing the components, the prepared electrolyte is heated and stirred for 2 h at 70 ± 2°C [101]. Afterwards it is cooled and stored at room temperature before the beginning of the conversion coating [101], or only cooled to the processing temperature.

Additional materials can also be used to boost the quality of conversion coating, e.g. surfactants increase the wetting of zinc substrate and produce a more uniform film [102].

The composition of a TCC treatment solution, the operating pH and temperature of the bath, and immersion time influence the structure, thickness, and colour of the film. The treatment solution must be sufficiently acidic to maintain the metal cations and enable them to deposit as the conversion coating. The pH of the treatment solution can be varied depending on the solution constituents. For the TCC processes, the pH level of the treatment solution varies typically from 1.5-5.0, the temperature range is 40-60°C and the processing time is 15-100s [24, 102]. However, for aluminium substrates, the immersion time usually is longer (e.g. 15-20min) [42, 43].

A typical TCC process on a zinc-plated steel has the following sequences; zinc or zinc alloy plating, rinse, activate (diluted acid), immersing in the TCC treatment solution, drag-out rinse, rinse (counter-current flow), dry, seal and/or topcoat, and dry [15]. Prior to applying the TCC coating, the samples are activated by immersion in a 0.25 - 0.5% HNO_3 solution (pH 1) for 10s and then rinsed in DI water, which should not exceed 40°C [82, 103–106]. The bath pH of these solutions is around 1.6-2.2 [28] and is usually adjusted with dilute nitric acid (HNO_3) [107] or diluted hydrochloric acid (HCL) [27]. Conversion coatings can be formed by simple immersion into the passivating bath [33]. Drying is usually done in an oven at 80-90°C for 15min [105].

Bath formulation for a zinc surface: Sarli et al. [27] described a commercial TCC treatment solution applied to the zinc surface consisted of chromium nitrate, iron and cobalt nitrate, and organic acid. The pH was 1.8, temperature 60°C, and 60s immersion time. After the passivation, the samples were dried in an oven at 80°C for 15min. Wen et al. [106] prepared three treatment solutions with different anions for zinc-plated steel using Cr(III)-sulfate, -nitrate, and -chloride; the concentration ratio of Cr(III) to each anion was set to be 1/3. The solution was adjusted at a pH of 2 and applied at 60°C.

Bath formulation for an aluminium surface: One of the first formulations of the TCC treatment solution applied to the Al surface introduced in 1994 at US naval air systems command (NAVAIR), Patuxent River, Maryland, revealing 96 hours corrosion resistance of this conversion coating in 5 wt% NaCl salt spray test [108, 109]. TCC coating of NAVAIR was accepted by the European directives and Occupational safety and health administration (OSHA) and was licensed to many manufacturers, including Henkel Surface Technologies; SurTec International GmbH; Luster-On Products Inc.; Metalast International [110]; and Chemeon [94].

The NAVAIR group of baths contained Cr_2O_3, Na_2SO_4, and Na_2SiF_6 and was prepared one week before usage [108, 111]. A typical TCC treatment solution for the aluminium substrate contains hexafluorozirconate (H_2ZrF_6 or K_2ZrF_6), trivalent chrome oxides (Cr_2O_3 or $Cr(OH)_3$), chromium sulfate ($Cr_2(SO_4)_3$), and a fluoride (NaF) or fluoroborate (BF_4^-) salt. The bath has a pH in the range of 3.8-4.0 and

is adjusted with hydrofluoric (HF) or sulfuric acid (H_2SO_4) or sodium hydroxide (NaOH) [36, 40, 42, 112, 113].

Munson et al. [43], using ICP-OES analysis, determined the elemental composition of three TCC treatment solutions applied to the Al substrate, namely SurTec 650 E, V, C (Figure 2.3). The main chemical composition of all was Cr, S, Zr, and Fe. As can be seen from Figure 2.3, the Cr amount was quite the same for all three treatment solutions ($\sim$ 150 ppm). The nominal Zr concentration in all three baths was higher than the Cr concentration, and the Zr/Cr ratio was approximately 2:1 for all the three coating variants. SurTec 650 E is the first generation of the treatment solution based on the original NAVAIR formulation with Zr(IV) and Cr(III) salts. SurTec 650 V belongs to the second generation with the same general composition as 650 E with some added complexing agents. Different complexing agents were used in 650 C. SurTec 650 V, and C also contained Zn. SurTec 650 V had the highest S, Zn, and Zr amount in comparison to the others; while its Fe content was the lowest. SurTec 650 C, with 0.2 ppm difference, had the highest amount of Fe in comparison to the others, and while its Zr content was comparable to that of 650 V, its Zn and S content was around 100 ppm less than 650 V; however, in both cases higher than 650 E.

The TCC treatment solutions used for Al and Al alloys are Zr- and/or Ti-based [33]. It was shown that a coating formed of zirconium oxide alone has poor corrosion protection; however, adding small amounts of Cr(III) to its treatment solution enhanced its corrosion resistance [110]. Therefore, when the Cr content of the treatment solution which is used for the Al and Al alloys is compared with the one which is used for the Zn and Zn alloys, it can be seen that the amount of Cr is higher for Zn and Zn alloys.

Treatment solutions may also contain organic and inorganic additives. The organic ones are primarily added to improve adhesion to the underlying substrate, and to build an adequate base for the successive organic layers. Inorganic additives (e.g. copper, manganese, phosphate, etc.) are used with the aim of increasing the kinetics of the coating formation and enhancing the coating homogeneity [33]. One study [114] suggested that only when the treatment solution contained a suitable combination of

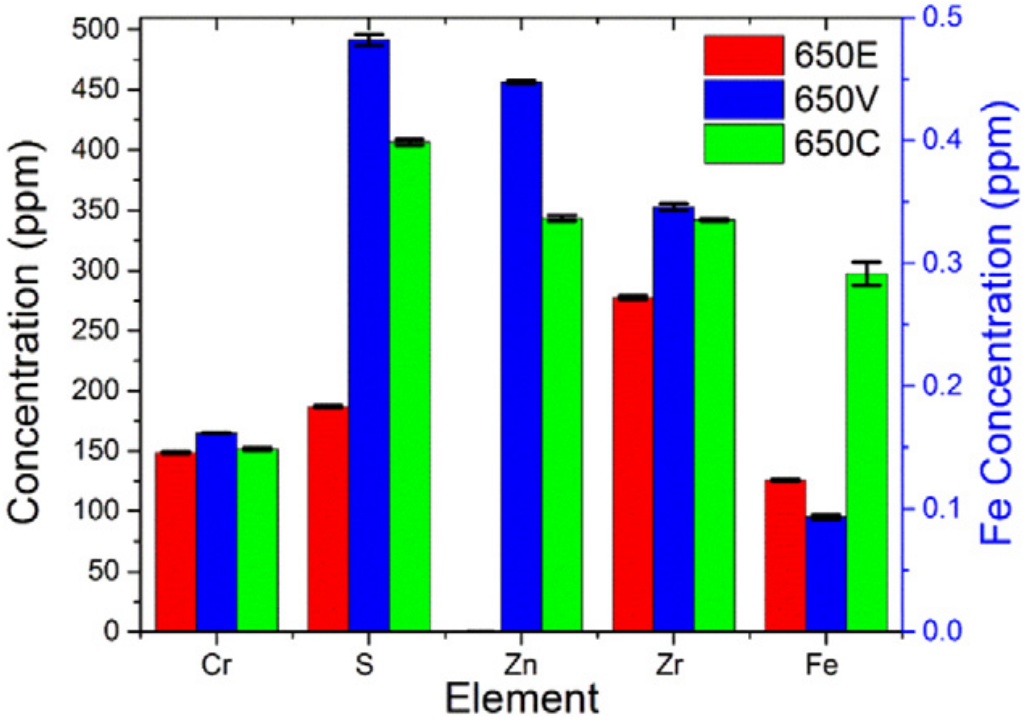

Figure 2.3 Elemental analysis of the TCC treatment solutions of SurTec 650 E (red), 650 V (blue), and 650 C (green) coating baths as determined by ICP-OES analysis. Data are presented as mean ± SEM (Standard Error of the Mean) for n ≥ 3 [43]

inorganic and organic substances were the morphology, homogeneity and corrosion protection of the coating satisfactory.

Unfortunately, selecting the correct composition of a TCC treatment solution does not guarantee a successful TCC process. An accomplished TCC coating for a selected substrate is a combination of choosing the right constituent for the treatment solution and selecting the suitable processing parameters.

A summary of the various TCC treatment solutions which have been described in literature is given in Table 2.2, together with their processing parameters and the substrate used. As can be seen most of the studies were done using proprietary products. Therefore, investigation using model TCC solutions promotes a fundamental understanding of the physical and chemical properties of these coatings [103].

RQ4: How do the processing parameters of a TCC treatment solution influence the formation of the coating?

The protective properties of a conversion coating are influenced strongly by the treatment solution composition; the bath pH and temperature; and the processing period. The film thickness is usually affected by the bath composition (e.g. chromium content) and immersion time; the reaction kinetics of the process is influenced by temperature and pH [5].

Treatment solution's pH: The pH of the passivation bath highly influences the uniformity of the formed film during the conversion coating process [33]. Because the pH of the solution affects the potential difference between the anodic and cathodic reactions which eventually influences the deposition rate. As can be seen from Table 2.2, the pH values of the processes vary depending on the substrate. A TCC solution is applicable for the aluminium substrate within a pH range of 3.8 to 4.0, while in the case of Zn, the bath is effective at pH values between 1.7 to 2.3. It is worth mentioning that, lower pH value causes a pickling attack on the zinc layer which brings about other complications.

Cho et al. [118] studied the effect of immersion time and bath pH on the microstructure and corrosion behaviour of TCC layers formed on the Zn surface. The layers were formed in a treatment solution containing chromium nitrate, cobalt,

Table 2.2 A summary of different TCC treatment solutions that were applied to the different substrates with their processing parameters of selected literature

Substrate	Process parameter	Bath composition	Trade name
Zn [27]	pH 1.8 at 60°C	Cr(III) + Co	(not mentioned)
Zn [80]	-	Cr(III)	Cr(III) Max blue (Glomax)
Zn [28, 82]	pH 1.9 at 25°C pH 1.8 at 25°C pH 1.6-2.1 at 60°C	Cr(III) + S Cr(III) Cr(III) + Co	UniFix Zn-3-50* UniYellow 3* SurTec S680 *(LABRITS)
Zn [25, 103]	pH 1.6-2.0 at 22°C pH 8.0-9.0 at 25°C pH 1.6-2.1 at 60°C pH 9.0-9.5 at 25°C pH 7.0-8.5 at 25°C pH 1.7-2.2 at 25°C	Cr(III) Cr(III) + Si Cr(III) + Co Cr(III) + Si Cr(III) + Si Cr(III)	Tridur Azul 3HPC Corrosil Plus 501 N SurTech 680 SurTech 555S SurTech 662 SurTech 666
Al [39, 92, 115]	pH 3.9 at 40°C	Cr(III) + Zr	SurTec 650 chromitAL
Zn [103]	pH 1.7-2.3 at 30°C	50 mL/L $Cr(NO_3)_3$(40%), 20 g/L $CoCl_2 \cdot 6(H_2O)$, 3 mL/L H_2SO_4	(not mentioned)
Zn [113]		H_3O^+, Cr^{3+}, $PO_4{}^{3-}$, F^-	Passerite 6001 (Henkel)
Al [43, 91]	pH 3.85 at 35°C	(not mentioned)	SurTec TCP (650 E, V and C)
Al [41, 42, 87, 90]	pH 3.8-4.0 at 30°C	$ZrF_6{}^{2-}$, F^-, Cr^{3+}, $SO_4{}^{2-}$	Alodine 5900RTU (Henkel)
Zn [107]	pH 1.8 at 60°C	10 g/L $Cr(NO_3)_3 \cdot 9(H_2O)$, 2.5 g/L $Co(NO_3)_3$	(not mentioned)
Al [112]	pH 3.8 at RT	$ZrF_6{}^{2-}$, F^-, Cr^{3+}, $SO_4{}^{2-}$	SurTech 650
Zn [105]	pH 1.8-2.0 at RT		Permapass Imunox 3K Permapass 7012
Zn [116]	pH 1.7-2.3 at RT	$Cr(NO_3)_3$, $CoCl_2$ each 2.5 g/L in DI water $Cr(NO_3)_3$, $NiCl_2$ each 2.5 g/L in DI water	
Al [117]	pH 3.9 at 40°C	$ZrF_6{}^{2-}$, Cr^{3+}, $SO_4{}^{2-}$ plus 0.01mol/L $FeSO_4 \cdot 7(H_2O)$	SurTec 650 chromitAL + Fe(II)
Al [44]	pH 3.9-4.0 at 40°C	$ZrF_6{}^{2-}$, Cr^{3+}	Socosurf TCS
Zn [106]	pH 2.0 at 60°C	Cr(III)-sulfate Cr(III)-nitrate Cr(III)-chloride	(not mentioned)
Zn [104]	pH 2.0 at 60°C	0.1 mol/L Cr(III) nitrate, 0.1 mol/L oxalic acid, , and 0.007 mol/L cobalt nitrate	(not mentioned)
Zn [93]	pH 2.2 at 30°C	Cr(III)	OKUNO Chemical Industries Co. Ltd.
Al [94]	pH 3.5-4.0 at RT	$ZrF_6{}^{2-}$, Cr^{3+}, S	Bonderite T5900 (Henkel)

chloride, and sulphuric acid. The bath pH values were 1.1, 1.7 and 2.3. SEM images showed that the surface roughness of the studied films was decreased with increasing pH value. Moreover, the layer formed by the treatment solution with the pH 1.1 didn't show a uniform growth, due to the high dissolution rate of Zn and the fast deposition of the TCC coating.

Process immersion time: Three immersion times of 20, 40 and 60s in the bath with a pH value of 1.7 were examined in the study of Cho et al. [118]. It was suggested that the TCC coating was deposited on the Zn substrate with micro-cracks due to internal tensile stress in the coating. The thickness and density of micro-cracks were first increased with increasing the immersion time from 20 to 40s, and then they were both reduced by increasing the immersion time to 60s. The TCC film with the highest thickness showed a better corrosion protection, due to the increased anodic pitting potential and the reduced passive current density.

Qi et al. [119] studied the dependence of the coating thickness on immersion time for an etched, desmutted, and mechanically polished Al alloy (AA 2024-T351) treated in the dilute SurTec 650 treatment solution at 40°C. The coating thickness was measured by a cross-sectional analysis of the Transmission electron microscopy (TEM) micrographs. The results suggested that the layer first reached a maximum thickness after the commencement of the process and then was thinned at a later time. That is attributed to the changes in pH and Al^{3+} ion (substrate metal ion) content of the treatment solution at the coating surface.

The effect of the TCC process immersion time on the electrochemical behaviour of an Al alloy (AA 2024-T351) was studied with the aid of EIS and Potentiodynamic polarization (PP) measurements in a 0.05 mol/L NaCl solution [115]. TCC solutions were prepared using four different immersion times of 300, 600, 900, or 1800s, followed by immersion in DI water (pH 5) at 40°C for 120s, drying in the cool air stream and ageing at ambient temperature for 24 h in air. The electrochemical measurements revealed that longer immersion time (900 and 1800s) resulted in reduced corrosion protection performances. This was ascribed to the increased number of defects in the structure of the coating, which were mainly formed near intermetallic particles. Therefore, the results implied that the best corrosion resistance was achieved with

the TCC layer produced in the solution for 300 and 600s. The coatings were thicker at longer immersion times, although cracks were observed because of internal stress.

Process temperature: Increasing temperature is not only uneconomical but also might make the passivating bath very unstable [120]. Considering Table 2.2, in most of the studies, the process was carried out at room temperature (25-30°C) due to the energy cost minimization; however, elevated temperatures like 40 and 60°C were also studied.

Water immersion post-treatment: To study the effect of water immersion post-treatment temperature, after a TCC treatment solution was applied to an Al alloy (AA 2024-T351), the specimens were immersed in DI water (pH 5) at either 20 or 40°C for 120s [115]. The results of EIS and PP revealed that an immersion post-treatment in DI water at 40°C for 120s, enhanced the corrosion protection properties of the TCC coatings compared to 20°C [91, 115, 121]. When the samples were not post-treated in the DI water, detachment from the metal substrate was observed. This was attributed to the low pH value and fluorine enrichment at the base of the film. Meanwhile, immersion of specimens in DI water at 20°C indicated an improved adhesion of the conversion coating and subsequently, an enhanced corrosion protection. On the other hand, the specimen that underwent immersion in DI water at 40°C exhibited a thicker film with no sign of localized corrosion. This was ascribed to the considerable reduction of fluorine-rich species and an increased amount of oxide/hydroxides at the base of the coating [121].

Bath impurities: It was shown that the presence of impurities, such as Zn and Fe, in the treatment solution applied to the Zn-plated steel degraded the quality of the formed layer [5]. Zinc impurities decreased the zinc redox dissolution and increased the formation of zinc hydroxide rather than chromium hydroxides in the conversion coating. Iron impurities intervened in the precipitation of chromium hydroxides as well [122]. Since the corrosion protection of the film is mainly supplied by Cr(III) compounds (hydroxide and oxide), the lowest possible amount of Zn and Fe in the passivating bath is preferable. Otherwise, a higher concentration of chromium in a contaminated passivating bath is needed, to compensate for the required corrosion protection.

Type of anions: Wen et al. [106] studied the effect of three different anions in TCC treatment solutions applied to Zn-plated steel. The electrolytes were prepared using Cr(III) sulfate, nitrate, and chloride. The Cr(III) concentration was set to be 0.1 M and the concentration ratio of Cr(III) to the various anions was adjusted to be 1/3. The TCC treatment solutions were heated and stirred at 80° for 4 hours, the pH was adjusted to 2, and finally stored for 24 hours before usage. Open circuit potential (OCP) measurements were employed to assess the potential change as the immersion proceeded. The OCP curves (Figure 2.4) showed that the formation potential (ΔE) of the zinc-plated steel immersed in the TCC treatment solution was the highest for the bath prepared with nitrate, followed first by that of chloride, and then finally that of sulfate. A layer with large voids was observed in the SEM micrographs taken from the layer formed in the chloride-containing bath; this layer also underwent pitting corrosion. With the aid of SEM micrographs and OCP measurements, it was proposed that the sulfate, nitrate, and chloride ions potentially performed as passivating, oxidizing, and pitting agents, respectively. Hence, the morphologies and characteristics of TCC coatings are clearly influenced by the anions in the passivating bath.

Bath additives: Corrosion performance of the TCC layers can be improved by adding transition metal ions into the TCC treatment solution [23, 118]. With the aid of EIS and anodic polarization measurements, it was shown that the addition of Co(II) or Ni(II) ions into a TCC bath, applied to the zinc-coated steel, enhanced the corrosion protection of the layers formed in these solutions [116]. The cathodic and anodic current densities in the polarization curves of the layer formed in the TCC coating with transition metal ions (Ni^{2+} or Co^{2+}) were reduced in comparison with the corresponding of the layer produced in a TCC bath without these ions. This was attributed to the decrease of oxidation- (zinc substrate dissolution) and reduction- (oxygen penetration to the zinc substrate) reactions. The results showed the effective barrier properties of these coatings.

Tomachuk et al. [25, 28] studied three different TCC coatings on Zn-plated steel. With the aid of EIS and polarization curve measurements, it was confirmed that the layer formed in the TCC treatment solution containing cobalt (SurTec S680) presented better barrier properties compared to the layers formed in the treatment

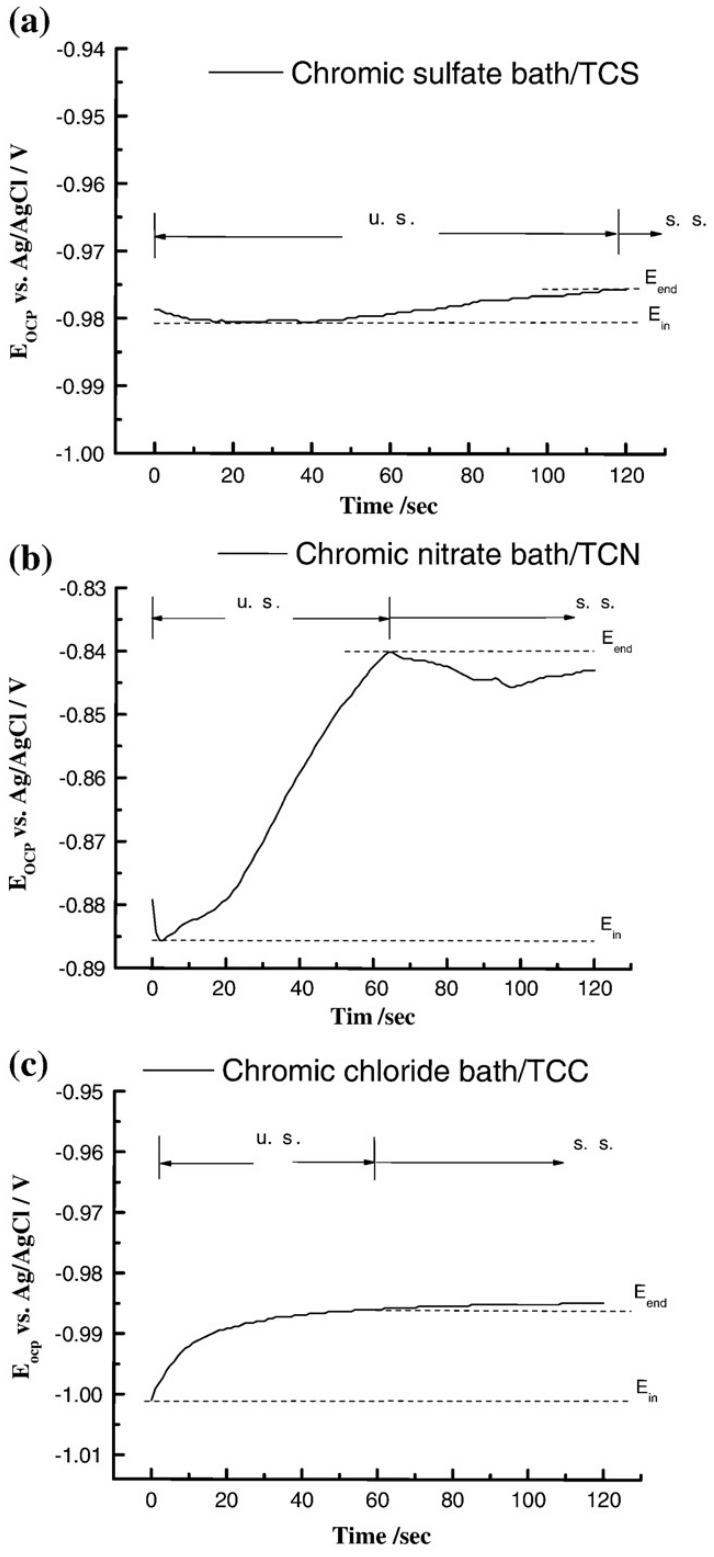

Figure 2.4 Open circuit potential vs immersion time of electro-galvanized steels immersed in the TCC treatment solutions containing (a) sulfate, (b) nitrate, and (c) chloride [106]

solutions without this ion [UNiFix Zn-3-50 (LABRITS) and UniYellow 3 (LABRITS)]. This was ascribed to the efficient corrosion inhibitive influence of Co added to the passive layer.

Co(II) was also reported as a reaction mediator in TCC treatment solutions, which increases the oxidation rate of Cr^{3+} to Cr^{6+} [123]. Therefore, it was suggested that the presence of cobalt in the TCC bath that results in the formation of Cr(VI) compounds may generate an effect like self-healing [116]. This, however, causes a lot of controversy about TCC coatings as being compatible with the European directives. Therefore, further studies should concentrate on the formation of Cr(VI) species in TCC coatings. Despite some discussions [46, 47], no detectable Cr(VI) was found on the TCC treated surface on the Al alloy [40, 90, 124]. It was reported that Cr(VI) was either formed in the TCC coatings by immersing the Al alloy in the air-saturated TCC solutions [42] or exposing the TCC treated samples to humid air [45]. It was suggested that when Al alloy (AA2024-T3) was immersed in an air-saturated TCC solution, oxygen formed hydrogen peroxide (H_2O_2) which diffused to the copper intermetallic sites. Since H_2O_2 is a strong oxidant, it should be capable of oxidizing Cr(III) to Cr(VI) [42]. In the case of samples exposed to humid air, Cr(VI) was mostly found near intermetallic areas [45].

The addition of a reducing agent at a pH value of 3.8 to 4.0 was suggested as a bath modification to avoid oxidation of Cr(III) to Cr(VI) [117]. The same study showed that adding Fe(II) species to a TCC treatment solution can prevent the formation of Cr(VI) compounds in the TCC film on the Al alloy (AA 2024-T351). This was ascribed to the preferential Fe(II)/Fe(III) oxidation by H_2O_2, and consequently, less available H_2O_2 to oxidize Cr(III) species. Findings in another study [125], demonstrated that the addition of copper sulfate to a TCC treatment solution can decrease the formation of H_2O_2 and Cr(VI) species, as revealed by Ultraviolet-visible spectrophotometry (UV-VIS) measurements. This was attributed to favouring the four-electron oxygen reduction mechanism at Cu-rich regions. With the aim of preventing Cr(VI) formation in the TCC coatings, Ely et al. [44] studied the effect of a commercial post-treatment (so-called PACS) containing lanthanum ion applied to the Al surface treated with a commercial TCC treatment solution (so-called Socosurf PACS). A chemical analysis of the TCC coating disclosed the presence of

lanthanum and the absence of Cr(VI) (below the limit of detection) ($< 0.1\,\mu g\,cm^{-2}$). This was attributed to the penetration of the post-treatment solution through the microstructural defects of the TCC layer that possibly induced the accumulation of lanthanum and restricted the formation of Cr(VI) due to the lack of Cr(III) ions resources to react with H_2O_2.

The oxidation of Cr(III) to Cr(VI) in the TCC films causes a lot of controversy surrounding these coatings as being compatible with the European directives. Especially, because the number of studies regarding the formation of Cr(VI) in the TCC coating formed on the Zn substrate is very limited and therefore, this occurrence can be further investigated.

Agitation during the TCC process: Generally, agitation of the treatment solution during the process speeds up the reaction and provides a more uniform film formation. However, no systematic study was found on this topic.

TCC coating colour: Tomachuk et al. [82] studied three TCC coatings with different colours including the layer formed in UniFix Zn-3-50 (LABRITS) with blue colour; UniYellow 3 (LABRITS) with yellow colour; and SurTec S680 with green colour. The EIS measurements in agreement with the results of polarization curves showed that the green-coloured TCC coating represented the best corrosion resistance followed first by the yellow-coloured and then blue-coloured. The green-coloured coating was also reported as a uniform layer. In this study, the coating thickness was reported as the summation of the thickness of the Zn and TCC layer. The thinnest film was the green-coloured (10.4 µm) which also contained Co in its treatment solution (SurTec S680) followed by the blue-coloured (10.8 µm), and the yellow-coloured was the thickest film (11.2 µm).

Ageing of the films: CCCs have microstructural imperfections and hydrated channels. Through the ageing process, the barrier properties of CCCs are enhanced due to condensing the film and collapsing these channels [41]. Considering the fact that microstructural defects were also observed in TCC coatings, the changes in barrier properties of these films during the ageing process were studied [41]. The protection performances of a TCC layer, ageing in the atmosphere, were daily evaluated by EIS measurements. It was reported that 3-7 days ageing improved

the barrier properties of approximately 30% of the coated samples. In their second relevant research, Li et al. [126] studied the effects of ageing time and temperature on the corrosion properties of the TCC coating on an Al alloy (AA2024-T3). It was observed that when ageing was done overnight at elevated temperature ($\leqslant 100°C$), the TCC layer underwent dehydration and condensation, which induced a more defect-free aluminium oxide layer. Moreover, the coating lost water and became much more hydrophobic, which resulted in improved corrosion protection performances. Finally, it was concluded that the moderate ageing period at room temperature improved the charge transfer resistance (R_{ct}) by a factor of four, due to the formation of an aluminium oxide layer on the metal sites exposed to the film microstructural defects; associated with an increased TCC coating's hydrophobicity. On the other hand, ageing at a higher temperature (150°C) resulted in excessive dehydration of the TCC layer, severe cracking, and detachment from the metal substrate.

Pretreatment process: To evaluate the importance of a pretreatment process (de-smutting [4]), anodic polarization test was done for an as-received control Al alloy (AA2024-T3), a TCC coated and a de-smutted AA2024-T3 in dilute Harrison's solution [5]. The results revealed that the breakdown potential of the TCC coated sample was 200 mV higher than the as-received control surface. Moreover, the cathodic polarization curves revealed that the TCC coating suppressed the oxygen reduction reaction on the Al surfaces. Besides, a non-coated sample that had been de-smutted also showed a protective behaviour in comparison to the control surface. This implied that de-smutting was a crucial step for enhancing corrosion protection [39].

It was formerly mentioned that the structure of the coating and subsequently its corrosion behaviour is influenced by the substrate chemistry. Optimized process parameters (e.g. temperature, pH, and composition of a treatment solution) should be specified for each system individually. However, a treatment solution that is applicable to different surfaces might be profitable for industrial usage. Table 2.3

[4]Smut is a residue of the alloying elements that are not dissolved in the caustic bath and can redeposit onto the etched surface. De-smutting is the act of removing excess alloyed metals from the Al surface after etching. This process is mostly done using mineral inorganic acids, such as hydrochloric, sulphuric and nitric acids [127].

[5]Harrison's solution is a dilute solution of 0.05 wt% NaCl + 0.35 wt% $(NH_4)_2SO_4$, which is also used for corrosion measurement [39].

lists commercial TCC treatment solutions applied to different substrates. As can be seen, the treatment solutions are applied to the Mg, Zn and Zn alloy, and Al and Al alloy. When there are some TCC treatment solutions that can be applied to the Zn and Zn alloys (e.g. Lanthane TR-175), there are also some TCC solutions that are applied to the specific type of surface (e.g. Finidip 124 for the Zn surface).

In summary, the TCC coating properties (e.g. coating structure, thickness, composition, and corrosion resistance) are greatly influenced by the TCC bath parameters (e.g. pH, temperature, composition), pretreatment, and post-treatment. However, the number of studies accomplished on each of the above-mentioned parameters is limited, especially when it comes to the TCC treatment on the Zn substrate.

RQ5: What kinds of methods have been used to study the TCC layers?

The morphology of the film has been primarily observed with SEM, TEM, and AFM. To study the chemical composition of a TCC film, spectroscopic methods like X-ray photoelectron spectroscopy (XPS), AES, Raman spectroscopy (RS), and Glow discharge optical emission spectroscopy (GDOES) were used. Analytical methods such as Inductively coupled plasma atomic emission spectroscopy (ICP-AES), Atomic absorption (AA), ICP-OES, titration, and UV-VIS were also employed to assess the chemical composition of the treatment solution or the leached TCC-treated specimen in diluted acids.

Table 2.4 shows the characterization methods which were used to study the TCC coatings. As can be seen, SEM is the method which was used the most to study the structure of the TCC film, followed by TEM and AFM. This table also indicates that XPS and afterwards RS were employed more often to study the chemical composition of the TCC layers. In many studies, several approaches were carried out to assess the physical or chemical characterization of the layer, to confirm the consistency of the results.

Apart from the methods in Table 2.4; spectroscopic ellipsometry [112, 113], Scanning Kelvin probe (SKP) maps [129, 130], and OCP vs immersion time were also used to study the deposition mechanism of TCC films [36, 41]. However, OCP was also used prior to PP or EIS measurements to reach a pseudo-equilibrium with the test solution [87, 131]. Fourier transform infrared reflection absorption spec-

Table 2.3 Commercial TCC coatings applicable to different substrates (The data were taken from the vendors' websites)

Cr(III)-based passivation product	Vendor	Application	Remarks
Iridite NCP, EXP, NR4-T NR2-I, 14-2.	MacDermid Enthone	Al	
Iridite 15		Mg, Mg alloy	
Tripass Tripass ELV (Co-free)		Zn, Zn alloy	
Perma Pass Passivates		Zn, Zn alloy	
Alodine T5900 Bonderite T5900	Henkel	Al, Ti, Mg	
T5900 RTU Alodine 871 Touch-N-Prep Alodine 1200S 5700		Al, Ti, Mg	
Aluminescent Tri-blue	Luster-On	Al, Mg	
Tri-descent Tri-black TZT		Zn, Zn alloy	
TCP-HF	Chemeon *	Al, anodize steel	*Formerly Metalast
Ecotri family	Atotech	Zn, Zn alloy	
Tridur		Zn, Zn/Ni alloy	
Rodip ZnX		Zn, Zn alloy	
Interlox 338		Al pretreat	
ChromitAl TCP (NAVAIR TCP licensee) SurTec 650 chromitAL	SurTec	Al	
SurTec 680/Chromiting		Zn and Zn alloys	Thick layer
SurTech 668		Zn	Blue
SurTech 675		Zn and Zn/Ni	Co-free
SurTech 662		Zn and Zn alloys	Co-free, blue
SurTech 684		Zn and Zn/Fe	Low temperature, thick layer
Finidip 124	Coventya	Zn	
Finidip 128 128.6 CF, 728.2 728.3		Zn-Ni (12-15%)	
Finidip 137 CF		Zn	
Finidip Silver Zn-Ni		Zn-Ni (12-15%)	
Lanthane black 760 CF Si 360 CF		Zn	
Lanthane TR-175		Zn, Zn alloy	

Table 2.4 Characterization methods used to study the TCC coatings (X sign shows the employed technique in the referred article)

		Structural characterization								
No.	**Article**	**Chemical**						**Physical**		
		XPS	**AES**	**ICP**	**RS**	**GDOES**	**EDXS**	**SEM**	**AFM**	**TEM**
1	[27]	X						X		
2	[15]									
3	[80]							X		
4	[47]									
5	[28]						X	X		
6	[39]	X			X					
7	[118]	X						X		
8	[106]	X						X		
9	[35]					X			X	X
10	[90]	X						X		X
11	[41]	X			X				X	
12	[107]							X		
13	[43]	X		X	X		X	X		
14	[42]				X		X	X		
15	[105]		X					X		
16	[116]							X		
17	[113]	X	X							
18	[91]	X								X
19	[117]				X			X		
20	[25]						X	X		
21	[82]							X		
22	[128]						X	X		
23	[38]	X		X						
24	[86]						X			
25	[44]	X						X		
26	[104]	X						X		
27	[114]	X								
28	[92]				X			X		X
29	[115]						X	X		
30	[121]						X			X
31	[122]				X					
32	[94]						X	X		

troscopy (FT-IRAS) [129], Rutherford backscattering spectroscopy (RBS) [33] were also used for compositional analysis. Time-of-flight secondary ion mass spectrometry (TOF-SIMS) is another surface-sensitive analytical method which was employed to analyse the surface chemical composition of the TCC coating [36, 44].

To study the corrosion behaviour of TCC coatings, especially in scientific research, electrochemical measurements were used first and foremost. However, in technical reports and patents, the most common corrosion test is the NSS test per ASTM B117 [48]. The electrochemical methods such as PP curves and EIS provide fast information about the kinetics of corrosion reactions. Moreover, electrochemical techniques are very practical to compare and characterize the corrosion resistance of different conversion coatings [82]. Most of the electrochemical measurements were performed at room temperature in naturally aerated NaCl (e.g. 0.05 mol/L), or Na_2SO_4 (e.g. 0.1 mol/L, 0.5 mol/L).

Table 2.5 summarizes the methods used to monitor the corrosion behaviour of the TCC layers in different papers. As can be seen, EIS was used intensively to study the corrosion properties of the TCC coated layer followed by PP and OCP.

Some examples of the methods which were used to investigate the physical and chemical characterizations of TCC layers are illustrated in the following; for instance, with the aid of EIS data, the equivalent electrical circuit model explaining the corrosion resistance of a system containing steel, zinc, conversion layer, and 0.5 mol/L Na_2SO_4 solution was provided [103].

The formation of the TCC coating on a deoxidized (unpolished) Al alloy (AA2024) was studied using OCP as a function of the TCC process immersion time [41]. In this study, the OCP during 10min of a TCC process was recorded for a sample immersed in 100 vol% full-strength Alodine T5900 solution (100% Trivalent chromium process (TCP) in figure 2.5); and another in a 50 vol% diluted of the same solution in DI water (50% TCP in Figure 2.5). Figure 2.5 shows that the OCP profiles measured for two passivation baths were similar in shape and magnitude. The cathodic shift within the first 50-75s of the OCP from -0.50 to -0.95 V vs Ag/AgCl, indicated that the treatment solution was aggressive towards the substrate. The dissolution was facilitated by the fluoride ions in the solution. As was also mentioned in another

Table 2.5 Corrosion tests used to study the TCC coatings (X sign shows the employed technique in the referred article)

		Corrosion Test			
No.	**Paper**	**NSS**	**Electrochemical measurements**		
			PP	**EIS**	**OCP**
1	[27]		X	X	
2	[15]	X			
3	[47]	X			
4	[28]		X	X	
5	[39]				
6	[80]	X		X	
7	[76]			X	
8	[118]		X	X	
9	[106]			X	X
10	[35]			X	
11	[90]		X		
12	[87]		X	X	X
13	[41]		X	X	X
14	[107]			X	
15	[82]		X	X	
16	[105]		X	X	X
17	[116]		X	X	X
18	[103]			X	
19	[117]			X	
20	[126]			X	
21	[25]		X	X	
22	[128]		X	X	
23	[38]			X	
24	[86]			X	
25	[44]		X		X
26	[93]			X	X
27	[92]				X
28	[115]		X	X	X
29	[121]			X	
30	[122]		X	X	X
31	[94]		X	X	X

study [36], the first step in the formation of the TCC coating was the dissolution of the oxide film to expose bare aluminium. It was supposed that in comparison with the 50 vol% diluted treatment solution, the 100 vol% full-strength of that produced a thinner oxide surface due to being enriched with fluoride ions. Afterwards, the OCP reached a minimum (-0.95 V vs Ag/AgCl) before a slight positive increase (to -0.90 V) during 100-200s. Thereafter, the potential stabilized at this value for the remaining immersion time. A slower cathodic shift in the OCP result was observed for the thicker oxide surface compared to the thinner oxide. Nevertheless, the ultimate OCP values for the thinner and thicker oxide surface were the same.

Hence, the processes that occurred in the three above-mentioned periods corresponded to the surface activation, conversion, and precipitation, respectively [132, 133].

The evolution of the OCP in a Zr-based conversion bath for AA 6014, cold-rolled steel and hot-dip galvanized steel (Figure 2.6) was shown that the decrease in potential from the initial to the minimum value depends on the type of substrate used [133]. This can be attributed to the fact that the chemical dissolution is influenced by the surface chemistry of the metal oxides [134] besides the thickness of the oxide layers [133]. Therefore, depending on variations of ionic and electronic conductivities of metal oxides with the type of substrate used, this drop (between the initial to the minimum value) occurs at different potentials.

In another study, the OCP development of a pure Al substrate in a 20 vol% diluted TCC solution (SurTec 650) was studied. This solution consisted of Cr sulfate plus potassium fluorozirconate (K_2ZrF_6), and adjusted to pH 3.8 with KOH/DI water. The OCP transient (Figure 2.7) decreased with time and stabilized after around 600s at approximately -1.4 V [112]. As was suggested before [36, 41], an initial sharp decrease of the OCP was attributed to the dissolution of the oxide layer due to the hydrofluoric acid attack. Furthermore, it is reported that the OCP transient resulting from the formation of the TCC coating took a longer time to reach the stable potential in comparison to the one from the CCC. Hence, the chemistry of both the Al surface and the treatment solution throughout the TCC process were not changed as fast as it would be for the CCC process. This was assigned to the lack of a strong oxidizing agent, such as Cr(VI), in the TCC treatment solution.

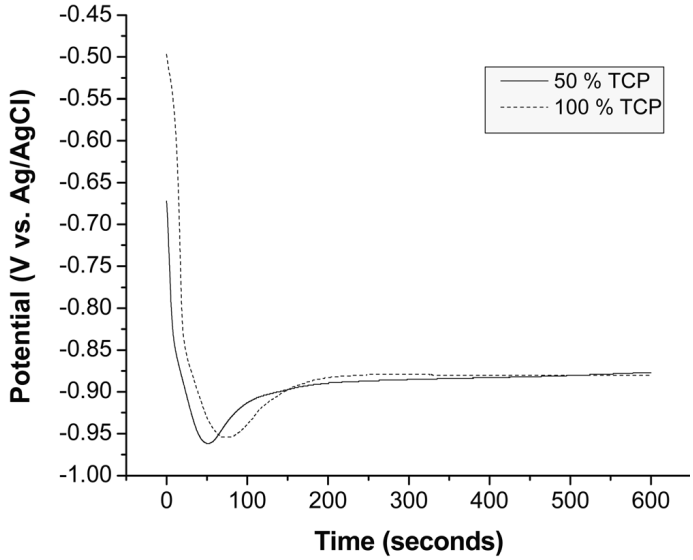

Figure 2.5 Transients of the OCP vs immersion time recorded during the formation of the TCC coating on the Al alloy (AA2024). Two different strengths of the Alodine 5900 RTU solution were used: full strength (100%) and diluted (50%). Coatings were formed at room temperature (20–25°C) [41]

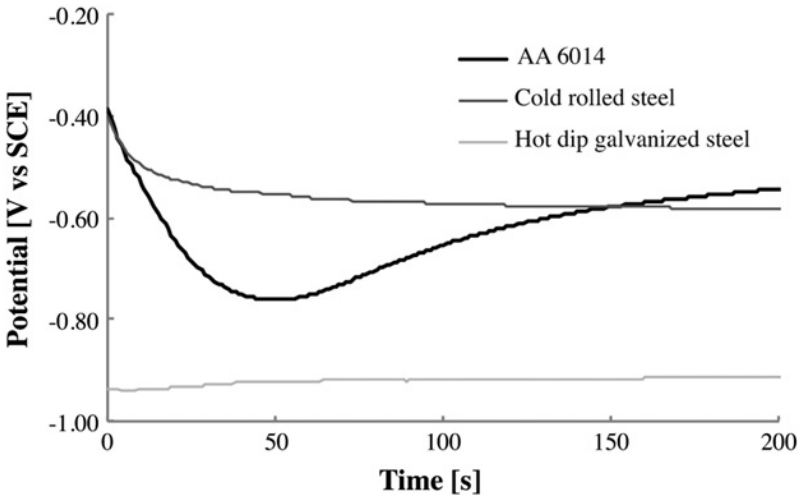

Figure 2.6 Transients of the OCP vs immersion time recorded during the formation of the Zr-based conversion coating for three different substrates [41]

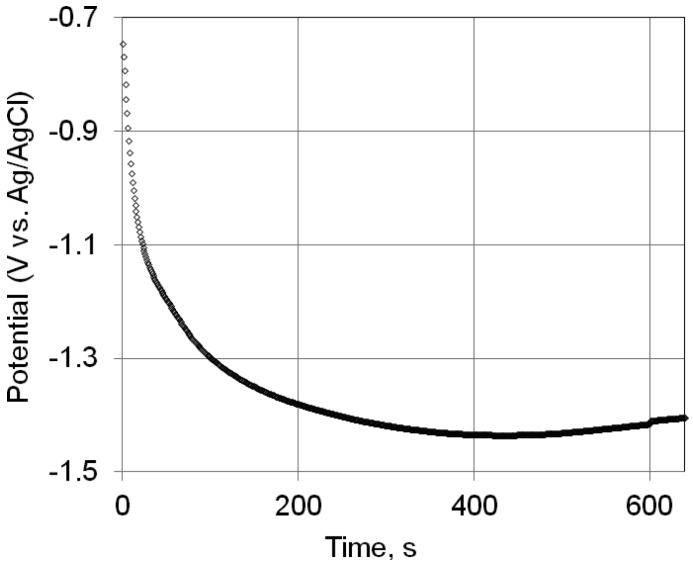

Figure 2.7 The OCP transient recorded for a pure Al substrate during the formation process of 20% TCC solution (SurTec 650 with pH 3.8) [112]

Spectroscopic ellipsometry is another effective characterization technique in which the thin film growth can be determined in real-time by employing light as a measurement probe [135].

Using in situ spectroscopic ellipsometry in the spectral region of 1.3–4.3 eV in real-time, the formation of the TCC film on the polished Al substrate was monitored in the research carried out by Dardona et al. [136]. The results obtained from in situ spectroscopic ellipsometry measurements evidenced three phases for the TCC film formation. The chemical thinning of the native oxide layer was introduced as an indispensable stage for the initiation of the TCC film growth, which lasted around 100s. This step was followed first by a linear TCC film growth at a constant rate of 0.4 nm s^{-1} up to around 50 nm thickness, and then a growth period to a final thickness of 125 nm at 880s [136].

In their second relevant study, in order to optimize the coating protection characteristics, Dardona et al. [112] investigated the role of applied potentials on the TCC growth kinetics and its composition, using in situ spectroscopic ellipsometry together with electrochemical measurements. The TCC treatment solution was 20 vol% SurTec 650 which was applied to a polished Al substrate at applied sample

potentials in real-time. To adjust the rates of cathodic and anodic reactions (the film formation kinetics), the electrode polarization was tested [112].

The current and the TCC film thickness development at different anodic (more noble potential) and cathodic polarizations (more active potential) from -1.0 to -1.6 V are shown in Figure 2.8. Under anodic polarizations (-1.0 and -1.3 V), the film formation showed three phases illustrated in Figure 2.8b. First, an initial induction stage indicating negligible or very slow coating growth, followed by first a prompt linear growth, and then a slower film growth. Conversely, under cathodic polarization (-1.5 and -1.6 V) the film formation started relatively slow at the intermediate stage, and afterwards a swift growth is observed. Therefore, it was proven that the sample polarization affects the formation kinetics and chemical composition of the TCC coating. In the end, it was suggested that the TCC films, which are formed using potential control, might provide a variety of conversion coatings with improved corrosion protection.

Neutron reflectivity (NR) is a powerful technique for studying inhomogeneities in either composition, structure or magnetization across an interface [137]. In situ NR was suggested as a useful tool to provide information about chemistry and structure of the interface between the substrate and the TCC treatment solution [138].

Dong et al. [36] used NR to determine the structure and composition of the TCC films on the Al alloy AA-2024. The treatment solution was an industrial product (METALAST TCP-HF with pH 3.75). In this work, the Electro-assisted (EA) deposition method was compared with conventional immersion deposition. In the EA method, proton reduction was controlled electrochemically. In other words, the consumption of hydrogen ions was controlled by the applied potential. Consequently, the film deposition was controllable and sustainable over a long period and the film thickness depended on the time under cathodic polarization. It was shown that the EA deposition produced a denser film with a more uniform film structure compared to the immersion deposition. Additionally, the Al substrate and additives in the precursor solution did not contaminate the film.

In their next relevant research, Dong et al. [138] used the electrochemistry measurement (OCP, PP) together with NR to monitor the corrosion process of the bare

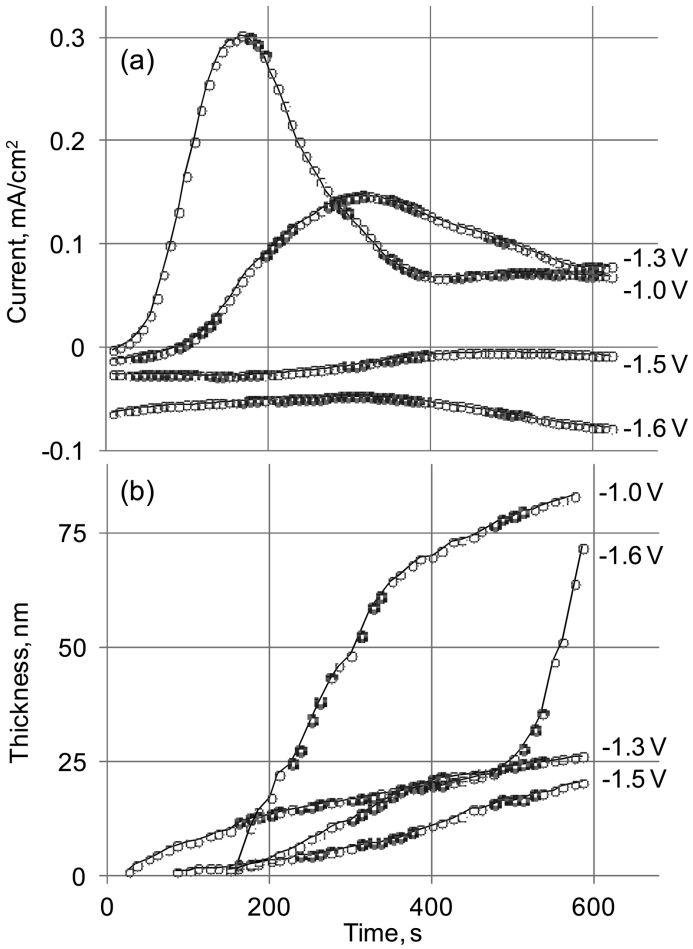

Figure 2.8 (a) Current development during a TCC process at applied sample potentials for pure Al substrate in 20% TCC treatment solution (SurTec 650, pH 3.8), (b) The corresponding TCC coating thickness as obtained from fitting of in situ ellipsometry data [112]

and the TCC coated Al alloy besides the morphology and structure of the TCC films in a chloride-containing aqueous solution. To observe the NR results of the corroding surface under potential control, a split cell that separated the anodic and cathodic reactions was used. A split cell clutching two Si wafer electrodes and a reference electrode was designed for this research. With the aid of this cell, two in situ corrosion experiments were performed on two different working electrodes. The original Al- coated wafer (ca. 1000 Angstroms of Al) was set as a control, and the TCC-coated Al on Si wafer was used to study the passivity of the film. During the test, the neutron beam interrogated the working electrode. A Si wafer was coated with a thin layer of gold to be used as the counter electrode. A chloride-containing aqueous environment was provided by injecting 1 wt% NaCl solution into the cell. The results revealed that the bare metal layer degraded uniformly under small anodic polarization over several hours. While the TCC-coated Al layer was stable and resistant up to an overpotential of +200 mV.

2.7 Conclusions

TCC coatings have been mostly compliant with the existing Registration, evaluation, authorisation, and restriction of chemicals (REACH) legislation while showing satisfactory corrosion performances on various substrates, including Zn/Zn alloys and Al/Al alloys. Therefore, to avoid the usage of carcinogenic chromate compounds, TCC coatings have been implemented by many industries as the most promising alternatives to CCCs, to date.

Not only are the TCC treatment solutions easy to apply but also they are uncomplicated in terms of wastewater treatment. The formed layer is resistant to elevated temperatures and may be produced in a variety of colours (Section 2.6). The TCC formation (e.g. the microstructure and composition of the formed layer) as well as its corrosion performance are influenced by various factors including the substrate material (Section 2.6); pretreatment processes (Section 2.6); formulation of the treatment solution (Section 2.6); process parameters (e.g. immersion time, pH, temperature, and agitation) (Section 2.6) as well as post-treatment (e.g. ageing at elevated temperatures) (Section 2.6). The optimal TCC process parameters (e.g. the

composition of the bath, immersion time, pH, temperature, and agitation) must be defined individually for each system. Therefore, novel formulations of TCC coatings are envisaged.

3 Material and Methods

3.1 Specimen preparation

3.1.1 Substrate preparation

Zinc plated (pre-galvanized) low carbon steel polished hull cell panels (10 x 7.5 cm^2) were supplied by Kiesow Dr. Brinkmann GmbH & Co. KG. The zinc film (that was used to protect the steel panels) was stripped off chemically by immersion in a 10 % diluted hydrochloric acid (HCl) solution (specific gravity 1.18 g/mL). Subsequently, the parts were immediately rinsed with DI water, to prevent further attacks of acid residue on the panels before commencing electroplating.

3.1.2 Zinc plating

The zinc layer was plated from a commercial alkaline zinc electrolyte, Protolux 3000 Atotech Deutschland GmbH. The panel was set up as the cathode of the cell whilst fully immersed inside the electrolyte and steel plates served as anodes (Figure 3.1). Direct current was applied to the cell by means of a power supply model HCS-3202 (1-36 V, 0-10 A) (Manson Engineering Industrial Ltd.). In order to deposit ∼8 µm of zinc on the steel panels, the electroplating was carried out with the current of 2 A/dm^2 for 30 minutes at room temperature (Table 3.1). To reduce hydrogen evolution on the substrate interface, the process was done with agitation via cathode movement. Without electrolyte agitation, the deposits will be streaked due to the marks caused by hydrogen. Once the treatment time was met the panels were removed from the electrolyte, rinsed with DI water and dried using hot air blower.

Evaluation of the deposition behaviour is done visually and through the distribution of the layer thickness by the aid of Energy-dispersive X-ray fluorescence (EDXRF).

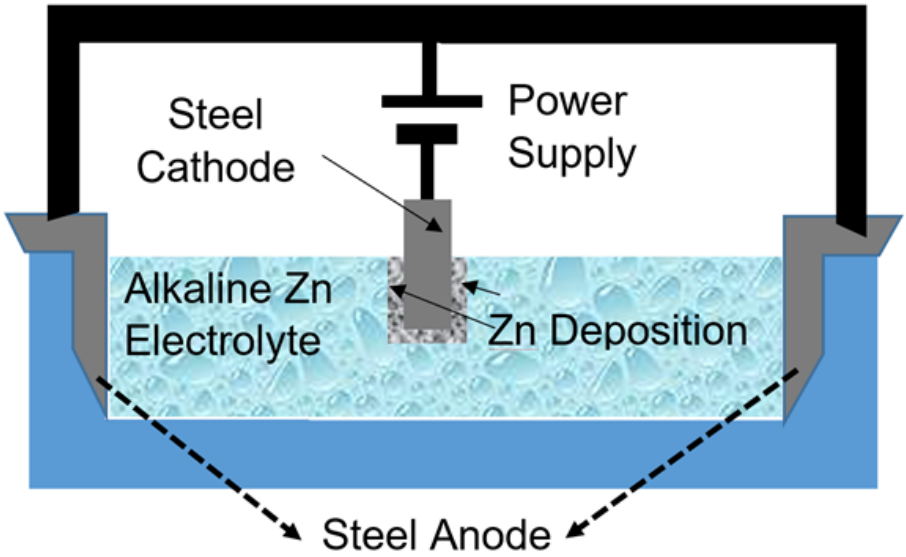

Figure 3.1 Schematic of the Zn electroplating bath

Table 3.1 Alkaline zinc electroplating operating parameters

Process parameters	**Values**
Temperature	24 °C (18 to 28 °C)
Current Density	2 A/dm^2
Current efficiency	60 %
Immersion time	30 min
Cathode Agitation	2 to 4 cm/s

3.1.3 Treatment solution

To apply the treatment solution, the panels were immediately rinsed after the electroplating process and dipped in 0.3 vol% HNO_3 to activate the surface prior to applying the TCC treatment solution. The zinc-plated steel sheets were passivated in different treatment solutions at 40°C. A matrix of eight different model solutions with two complexing agents including and excluding cobalt was prepared (Table 3.2).

Table 3.2 The composition and processing parameters of the model TCC treatment solutions

Number	**Specimen**
1	Cr + Ox
2	Cr + Ox + 1/2 Co
3	Cr + Ox + Co
4	Cr + F
5	Cr + F + 1/2 Co
6	Cr + F + Co
7	2Cr + 2Ox
8	2Cr + 2Ox + Co
Parameters	**Concentration(mol/L)**
Cr(III) (Higher concentration is shown as 2Cr)	0.08, 0.16
Co(II) (lower concentration is shown as 1/2 Co)	0.002, 0.004
Complexing agent	
Oxalic acid	0.1
Ammonium bifluoride	0.15
Processing parameters	
pH	1.8
Immersion time	40, 60, 80s
Working temperature	3, 18, 40°C

The same amount of chromium nitrate was used for all the first six TCC treatment solutions. The ratio of Cr to oxalate concentration in the electrolyte with this ion was 1 to 1.3. To study the effect of Cr concentration on the properties of the layers formed, a bath with double concentration of Cr and oxalate was prepared and named as the specimens 7 and 8 in Table 3.2. The cobalt-containing TCC solutions were prepared with two different concentrations of Co. All chemicals were reagent grade and were obtained from Carl Roth GmbH + Co KG. The immersion time and process temperature applied for the morphology studies, compositional analysis, and corrosion tests were 60s and 40°C, respectively. To study the kinetics of the process, other immersion times, 40 and 80s, as well as more passivation bath temperatures, 3°C, and 18°C were also applied. Agitation was performed by manual shaking during immersion time. Afterwards, the samples were rinsed with DI water and dried in an oven for 15 minutes at 80°C. The samples were then left to stabilize at room temperature for a minimum of 24 hours in accordance with the American society for testing and materials (ASTM) B201 standard [139]. To study the annealing effect on the coatings, some specimens were heated in a forced convection oven (MEMMERT oven (Memmert GmbH + Co. KG)) for 6 hours at 210°C.

3.2 Experimental techniques

3.2.1 Morphology characterization

3.2.1.1 Focused ion beam scanning electron microscope

Focused ion beam scanning electron microscopy FIB-SEM combines two beams (electron and ion) in one single apparatus, which leads to an instrument that combines all the capabilities of Focused ion beam (FIB) with SEM [140, 141]. This method operates by employing a gallium (Ga) FIB column and a field emission SEM column. Impinging low Ga^+ beam current produces secondary electrons emitted from the sample surface. To sputter or mill the sample, a higher current beam is typically used. Moreover, the ion milling process can be observed and controlled with SEM

during the analysis. Figure 3.2 (a) shows a typical FIB-SEM column configuration with a vertical electron column with a 54° tilted ion column to the vertical.

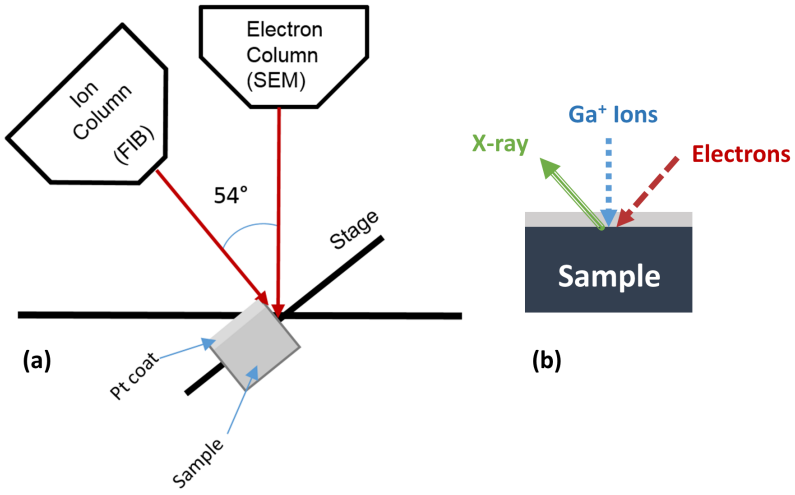

Figure 3.2 Simplified schematic diagram of (a) a typical focused ion beam combined with a scanning electron microscope, (b) a dual-beam FIB-SEM configuration with energy-dispersive X-ray spectroscopy

The cross-sectional structure of the formed TCC layer was observed via cryo-sample preparation in conjunction with FIB-SEM. The thickness of the films was also measured using the cross-sectional micrograph. Specimens were initially immersed in liquid nitrogen (-200°C) for 1 minute and immediately bent. This process caused the conversion coating to crack and facilitated the observation of film thickness. Since the coatings were not conductive, the samples were then transferred to a Gatan 682 Precision Etching and Coating System (PECS), where the surface of the specimens was sputtered with a ∼40 nm thick tungsten film to improve their surface conductivity. Following that, the sample was transferred to the SEM device for imaging. A Zeiss Auriga 60 (Carl Zeiss, Germany) Dual Beam FIB-scanning electron microscope (SEM) system with a Ga ion beam at 30 kV and 50 pA current were used to analyse the cross-sectional FIB-SEM of the specimens. Prior to ion milling, to protect the coating from any damage caused by the ion beam, a 500 nm thick platinum layer was deposited onto the area of interest. The cross-section milling was performed at a tilt angle of 54° for all the samples.

Energy-dispersive X-ray spectroscopy is a chemical microanalysis technique used in conjunction with SEM. In this method, the X-ray spectrum emitted by a solid

sample during bombardment with a focused beam of electrons is detected (Figure 3.2 (b)) [142]. The information collected comes from the depth probed which is dependent primarily on the energy of the electron beam, and on the material being probed [143].

To detect the chemical composition of the Zn surface, the FIB-SEM associated with EDXS was used. However, due to the relatively high sampling depth of EDXS (∼1 µm) to detect the elemental composition of TCC layers, other techniques such as AES and ICP-OES were employed.

3.2.1.2 Atomic force microscopy

AFM is a technique by which the shape of a surface can be seen in three dimensional (3D) detail down to the nanometre scale [144]. AFM does not form an image by focusing light or electrons onto a surface, as an optical or electron microscope does. As is shown in Figure 3.3, this method works by scanning near an atomically sharp probe over the sample surface, employing the forces and energy dissipated between the probe tip and the specimen surface to build up a map of the height or topography of the surface as it goes along [145]. AFM has the advantages of being operated in air, liquids, and at room temperature and pressure, besides being able to analyse a wide range of materials such as conductive and non-conductive [144, 145]. In this work, the non-conducting surface of the formed TCC layers was observed using AFM. Surface roughness values were also obtained from the topographical data obtained from AFM using a Dimension Icon AFM from Bruker Corporation. Mapping was performed in PeakForce tapping mode using Bruker ScanAsyst-Air HPI probes, with a tip radii ∼2 nm, silicon nitride cantilever, and 0.25 N/m spring constant. All images were obtained with a scan rate of 1.0 Hz. AFM images and mean roughness values were analysed quantitatively by means of NanoScope Analysis 1.5 Software (Bruker). Average roughness (R_a) is one of the most commonly used roughness statistics. Because it is a simple parameter to obtain, and it is defined as follows (Equ. 3.1) [146].

$$R_a = \frac{1}{L}\int_0^L |Z(x)|\,dx \tag{3.1}$$

Where Z(x) is the function that describes the surface profile analyzed in terms of height (Z) and position (x) of the sample over the evaluation length "L" (Figure 3.4). Thus, the R_a is the arithmetic mean of the absolute values of the height of the surface profile Z(x).

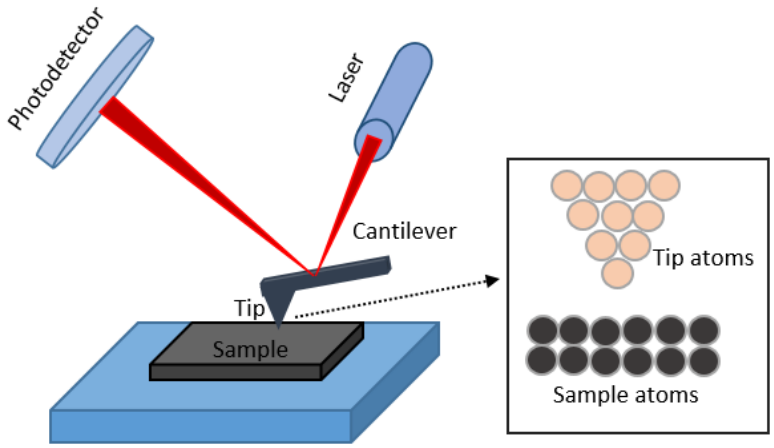

Figure 3.3 Simplified schematic diagram of a typical atomic force microscopy configuration

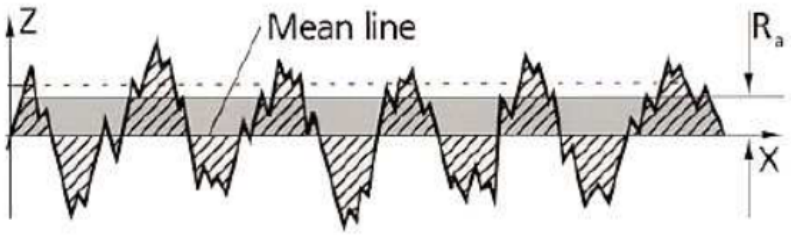

Figure 3.4 Profile of a surface (Z(x)). It represents the average roughness R_a, which is the RMS roughness based on the mean line [146]

3.2.2 Characterization and analytical techniques

3.2.2.1 Energy-dispersive X-ray fluorescence

EDXRF is used for elemental analysis applications. In this method, an X-ray tube emits a primary X-ray to the sample (Figure 3.5), which causes all of the elements in the sample to excite at the same time. Simultaneously, the fluorescence radiation emitted from the specimen is collected by an energy-dispersive detector in

combination with a multi-channel analyser. Afterwards, the detector organizes the received photons according to energy and counts the number of photons that relate to different energy levels. Therefore, the energy of the detected fluorescent X-ray is used to identify the elements in the sample. The concentration of the detected elements is reflected by the intensity of the X-ray [147].

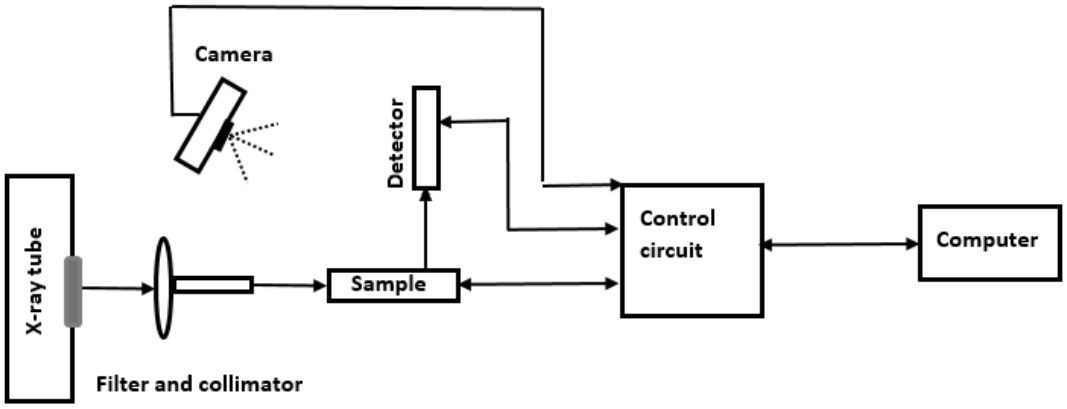

Figure 3.5 Simplified schematic diagram of a typical energy-dispersive X-ray fluorescence configuration

In this work, the amount of deposited chromium in the TCC layer was measured by EDXRF using a FISCHERSCOPE X-RAY XDV-SDD. The X-ray detector was equipped with a large silicon drift detector with an effective detector area of 50 mm^2. The micro-focus X-ray tube featured a 50 kV power supply, a tungsten target, a beryllium window, a collimator with 1 mm diameter, and an Al 100 µm filter. The measurements were done at different points of each sample with the aid of a programmable XY-stage and for a measurement time of the 30 s.

3.2.2.2 Inductively coupled plasma optical emission spectroscopy

ICP-OES is a powerful technique for the determination of elements in a sample. As is shown in Figure 3.6, with the aid of this tool, liquid samples are injected into a radio-frequency (RF)-induced argon plasma using a nebulizer. As soon as the sample

mist reaches the plasma, due to collisional excitation at high temperature, it is dried, vaporized and energized. The atomic emission emerging from the plasma is collected with a lens or mirror, observed in either an axial or radial configuration and imaged onto the entrance slit of a wavelength selection device. Single-element measurements can be done with a simple monochromator-photomultiplier tube combination, and simultaneous multi-element measurements are performed for up to 70 elements with the combination of a polychromator and an array detector [148].

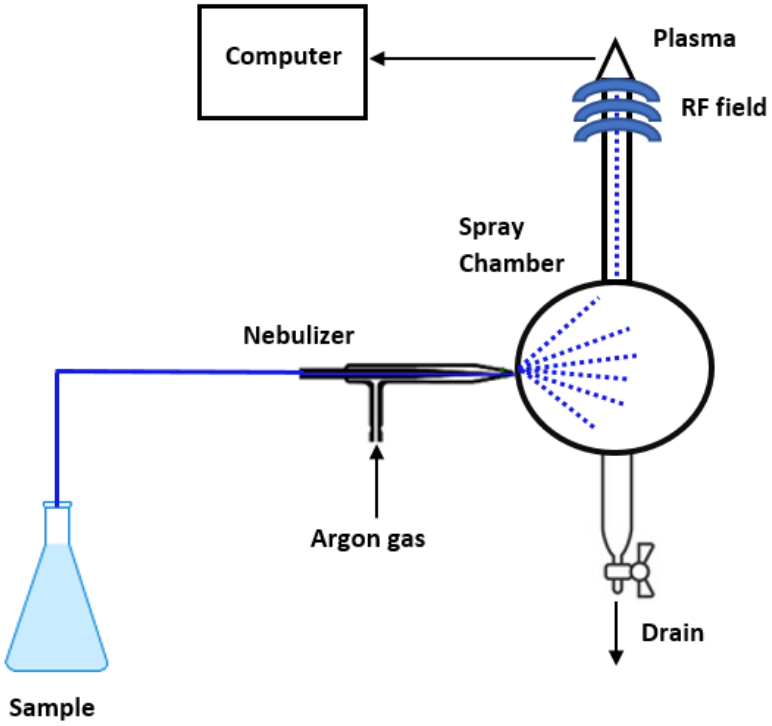

Figure 3.6 Simplified schematic diagram of a typical inductively coupled plasma optical emission spectroscopy configuration

In this work, the amount of dissolved chromium and cobalt obtained from the leached conversion coatings in 10 vol% HCl was evaluated employing a Spectroblue ICP-OES model FMX 36 using SPECTRO SMART ANALYSER software. The device is equipped with a SPECTRO UV-PLUS gas purification system. The optical chamber was filled with argon and hermetically sealed. To ensure the availability and stability of the gas flow, the argon atmosphere was circulated continuously by means of a membrane pump. The status of the optical system was monitored using SPECTRO's Intelligent Calibration Logic (ICAL). An air-cooled Inductively

coupled plasma (ICP)-generator was operated at 27.12 MHz ensuring the stability of the forward power. All experimental ICP operating parameters (Table 3.3) were controlled via software. The analytical curves were prepared separately for chromium and cobalt with five different standard solutions (0.02, 0.05, 0.1, 0.5, 1, 5 mg/L). The pH of the solutions was adjusted (pH 4-7) with analytical grade 1 vol% HNO_3. SRM NIST 1643e (Standard reference material National Institute of Standard and Technology) was utilized to perform the quality control of the method by using a 100 µg/L Cr(VI) intermediate solution. A volume of 100 µg/l yttrium solution was added to all standards, samples and blank tests as an internal standard.

Table 3.3 Instrumental and operating parameters for ICP-OES

ICP-OES parameter	Type or value
Spray chamber	Cyclonic
Nebulizer	See Spray
RF power	1450 W
Coolant gas flow rate (Ar)	13 L/min
Auxiliary gas flow rate (Ar)	0.8 L/min
Nebulization flow rate (Ar)	0.8 L/min
Wavelength for chromium	276.716 nm
Wavelength for cobalt	228.616 nm
Plasma torch	Quartz, demountable, 2.0 mm Injector tube
Sample aspiration rate	2 mL/min
Replicate read time	49s per replicate

3.2.2.3 Auger electron spectroscopy

AES is a widely used surface analytical technique by which the composition and chemical species present on a solid surface are determined [149]. This technique provides high sensitivity chemical analysis in the vicinity of 5 to 20 Å of the surface. The specimen is excited by an electron beam that can be focused into a fine probe. The depth from which the AES provides chemical information is typically less than 3 nm. However, elemental depth profiles to depths of up to a few micrometers can be measured, when the spectrometer is equipped with a source of ions with energy in the range of a few hundred electron volts to about 5 keV [150]. Inert gases (e.g.

Ar) are commonly used as ion sources. When the energetic ions strike the sample, a small amount of energy which is conveyed to the atoms on the surface, causes them to leave. In this destructive technique, the sample surface is eroded through ion sputtering and the analysis is repeated and continued for a known time with the interchanging of erosion and analysis until the required depth is reached. Under monitored conditions the layer removed can be calculated. The remaining surface is then analysed by AES which provides a depth distribution of present elements in the sample [151]. To measure the energy distribution of electrons emitted from the test sample surface, an electron spectrometer is required. A spectrometer includes an electron energy analyser and an electron detector as the output.

The principle of electron energy analyser is to measure the energy of the emitted Auger electrons. The Concentric hemispherical analyser (CHA) is one of the fundamental devices used for AES. A CHA contains three parts including a retarding and focusing input lens assembly, an inner and outer hemisphere, and an electron detector (Figure 3.7). The electrons emitted from the surface go through the input lens, where they are focused, and their energy is retarded for a better resolution. Afterwards, electrons enter the hemispheres through an entrance slit. The potential difference which is applied to the hemisphere aids the electrons with a small range of energy differences to reach the exit. In the end, electrons are analysed by an electron detector [152].

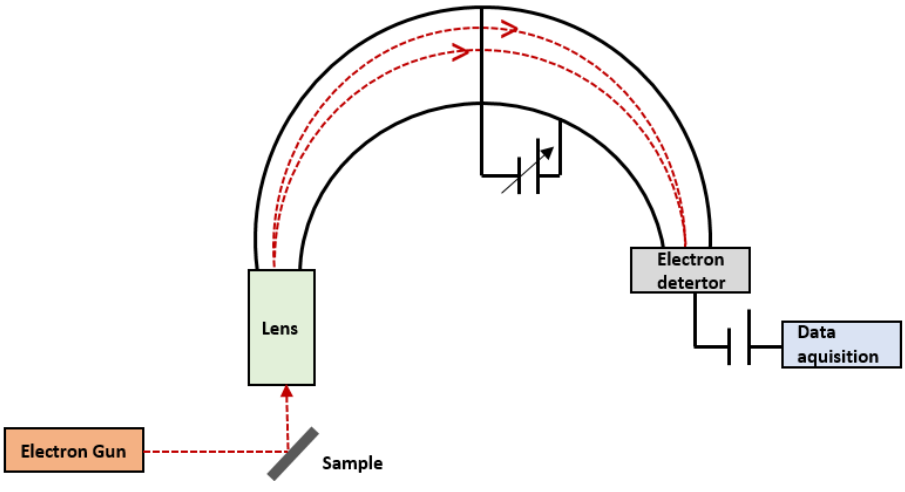

Figure 3.7 Simplified schematic of a concentric hemispherical analyser

AES depth profiling was performed to investigate the elemental composition profiles of the TCC layers using a Thermo VG Scientific Microlab 350 instrument with the Avantage processing software. The spectra were acquired at an accelerating voltage of 10 keV and a primary electron beam current of 14.1 nA. The beam diameter was approximately 30 nm with an incident angle of 60° with respect to the surface normal. The surface was scanned during the measurement over an area of 20 μm^2. The measurement was carried out by a CHA and a detection angle of 0°. The energy resolution of the detector was 0.25 %. The Auger spectra were detected with a step width of 0.7 eV and a dwell time of 200ms. Sputtering was carried out using a 1 keV Ar ion beam of approximately ∼700 nA over an area of 1x1 mm^2 and an incident angle of 43.4°. The base pressure in the analysis chamber was 10^{-9} mbar. The depth profiling was discontinued at the point in which the Zn signal reached a constant value (∼100 % zinc atomic concentration).

3.2.2.4 Coulometric Karl Fischer titration

Karl Fischer titration (KFT) is a well-established analytical method for the determination of water content in various types of samples [153]. The reactions, which take place during the titration of a water-containing sample, can be summarized as Reaction 3.2, in which RN represents a base. Iodine (I_2) reacts quantitatively with water according to this reaction and therefore, this chemical relation forms the basis of the water determination.

$$H_2O + I_2 + [RNH]SO_3CH_3 + 2RN \rightleftharpoons [RNH]SO_4CH_3 + 2\,[RNH]I \tag{3.2}$$

The Coulometric Karl Fischer titration (cKFT) is a version of the classical KFT in which the iodine is generated electrochemically at the anode. This is a much more rigorous technique for measuring water content in a specimen, which is based on a direct relationship between the passed electric charge and the produced amount of iodine [154].

To determine trace amounts of water in the layer, the experimental setup comprised of a cKFT and a vial with a septum cap, as a vaporiser (Figure 3.8). The total area size equal to 110 cm^2 was prepared for each sample. Samples were cut into pieces of (1 x 5 cm^2) to be fitted inside the vials that were connected from their septum cap through a nozzle and a pipe to the device. The accuracy of the coulometric Karl Fischer system was checked beforehand with a Hydranal water [1]. The evaporation of water in the samples was done at a temperature of 120°C. This temperature assures the reproducibility of realistic drying conditions of the electrode. A dry argon gas stream (with water fugacity (fH_2O) < 10 ppm) as a carrier gas moves water in the vial (water content of the sample) to the cKFT (831 KF Coulometer, Deutsche Metrohm GmbH & Co. KG). The transferred water was quantified using a fritless generator electrode. The flow rate of argon gas was kept constant at 100 ml/min by a mass flow controller. This measurement was done in two sequential steps. The samples in the vial with a septum cap were flushed with the dry argon stream at room temperature during the first step, and the amount of water left the samples was monitored by the cKFT. Afterwards, in order to facilitate the evaporation of more strongly bound water in the samples, the vial containing the samples was put in the evaporation unit where it was heated to 120°C. The duration of the second step was 15 min. To evaluate the raw data of the cKFT, water drift values, and blank values need to be taken into account. The water drift comes from water diffusion into the titrator setup and piping system. The drift value was constantly stable below 7 µg min^{-1} for all experiments before a measurement was started. The blank values originate from the water contained within the empty vial with a septum cap (sample containers). The water content of the empty glass vials was measured the same as the one with samples. For all measurements done with KFT for solids, drift and blank value corrections are self-evident.

3.2.2.5 Ultraviolet-visible spectrophotometry

UV-VIS is a quantitative analytical technique concerned with the absorption of near-ultraviolet (180–390 nm) or visible (390–780 nm) radiation by chemical species in

[1] "Hydranal - Water Standard 0.1" of Fluka Analytical,Fluka, lot#SZBG0290V, Standard for Karl Fischer titration with water content 0.1 ± 0.005 mg g^{-1}

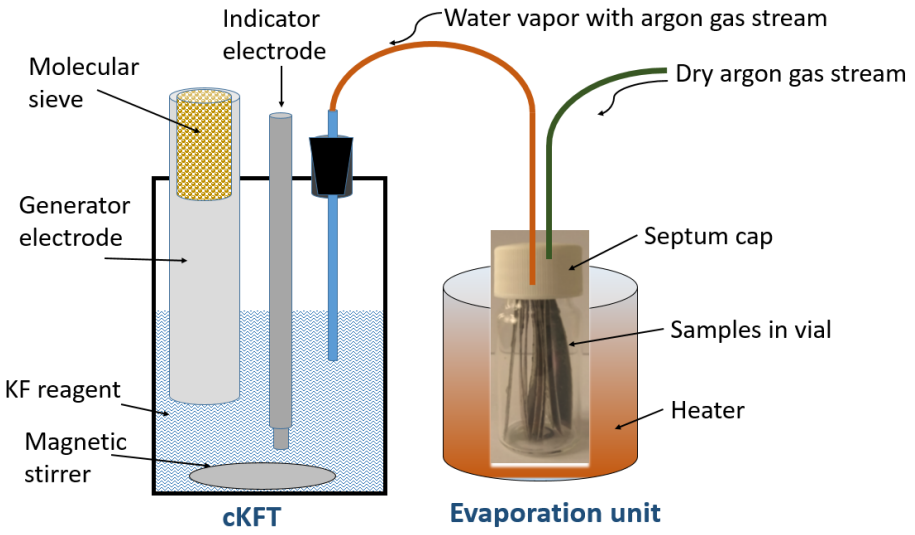

Figure 3.8 Schematic of the experimental setup of the coulometric Karl Fischer titrator

solution or in the gas phase [155]. This technique relies on a sample containing species that absorb light in the near-ultraviolet and the visible parts of the electromagnetic spectrum, whereby, the energy that gives rise to electronic transitions is provided [155, 156]. This technique can be developed to non-absorbing analytes by exploiting a selective reaction of the analyte with an appropriate reagent to form an absorbing chemical species [155]. The various colours of visible light and the complementary colours of solutions are absorbed at particular wavelengths that are shown in the literature [155]. When experimental conditions are controlled, the amount of radiation absorbed is directly related to the concentration of the analyte in solution. This relationship is known as Beer-Lambert law. According to that (Equation 3.3) the absorbance is proportional to the concentration of the substance in solution. Therefore, UV-VIS can also be used to measure the concentration of a sample [157].

$$\log(\frac{I_0}{I}) = \log(\frac{100}{T(\%)}) \equiv A = \epsilon.c.d \tag{3.3}$$

where
$A = \log(\frac{I_0}{I})$ is the absorbance, I_0 is the intensity of the incident light, and I is the intensity of the transmitted light,
$T = \frac{I}{I_0} \cdot 100$ in % is the transmittance,
ϵ is the molar extinction, which is constant for a particular substance at a particular

wavelength
c is concentration of the sample (mol/L)
d is the path lenght (cm)

When the absorbance of a series of known concentrations of sample solutions are measured and plotted versus their corresponding concentrations, the produced graph of absorbance against concentration is linear if the Beer-Lambert law is obeyed.

Many ionic and covalent compounds of transition metals are coloured. As light passes through a material, it absorbs some of the wavelengths induced by electronic excitation [158].

In this work, the concentration of hexavalent chromium was analysed by means of a SPEKOL 11 spectrophotometer (Carl Zeiss Jena, Germany). The method is based on the colorimetric determination of the Cr(VI) content. Dissolved hexavalent chromium is reacted with 1,5-diphenylcarbazide dye in acidic conditions (pH level 4-7). As a result Cr(VI) is reduced to Cr (III), and 1,5-diphenylcarbazide ($C_{13}H_{14}N_4O$) is oxidised to 1,5-diphenylcarbazone ($C_{13}H_{12}N_4O$) (Reaction 3.4). The obtained complex has a magenta (reddish-purple) colour [159].

$$2\,{CrO_4}^{2-} + 3\,C_{13}H_{14}N_4O + 8\,H^+ \longrightarrow [{Cr}^{3+}(C_{13}H_{12}N_4O)2]^+ \qquad (3.4)$$

According to the literature [155], when the colour observed is violet, the wavelength is 520–550 nm, and the absorbed colour is yellow-green. The optimal wavelength to measure this absorbance is 540 nm and the molar absorptivity is 3.14×10^4 [160]. Therefore, the absorbance of the obtained solution was measured at a wavelength of 540 nm with the blank as a reference in a cuvette with a path length of 5 cm.

3.2.2.6 X-ray diffraction

XRD is a non-destructive method capable of characterizing crystalline materials. It gives information on structures, phases, preferred crystal orientations (texture), and other structural parameters, such as average grain size, crystallinity, strain,

and crystal defects [161]. In order to study the structure of the TCC coating, an X-ray diffractometer Bruker AXS D 5000 operating with Cu-Kα radiation and Bragg Brentano geometry was used to analyse a sample area of 1 cm^2. The XRD pattern was recorded with a step size of 0.02° for 2θ ranging from 20 to 100° and a measuring time of 1.4s per step.

3.2.3 Corrosion characterization

3.2.3.1 Neutral salt spray corrosion test

NSS is one of the most widely used accelerated tests for evaluating the corrosion resistance of coatings on metals [162, 163]. The aim of this accelerated test is to evaluate the relative corrosion resistance of samples in a corrosive environment that try to mimic severely corrosive conditions. Test specimens are placed in an enclosed chamber and exposed to a continuous indirect spray of sodium chloride-based fogs with a pH range between 6.5 and 7.2. The spray of salt water solution falls out on to the specimens at a rate of 1.0 to 2.0 ml/80 cm_2/hour, in a chamber temperature of +35°C. The cabinet climate is maintained under constant steady state conditions. The test duration varies typically between 8 to 3000 hours. The test for X hours is not an indicator of any number of years that coating will resist corrosion. This standard corrosion test follows standardized protocols including ASTM B117 [48] and DIN 50021 [164] for conducting the test and evaluating the results. The above-mentioned standards have been accepted by the automotive industry [165]. Thus, although there is not enough evidence to prove that this test generates consistent reproducible results, NSS test has been used continuously.

The NSS test was conducted in this work not only to evaluate the corrosion resistance of TCC coating (Section 6.1), but also to determine the formation of Cr(VI), when TCC coatings are kept in the NSS chamber for 24 hours (Section 7.3.2).

3.2.3.2 Potentiodynamic polarization curves and electrochemical impedance spectroscopy

The corrosion protection of TCC films was assessed by potentiodynamic polarization and electrochemical impedance spectroscopy. The measurements were done with a BioLogic SP-150 potentiostat, using the commercial software package EC-LAB (version 10.32). The tests were carried out in a three-electrode corrosion flat cell kit from Biologic with a contact surface area of 1 cm^2. The potential of the working electrode was measured against a Saturated calomel electrode (SCE) (+241 mV vs Standard hydrogen electrode (SHE)), and a platinum mesh was used as the auxiliary electrode. The reference electrode was fixed as near as possible ($\sim$ 5 mm) to the working electrode to minimize the IR drop. The potentiodynamic polarization experiments were performed in a naturally aerated 3.5 wt% NaCl aqueous solution at a controlled temperature of ($\sim 40°C$) and pH around 6 (very similar to the environment of a NSS chamber). To allow the working electrode to reach a steady-state, the OCP was monitored for 30 minutes (until stable) after immersion of the working electrode in the corrosion cell and prior to the beginning of each test. The potentiodynamic polarization with a scan rate of 0.167 mV/s was performed from a cathodic potential of – 250 mV to 250 mV with respect to the OCP.

To perform the EIS analysis, the following procedures were performed: (i) 30 min OCP measurement; (ii) EIS measurement with a sinusoidal 10 mV voltage perturbation with frequencies ranging from 10^5 to 10^{-2} Hz at the OCP level. The EIS experiments as well were performed in a naturally aerated 3.5 wt% NaCl aqueous solution at a controlled temperature of ($\sim 40°C$) and pH around 6. Despite the fact that for the NSS test 5 wt% NaCl is used, a lower concentrated NaCl solution was used for electrochemical tests to reduces the degradation processes kinetics and to better understand the electrochemical behaviour of TCC layers [68]. Impedance spectra were modelled using an equivalent circuit analysis and complex non-linear least-squares fitting of the data to a suitable equivalent circuit. All tests were repeated ten times for each sample to test reproducibility.

3.2.4 Surface characterization

3.2.4.1 Contact angle

To measure the wettability of a surface, the water contact angle technique is commonly used. This method provides information about hydrophobicity or hydrophilicity of a solid surface which plays a crucial role in the interaction solid surface with liquids [166]. The contact angle between a liquid and a solid is the angle within the body of the liquid formed at the gas–liquid–solid interface [167]. As can be seen in Figure 3.9, when the liquid spreads on the surface, a small contact angle is formed; while, when the liquid drops on the surface, a large contact angle is formed. Wetting of a solid surface by liquid can be quantitatively explained from the tangential angle at liquid–solid–vapour interface liquid (droplet profile). This angle of contact (θ_a) is expressed as the Young's angle (Figure 3.9) and is obtained by a mechanical equilibrium (Equation 3.5) among the three parameters defined as: the liquid surface tension (Υ_{LV}), the solid surface tension (Υ_{SV}), and the liquid-solid interfacial tension (Υ_{SL}).

$$\Upsilon_{SV} = \Upsilon_{SL} + \Upsilon_{LV} cos\theta_a \tag{3.5}$$

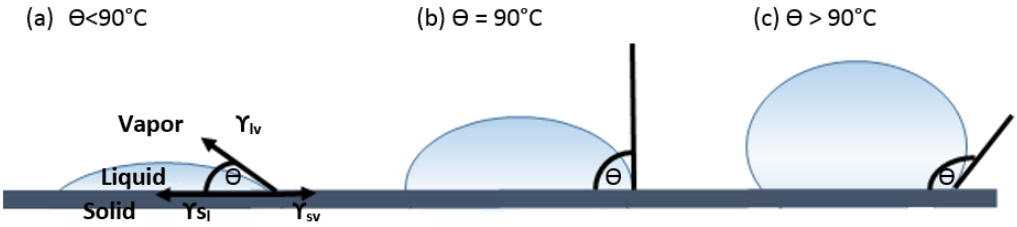

Figure 3.9 Schematic of a contact angle formed by the sessile liquid drops method on a TCC c coating surface

To verify the wettability of the coating surfaces, contact angles were obtained using a Krüss Drop Shape Analyser (DSA 10, Kruess GmbH, Hamburg, Germany) with analytical grade DI water and diiodomethane (>99%, Acros Organics, Geel, Belgium). Initial drops of 3μL were dispensed onto the solid surface and their drop shape profiles were fitted with the "sessile drop" method in the software. A

motor-driven syringe slowly increased the volume of the test liquid droplet to enable the determination of the contact angle, θ_a. The needle tip remained immersed within the top half of the droplet. The shape of the droplet was monitored with a CCD camera and contact angles were determined using the Drop Shape Analysis software (DSA version 1.0, Kruess). The angles were fitted with the tangent method for both left and right sides of the drop (Equation 3.6)

$$f(x) = a + bx + cx^{0.5} + d/lnx + e/x^2 \tag{3.6}$$

This curve is then differentiated, and the gradient at liquid–solid–vapour interfacial point (θ_a) is calculated. Ten contact angles at different positions of 3 surfaces for each coating were measured in the open air at ambient conditions (T = 20 ± 2°C).

4 Characterization of Zn layer

4.1 Morphology of the Zn layer

Low magnification of a top-plane FIB-SEM micrograph of the alkaline Zn plated steel is shown in Figure 4.1 (a). At some spots, small deposit structures coalesced on top of the surface. The surface morphology at higher magnification (Figure 4.1 (b)) shows no visible sign of grain-like structures or boundaries.

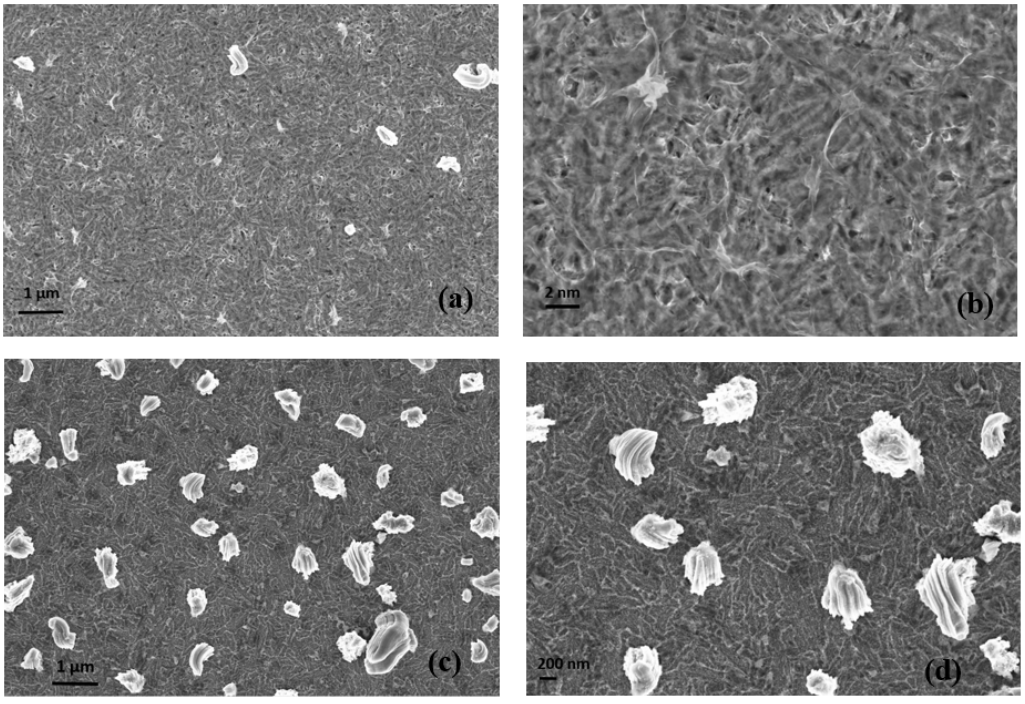

Figure 4.1 FIB-SEM micrograph of alkaline zinc electro-deposited steel (a) low magnification of as-received sample, (b) high magnification of as-received sample, (c) low magnification of heat-treated sample, (d) high magnification of the heat-treated sample

To study the influence of elevated temperature on the Zn surface structure, the FIB-SEM was carried out after the Zn plated steel was kept in an oven for 6 hr and 210°C. The surface structure of the heated Zn layer is shown in Figure 4.1 (c) with low magnification and Figure 4.1 (d) with high magnification. As can be seen, the number of protrusions on the surface was increased in the heated sample in comparison to the non-heated (deposited) sample. The images (Figure 4.1 (c) and (d)) indicate that a Zn surface was covered with random nodular shape after heat treatment. The formation of such a structure also was seen in previous studies [29, 168] and is categorized as "curved whiskers" [168, 169]. Electroplated Zn coatings have been identified to be prone to whiskers growth [170].

Zinc whiskers were observed from Zn electro-deposits following exposure to thermal treatment (150°C for 1 h), furthermore, they were protruded out of CCC and TCC surfaces [29]. However, elemental analysis and grain pattern investigations of the above-mentioned study failed to discover the cause of Zn whisker initiation.

It was suggested that the temperature, zinc coating thickness, type of substrate, and residual compressive stress (both micro-stress and macro-stress) are the primary influencing parameters on the formation of zinc whiskers [170]. Many of the suggested factors for the formation of Zn whiskers were interdependent, and there are not many investigations carried out on the role of parameters. However, there is no concrete agreement among the scientist for the growth of Zn whiskers. Therefore, there is no generally accepted mechanism for the formation and growth of zinc whiskers [169, 170].

To observe the cross-section and thickness of the zinc electro-deposited steel, the sample underwent the cryo-freeze fracture preparation process (Section 3.2.1.1). A cross-sectional view of the Zn layer is indicated in Figure 4.2 (a). A region composed of columnar grain with vertical grain boundaries can be distinguished in the Zn coating. This structure was also observed in a previous study [171] which investigated the Zn coating structure with Electron backscatter diffraction (EBSD). A Band contrast (BC) image corresponding to an area by EBSD of this study is shown in Figure 4.2 (b). This picture indicated the steel substrate at the bottom of the sample, and two regions in the Zn coating one consisted of columnar grain with vertical grain

boundaries and one belong to larger grains at the root of the whisker with oblique grain boundaries [171].

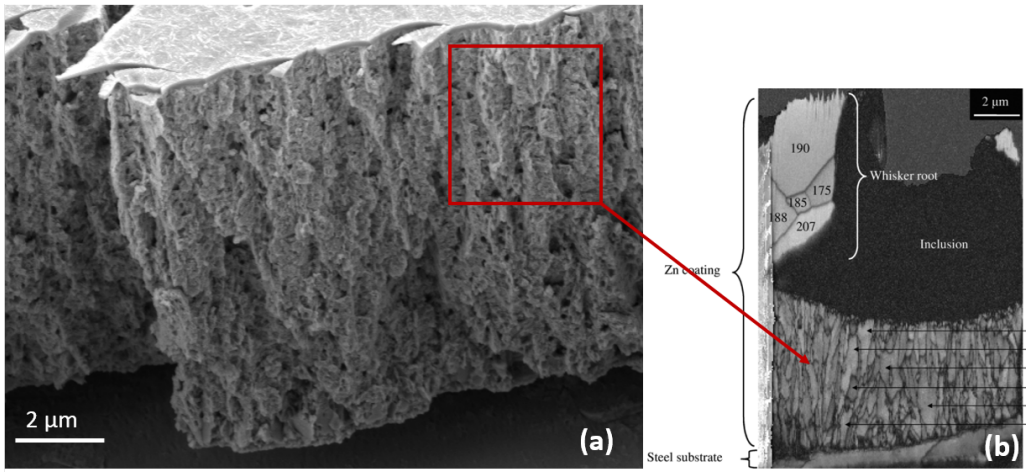

Figure 4.2 (a) SEM analysis of the Zn layer cross-section of the current study, (b)EBSD pattern quality map depicting the grain structure of the Zn-coating on the sample extracted at the root of a whisker of another study [171]

The morphology and structure of the TCC-treated electroplated Zn steel will be discussed in detail in the next chapter (chapter 5). However, in the following, there will be a short introduction of the TCC-treated morphology in the context of Zn underneath layer.

Figure 4.3 shows the SEM images of a deposited TCC-treated (Cr + F + Co) electroplated Zn steel at two different positions ((a) and (b)), and two positions of the same heat-treated sample at two different positions ((c) and (d)). As can be seen, the number of protrusion structures was increased after heat treatment.

Figure 4.4 (a) and (b) show the SEM images of another TCC-treated (Cr + Ox + Co) electroplated Zn steel at two different positions. The SEM images of the same heated sample at two different positions are shown in Figure 4.4 (c) and (d). So, it can be seen that the size of the protrusion structure was increased after heat treatment. However, these structures are not covering the whole surface of the TCC surface.

Taking the same magnification of images in both pictures (Figure 4.3 and Figure 4.4) into account, it is obvious that the number of protrusion and its size is increased

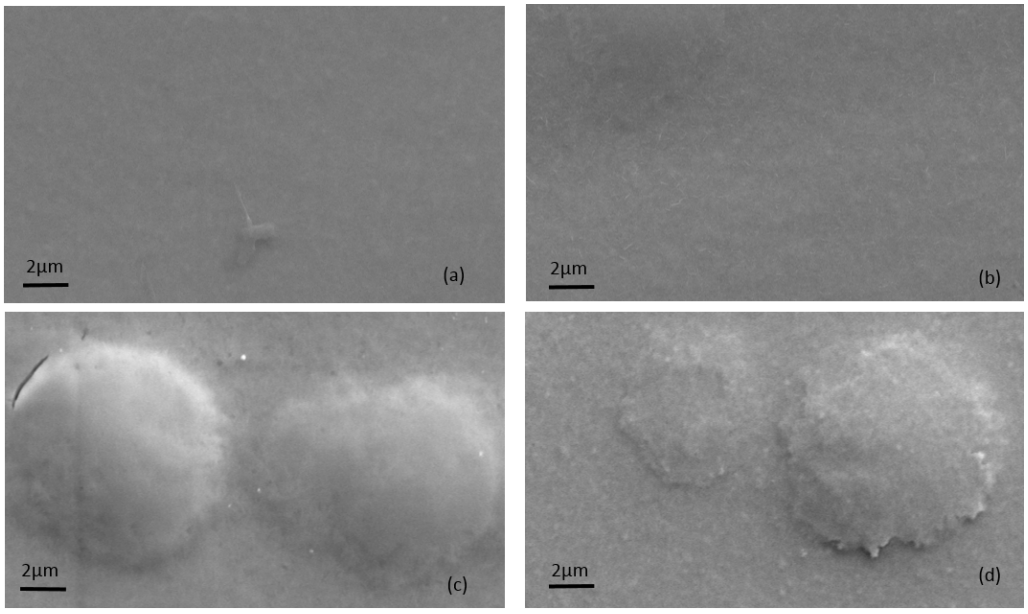

Figure 4.3 SEM images of the TCC-treated (Cr + F + Co) electroplated Zn steel at two different positions of (a) and (b) as-received, (c) and (d) heat-treated specimens

after the heat treatment in Figure 4.3 and Figure 4.4, respectively. Another study [29] was shown that the number and size of protrusions on the Zn coating surface which showed whiskers was increased after heat treatment. The formation of Zn whisker is not the aim of this study. However, it is worth mentioning that these whiskers or protrusions do not occur in all cases. Moreover, to study the TCC coating, it was attempted to choose Zn surfaces with less of these effects.

4.2 Elemental composition of the Zn layer

To get an idea about the composition of the Zn layer, EDXS was carried out around (Figure 4.5 (a)) and on (Figure 4.5 (b)) the protrusion structure of the Zn surface.

Table 4.1 (a) lists the composition measured by EDXS of a point around (Figure 4.5(a)) and on (Figure 4.5(b)) the protrusion of the Zn layer. As can be seen, Zn, C, and O were identified in both cases (Table 4.1 (a) and (b)). The Zn amount was 95 wt% and oxygen content was 3 wt% for the point around the protrusion

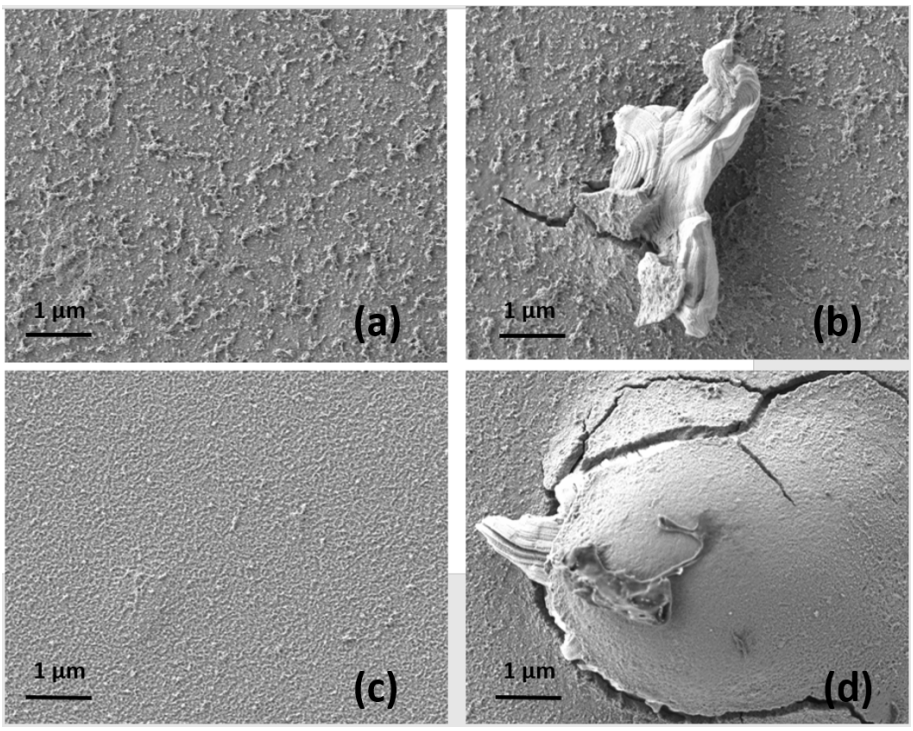

Figure 4.4 (a) and (b) SEM images of an as-received TCC-treated (Cr + Ox + Co) electroplated Zn steel at two different positions, (c) and (d) SEM images of a heated TCC-treated electroplated Zn steel at two different positions

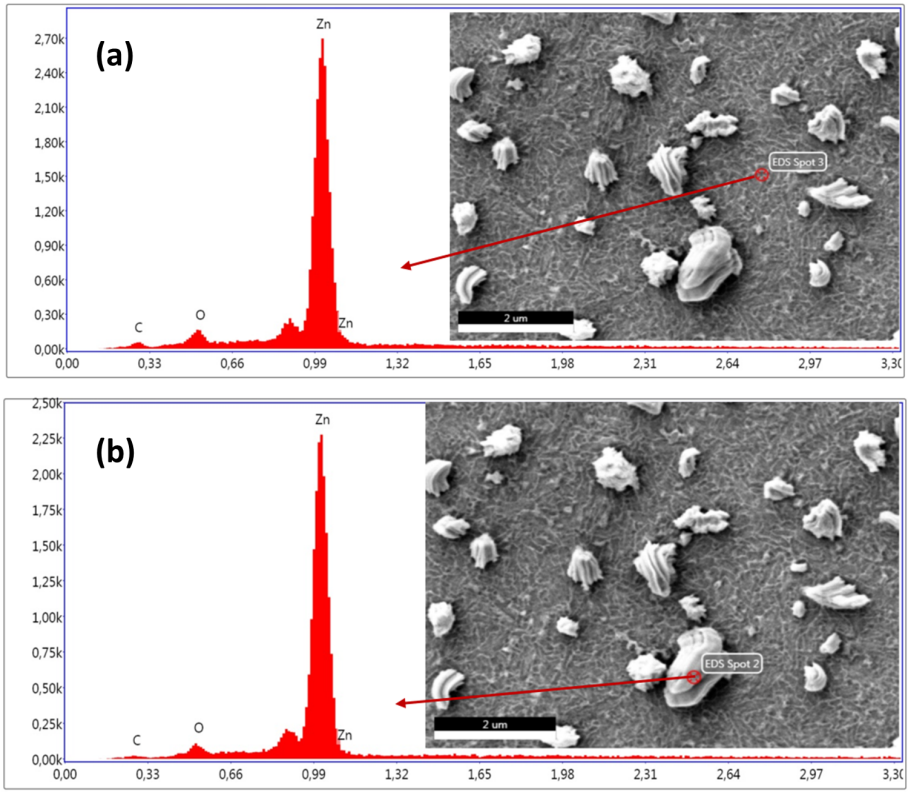

Figure 4.5 EDXS analysis of (a) a point around the protrusion, and (b) a point on the protrusion

(Figure 4.5 (a)) and these values were respectively 97 and 2 wt% for the point on the protrusion (Figure 4.5 (b)). The amount of carbon was double for the point around the protrusion (Figure 4.5 (a)) in comparison to the point on it (Figure 4.5 (b)). A previous study [29] also showed a similar results for the elemental composition of the Zn whiskers over its surface. It was agreed that slight localised differences might occur due to absorbed electroplating additives. In both cases (this study and a previous one [29]) a Zn content of more than 90 wt% was found on and around the whisker. However, Zinc whisker studies by Lahtinen et al. [172] indicated the elemental composition changes with Cl and S on and around a hot-dip galvanizing whisker over long term growth (20 years) in an active environment. These impurities were ascribed to airborne pollutants. The experimental circumstances in this work would preclude a similar condition.

Table 4.1 The composition measured by EDXS of (a) a point around the protrusion of the electroplated Zn surface in Figure 4.5 (a), and (b) a point on the protrusion of the electroplated Zn surface in Figure 4.5 (b)

Element	**(a) wt%**	**(b) wt%**
Zn	95	97
C	2	1
O	3	2

4.3 X-Ray Diffraction analysis of the Zn layer

Figure 4.6 shows a XRD pattern of the electroplated Zn layer. The Bragg reflections with 2θ values of 56.602° and 70.661° correspond to (110) and (110) planes that are typical for Zn and ZnO, respectively [173]. Both diffraction peaks were indexed according to the hexagonal lattice of Zn and ZnO. Moreover, the intensity of the Zn peak is much higher than ZnO. Apart from these peaks, no impurities were found, implying a good crystalline structure of the samples. It can be seen, that this Zn layer has a strong preferred orientation (for Zn at 70.661° relating to (110)). Therefore, only one set of specific lattice planes can be detected. XRD was also used to characterize the TCC films. However, because these films were much thinner than the Zn plated layer, the XRD spectra of the zinc layer was more predominant than

the one from the TCC layer. That is why the diffraction patterns of the TCC films were the same as the one for the Zn layer. Two examples of the XRD analysis of the TCC films are presented in Appendix 3 in Figures A.2 and A.3.

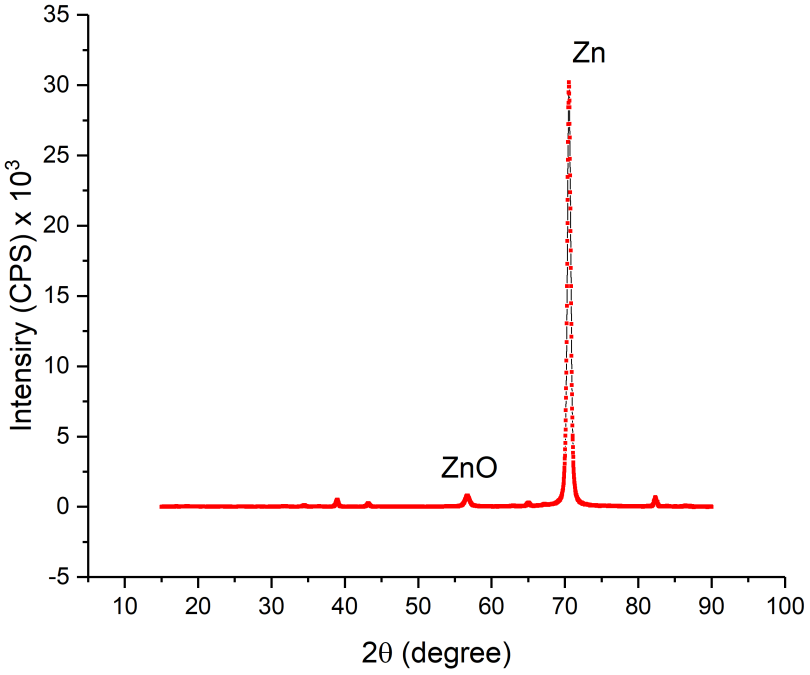

Figure 4.6 XRD analysis of the Zn layer

4.4 Atomic force microscope analysis for the Zn layer

An AFM image of the electroplated Zn surface is shown in Figure 4.7. The Zn layer seems relatively smooth, with the mean roughness of 10.6 ± 0.4 nm (obtained from the NanoScope Analysis 1.5 Software, mentioned in Section 3.2.1.2).

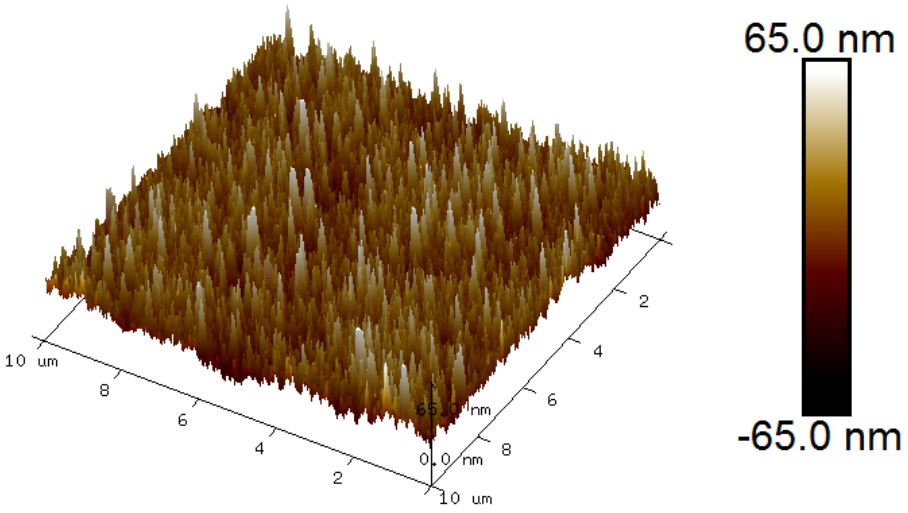

Figure 4.7 AFM micrograph of the alkaline Zn-plated steel a surface area of 10 X 10 µm^2

5 Physical and Chemical Characterization of Trivalent Chromium-based Conversion Coatings

5.1 Morphology and physical characteristics

5.1.1 Focused ion beam scanning electron microscopy

Figure 5.1 depicts the FIB-assisted cross-sectional SEM micrographs corresponding to the layers formed in different treatment solutions with the immersion time of 60s. The TCC coating shows a two-layered structure comprised of an outer thin barrier layer plus an inner thicker layer with a porous structure. Previous work also showed a two- [36, 90, 119] or three- [104] layered structure of the TCC coatings. The as-prepared TCC coating on zinc-plated steel was reported [104] as being composed of three layers; an inner layer contacting the substrate, an intermediate layer, and a thin outer layer with a thickness of ca. 20-40 nm. The middle layer, which contributed to approximately two-thirds of the total coating thickness, was observed as more porous than the other two layers. As can be seen in Figure 5.1 (a) and (b) the inner film formed in the oxalate-containing passivating bath covered the zinc substrate with relatively uniform and less porous morphology. However, the images in Figure 5.1 (c) and (d), represent a non-uniform structure with cavities for the conversion coatings produced by fluoride-containing treatment solutions. After heat treatment,

the coating was still composed of two layers (Figure 5.1 (e)). However, both the inner and outer layers became denser as compared to the as-prepared counterpart. Another study [104] also showed that the size and the number of cavities in the TCC coatings were reduced after heat treatment. The thickness of the coatings was measured from the cross-sectional micrographs, and the average of the summation of the inner and outer thickness of each coating is listed in Table 5.1.

The results indicate that the films formed in the fluoride-containing solution have a higher thickness than the layers formed in oxalate-containing treatment solutions (430 nm for Cr + F, 230 nm for Cr + Ox). Additionally, layer thickness measurements reveal that adding cobalt to the passivating solution did not affect the coating thickness significantly (220 and 240 nm for the films with Co). Furthermore, comparing Figures 5.1 (c) with (d), or (a) with (b), it is noticeable that the number of micropores was decreased by adding cobalt to the treatment solution. The cross-sectional analysis (Table 5.1) reveals that the layers were dehydrated by the heat treatment and their thickness decreased (e.g. the thickness of the sample Cr + Ox + ½ Co was reduced from 220 nm to 185 nm). Moreover, the layer formed in cobalt-containing solution had undergone less thickness reduction during annealing, compared to the film produced by the cobalt-free solution (e.g. from 430 nm to 280 nm for the sample Cr + F in comparison with 340 to 300 nm for the sample Cr + F + Co). This can be attributed to the high density of pores in cobalt-free samples that shrank during heat treatment.

Table 5.1 Thickness of TCC layers, as-prepared and heated samples are presented as the average ± standard error of six measurements

Specimen	**Average thickness (nm)**	
	As-prepared	**Heated**
Cr + Ox	230 ± 11	160 ± 7
Cr + Ox + 1/2Co	220 ± 10	185 ± 8
Cr + Ox + Co	240 ± 12	200 ± 5
Cr + F	430 ± 22	280 ± 10
Cr + F + 1/2Co	330 ± 13	290 ± 9
Cr + F + Co	340 ± 17	300 ± 6

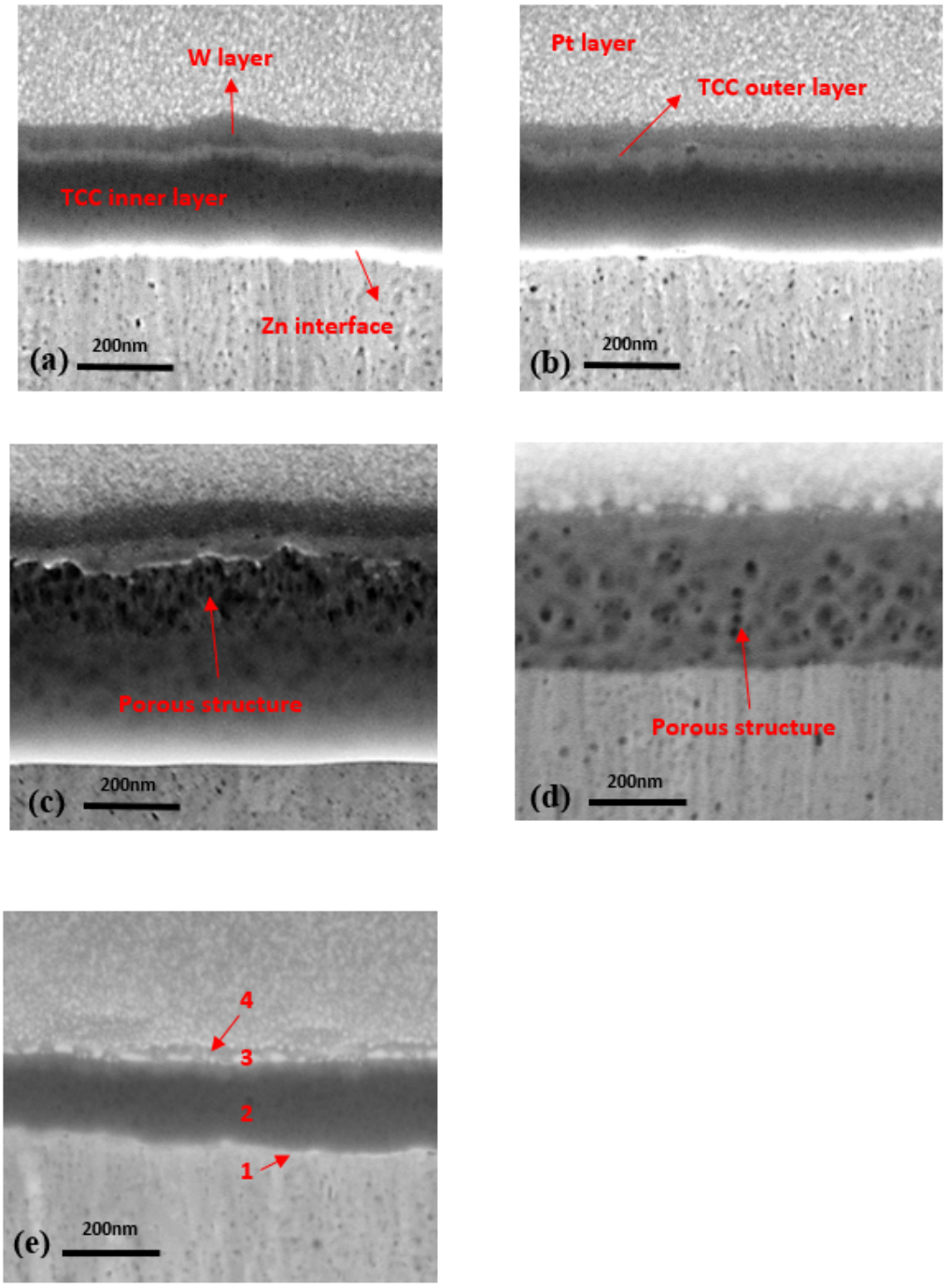

Figure 5.1 FIB-SEM cross-sectional view images of as-prepared TCC coatings (a) Cr + Ox, (b) Cr + Ox + Co, (c) Cr + F, (d) Cr + F + Co, (e) Cr + Ox after heat treatment. Indicated numbers are (1) Zinc substrate, (2) TCC inner layer, (3) TCC outer layer, (4) W layer

5.1.2 Atomic force microscopy

Since the surface of the formed TCC layers was non-conductive, AFM has the advantage of providing topographical images of the coating surface without applying a conductive coating (e.g. tungsten sputtering for SEM images in Figure 5.1). Top view AFM images (Figure 5.2) are shown over a 10 x 10 µm^2 area. Images reveal smoother morphologies with less microstructural defects for the coatings formed in cobalt-containing treatment solutions (Figure 5.2 (b) and (d)).

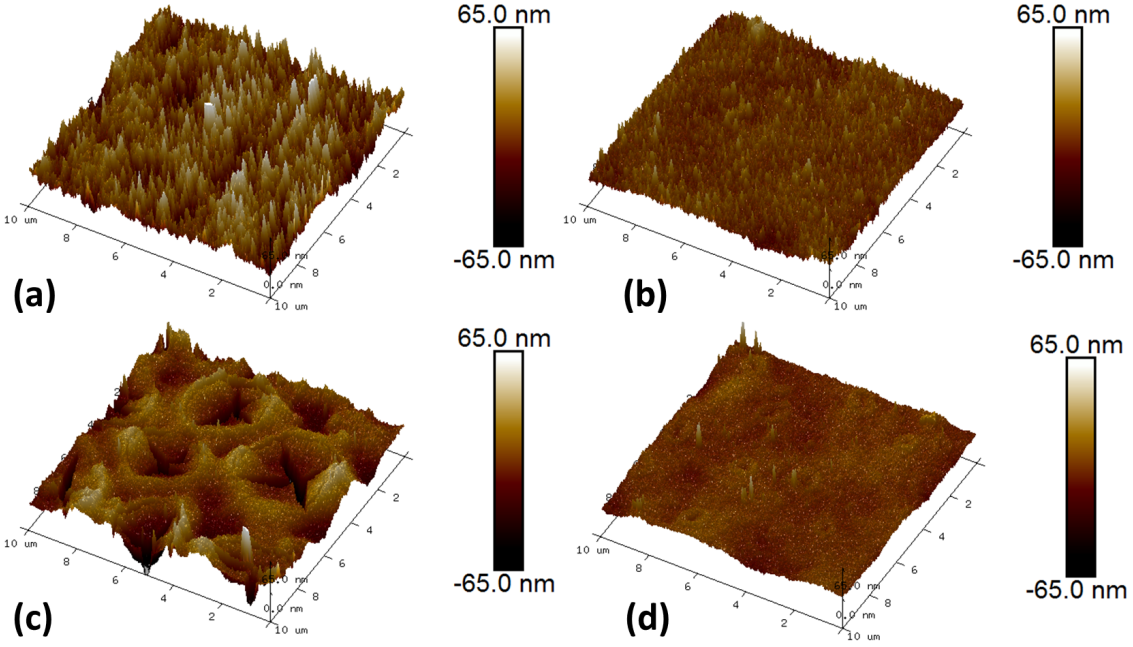

Figure 5.2 AFM top-view images of TCC coatings with a surface area of 10 x 10 µm^2 (a) Cr + Ox, (b) Cr + Ox Co (c) Cr + F ,(d) Cr + F + Co

Considering Figure 5.2 (c), at first glance, the observed shape might be mistaken with an artefact of the AFM cantilever. Figure 5.3 (a) and (b) present the SEM top-view images of the same sample with low and high magnification, respectively. Figure 5.3 (a) indicates that the surface was formed of a sun-cross like structures [1] with different sizes, approximately in the range of 1-2 µm (Figure 5.3 (b)). These structures conform to the surface topography seen in Figure 5.2 (c). Therefore, SEM

[1] A sun cross is a solar symbol consisting of an equilateral cross inside a circle. The design is frequently found in the symbolism of prehistoric cultures [174].

and AFM top-view images show similar structural patterns for the film formed in the fluoride-containing solution (Cr + F).

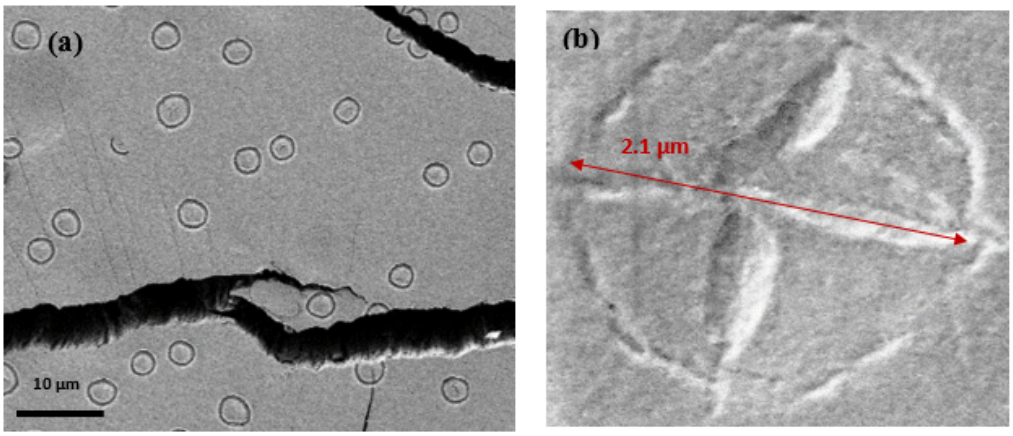

Figure 5.3 Top-view SEM images of Cr + F surface without being sputtered (a) with low magnification, (b) with high magnification

Average roughness values of the surface obtained from the AFM topographical images are listed in Table 5.2 (discussed in Section 3.2.1.2). The non-passivated zinc surface showed a relatively low roughness (10.6 nm). Regarding the passivated samples, the results imply that cobalt addition to the treatment solutions reduced the R_a value of the layer (e.g. from 15.3 nm for the film produced by the fluoride-containing treatment solution (Cr + F) to 7.6 nm for the film made by the same solution plus the addition of cobalt (Cr + F + Co)).

Table 5.2 Average roughness of TCC coatings measured over an area of 10 x 10 µm^2 are presented as the average ± standard error of six measurements

Specimen	**R_a (Average roughness) (nm)**
Zinc substrate	10.6 ± 0.4
Cr + Ox	13.0 ± 0.6
Cr + Ox + 1/2Co	12.1 ± 0.3
Cr + Ox + Co	10.3 ± 0.2
Cr + F	15.3 ± 0.8
Cr + F + 1/2Co	9.8 ± 0.2
Cr + F + Co	7.6 ± 0.4

5.1.3 Influence of chromium amount on the formed layers

The effect of a higher amount of Cr in the TCC treatment solution on the structure of the formed layer was also investigated. Figure 5.4 shows the SEM cross-sectional images of the layer formed in the TCC treatment solution with double the amount of Cr (samples 7 and 8 in Table 3.2). Figure 5.4 exhibits the structure of samples 2Cr + 2Ox (Figure 5.4(a)) and 2Cr + 2Ox + 2Co (Figure 5.4(b)). It is obvious that the formed films consist of an inner and an outer layer (the same as in the cases of previous samples, Figure 5.1). The two-layered structure of the film can also be seen for the layers that were heat-treated (Figures 5.4(c) and 5.4 (d)), which is also consistent with the previous result (Figure 5.1 (e)). Table 5.3 listed the average thickness measured from the SEM cross-section. As can be seen, in good agreement with the results that were shown in Table 5.1, the presence of Co in the treatment solution does not result in a higher thickness of the film (e.g. 290 nm for the 2Cr+ 2Ox layer in comparison with 218 nm for the 2Cr + 2Ox + Co layer). In the same trend as that observed in Table 5.1, the average thickness of the layers was also reduced following a heat treatment (e.g. 290 nm for the prepared 2Cr+ 2Ox layer in comparison with 237 nm for the heated one). As expected, the thickness of the film was increased by increasing the Cr amount in the TCC treatment solution (e.g. 290 nm for 2Cr + 2Ox in compared with 230 nm for Cr + Ox). However, for the Co-containing layer, this increase was not observed (i.e. 218 nm for 2Cr + 2Ox + Co, while 240 nm for Cr + Ox + Co).

Table 5.3 Thickness of TCC layers with higher Cr amount, as-prepared and heated samples are presented as the average ± standard error of six measurements

Specimen	**Average thickness (nm)**	
	As-prepared	**Heated**
2Cr + 2Ox	290 ± 6	237 ± 9
2Cr + 2Ox + Co	218 ± 17	173 ± 3

AFM analysis was performed to compare the surface of oxalate-containing TCC coating with a low and high amount of Cr. Figure 5.5 shows the AFM top-view images of these layers with a surface area of 5 X 5 μm^2. In accordance with the images observed in Figure 5.2, comparing Figures 5.5 (b) and (d) implies that adding Co to

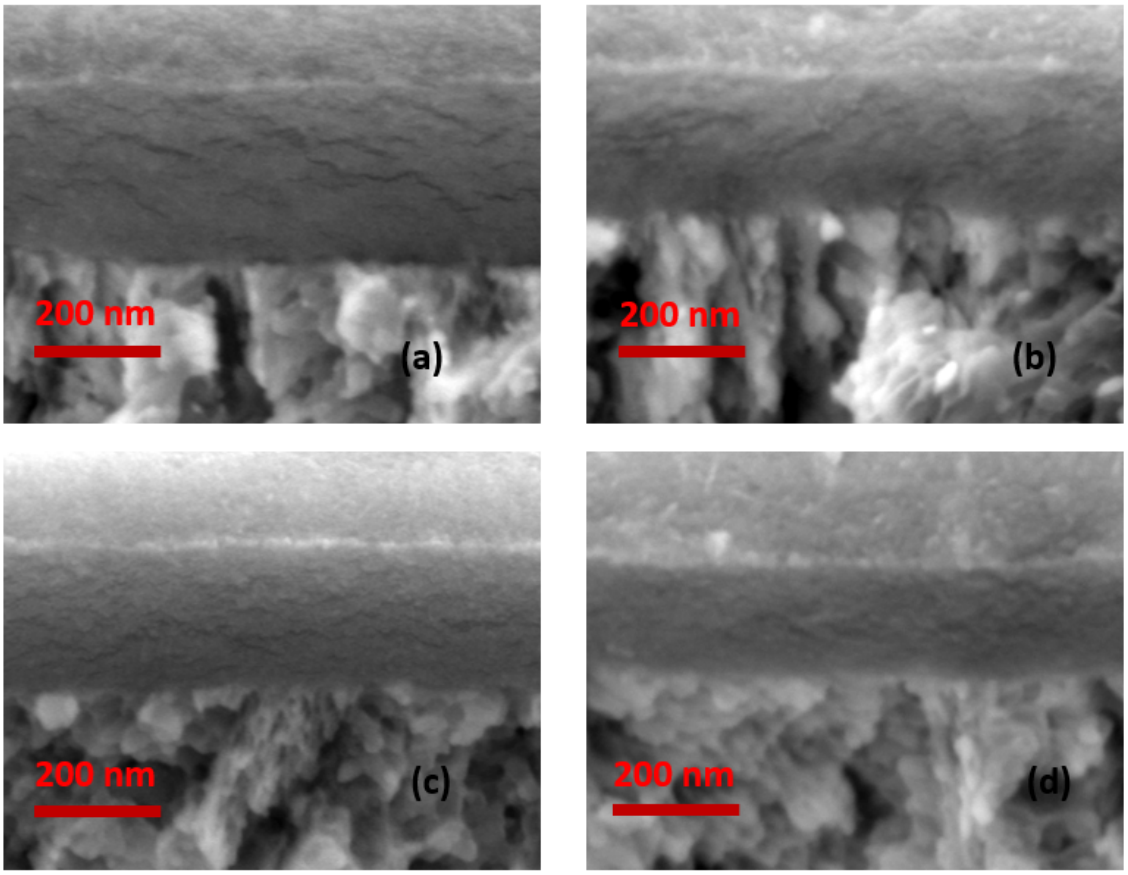

Figure 5.4 SEM cross-sectional view images of TCC coatings (a) 2Cr+ 2Ox, (b) 2Cr + 2Ox + Co, (c) 2Cr+ 2Ox (heated), (d) 2Cr + 2Ox + Co (heated)

the TCC treatment solution produces a smoother surface. Besides, the roughness value of these layers, which were obtained from AFM images, are listed in Table 5.4. The results indicate that adding cobalt to the treatment solution reduces the roughness. The increase of Cr(III) content to the TCC solution also seems to reduce the roughness of the film, probably through producing a more coherent film. For example, the roughness value is $\sim$ 12 nm for Cr + Ox and $\sim$ 8 nm for the 2Cr + 2Ox. Therefore, adding Co to the treatment solution reduced the roughness of the layer from $\sim$ 8 nm for 2Cr + 2Ox to $\sim$ 5 nm for 2Cr + 2Ox + co (the same as the results shown in Section 5.1.2).

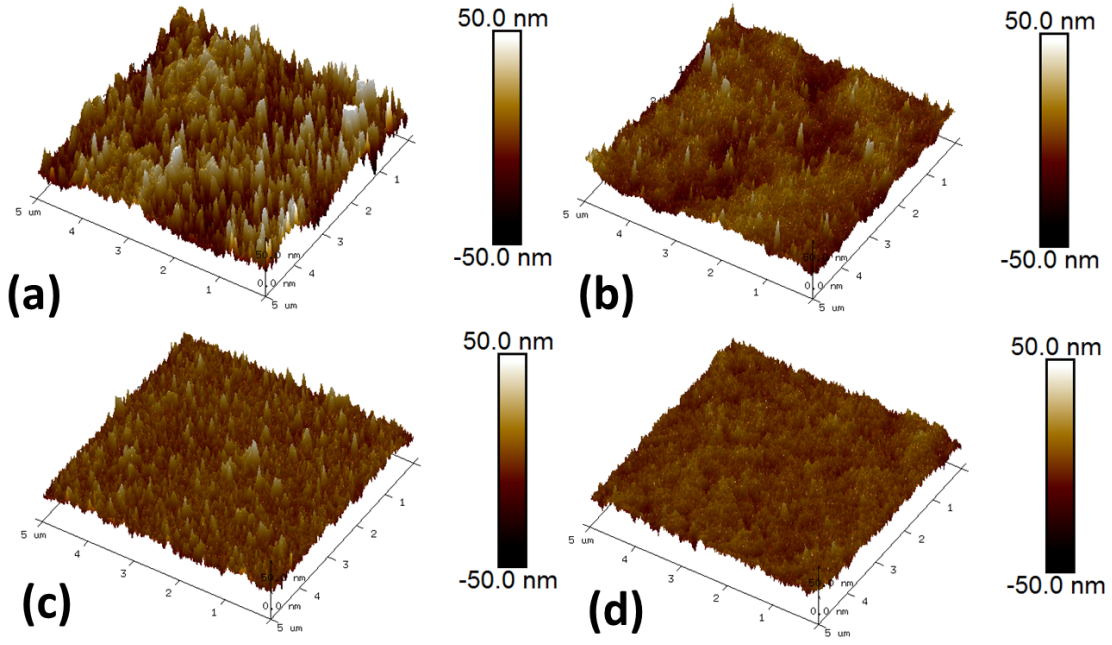

Figure 5.5 AFM top-view images of TCC coatings with a surface area of 5 X 5 µm^2 (a) Cr + Ox, (b) 2Cr + 2Ox, (c) Cr + Ox + Co, (d) 2Cr + 2Ox + Co

Table 5.4 Roughness of the oxalate-containing TCC coatings with low and high Cr measured over an area of 5 x 10 µm^2 are presented as the average ± standard error of four measurements

Specimen	R_a (Average roughness) (nm)
Cr + Ox	12.1 ± 0.3
Cr + Ox + Co	7.3 ± 0.4
2Cr + 2Ox	8.3 ± 0.5
2Cr + 2Ox + Co	5.4 ± 0.3

5.2 Influence of immersion time and process temperature

To shed light on the growth kinetics of the TCC coatings, the effects of immersion time and bath temperature on the layer thickness and the amount of deposited chromium were investigated. Firstly, the zinc layer was subjected to the passivating bath for three different immersion times (40, 60 and 80s at 40°C). The thickness of the formed layers was evaluated by means of FIB-SEM and the amount of deposited chromium was measured by EDXRF. Figure 5.6 indicates that for all cases, the increase of immersion time from 40 to 60s, led to higher thicknesses and chromium content. However, the immersion time of 80s did not in all cases produce a thicker film. This implies that a part of the passivated film might have been dissolved between 60 to 80s. Despite a correlation between thickness and Cr content, adding cobalt to the fluoride-containing solution did not increase the thickness of the layers formed during any immersion time, although it increased the amount of deposited Cr in the layer.

Additionally, the influence of bath temperatures was studied by applying solution treatment for the 60s of immersion time at three different temperatures (3, 18, and 40°C). Figure 5.7 indicates that the layers formed in treatment solutions at 3°C with the same complexing agent, had almost the same amount of deposited Cr and layer thickness. With increasing temperature from 3 to 40°C, the thickness of the coating, as well as the amount of deposited Cr was increased. For example, adding cobalt to the oxalate-containing treatment solution showed higher Cr content as well

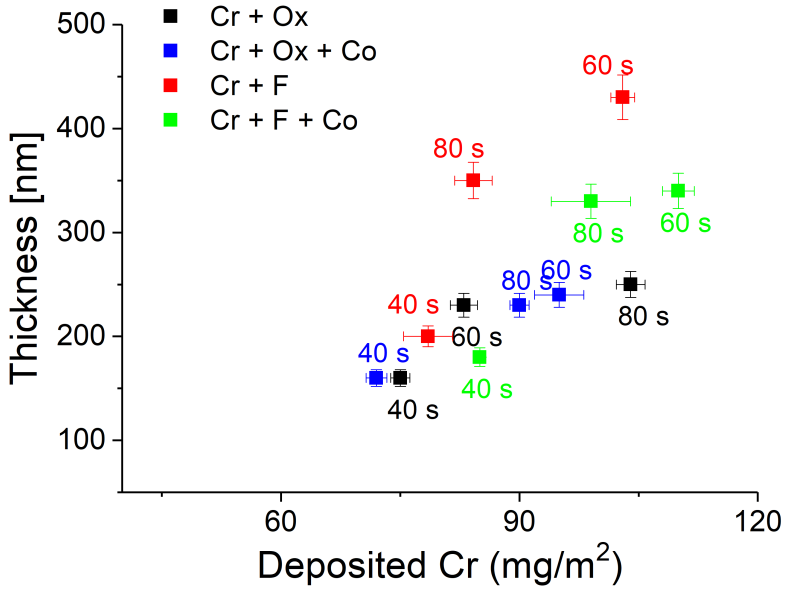

Figure 5.6 Effect of passivating immersion time on the formation of TCC coatings, thickness(nm) from cross-section FIB-SEM, and Cr amount(mg/m^2) from EDXRF coatings

as a higher thickness of the formed layers with increasing bath temperature. The same applies to the layers formed in fluoride-containing solutions, except for the fact that for this case the thickness did not increase with increasing the deposited Cr. In summary, the rate of film formation was enhanced at a higher temperature.

5.3 Chemical characteristics

5.3.1 Inductively coupled plasma optical emission spectrometry

To investigate the composition of layers, the solution from leaching the TCC coating in 10 vol% HCl was analysed by ICP-OES (Table 5.5). The data indicate that the amount of chromium observed in the extracted solution of the films formed in the fluoride-containing treatment solution (e.g. 106.6, 109.4, and 110.4 mg/L)

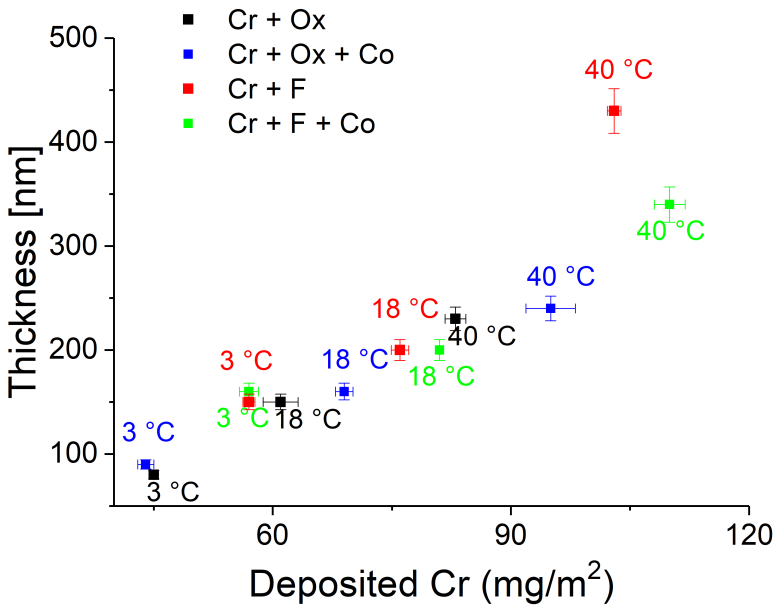

Figure 5.7 Effect of passivating bath temperature on the formation of TCC coating, thickness(nm) from cross-section FIB-SEM, and Cr amount(mg/m^2) from EDXRF coatings

was more than in the case of the oxalate-containing solution (e.g. 60.8, 64.9, and 68.2 mg/L). However, more cobalt was incorporated into the layers formed in the oxalate-containing treatment solution (e.g. 12.1 mg/L for Cr +Ox + Co sample, while 6.3 mg/L for Cr + F + Co sample). As expected, the amount of detected Co in the samples produced in TCC baths without this component (i.e. Cr + Ox and Cr +F) was less than the Limit of detection (LOD) of the device. For the treatment solutions with either complexant, the Cr content of the layer was higher when cobalt was also present in the passivating bath (e.g. 60.8 mg/L for Cr + Ox and 68.2 mg/L for Cr + Ox + Co). This effect was also observed in Figure 5.7 for bath temperature of 18 and 40°C. For both of these temperatures, and either of the complexing agents, the amount of deposited Cr was more, when Co was also present in the TCC bath.

Table 5.5 Total dissolved cobalt and chromium of leached TCC coatings, analysed by ICP-OES are presented as the average ± standard error of ten measurements

	Measured amount of cobalt and chromium	
Specimen	**Cr (mg/m²)**	**Co (mg/m²)**
Cr + Ox	60.8 ± 0.4	<LOD
Cr + Ox + 1/2Co	64.9 ± 0.2	5.9 ± 0.3
Cr + Ox + Co	68.2 ± 0.3	12.1 ± 0.2
Cr + F	106.6 ± 0.3	<LOD
Cr + F + 1/2Co	109.4 ± 0.2	2.9 ± 0.2
Cr + F + Co	110.4 ± 0.4	6.3 ± 0.4

Remark: LOD is 0.05 µg cm^{-2}

5.3.2 Auger electron spectroscopy

Depth profiling was carried out by evaluating the Auger intensities of the major constituent elements in the layer. The Auger parameters for the measured elements are listed in Table 5.6. As can be seen from Table 5.6, there are two peaks allocated to cobalt, at Co1($L_3M_{23}M_{45}$) ∼ 705 eV and Co2 ($L_3M_{45}M_{45}$) ∼ 772 eV. There is another peak, F-Co at 660 eV, which is a superposition of two Auger peaks of the F KLL Auger peak and the Co $L_2M_{23}M_{23}$ Auger peak. In the case of fluoride-containing samples, the peak reflects the F concentration because the part of Co which contributes to this peak is negligible. AES depth profile of the passivated samples presented Zn, O, C, and Cr as the primary coating elements. For all coatings, the signal of zinc reached a constant value as the oxygen signals decayed to zero at the same depth. The Auger depth profiles were quantified by using the elemental sensitivity factors of the spectrometer software (Table 5.6). The quantitative depth profiles were once evaluated using the Co1 peak and another time using the Co2 peak. The depth scale was calculated by converting the sputtering time scale into the depth with the known thickness of each sample from FIB-SEM. The sputtering time at which Zn atomic concentration reached 80% was specified as the conversion coating thickness. The quantitative Auger profiles of the four samples are depicted in Figure 5.8.

Table 5.6 Auger parameters for the measured elements with the elemental sensitivity factors obtained from the Avantage processing software

Element	Auger transition	Auger peak position	Measured range	Sensitivity factor
C	KLL	∼262 eV	230 eV ... 287 eV	0.6
O	KLL	∼514 eV	440 eV ... 800 eV	0.96
Cr	$L_3M_{45}M_{45}$	∼575 eV	440 eV ... 800 eV	0.09
F	KLL	∼660 eV	440 eV ... 800 eV	0.38
Co	$L_3M_{23}M_{45}$ (Co1)	∼705 eV	440 eV ... 800 eV	0.41
Co	$L_3M_{45}M_{45}$ (Co2)	∼772 eV	440 eV ... 800 eV	0.52
Zn	$L_3M_{45}M_{45}$	∼993 eV	930 eV ... 1040 eV	0.58

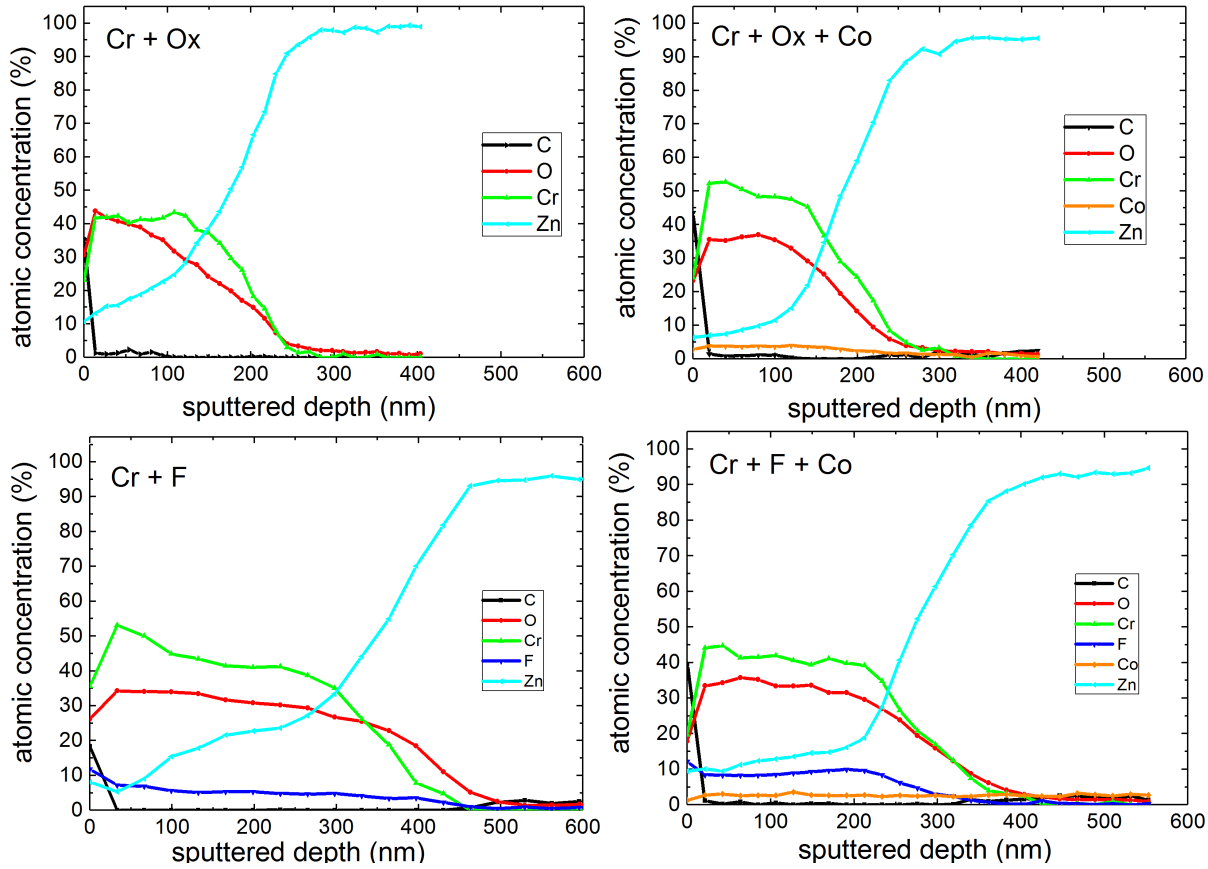

Figure 5.8 Quantitative Auger depth profiling of TCC coatings, (a) Cr + Ox, (b) Cr + Ox + Co, (c) Cr + F, (d) Cr + F + Co

The oxygen content within the layer increased initially compared to the level at the surface, then stabilized before declining at a depth corresponding to the zinc substrate. The concentration of all elements except zinc decayed with further depth profiling into the coating. For almost all samples, carbon was only seen at the very surface, which might be the consequence of exposure to the ambient atmosphere. In the case of fluoride-containing treatment solution, the results indicate enrichment of fluorine with a comparable amount of chromium in the layer. It is proposed that the layers consisted of a mixture of metal (Cr, Zn and perhaps Co)-oxide, hydroxide, fluoride, and possibly oxyfluoride species. The Cr, F and Co concentrations of the relevant samples are compared in Figure 5.9. The AES results do not indicate a significant difference in Cr intensity between the layer formed in fluoride and oxalate-containing baths (Figure 5.9 (a)). Besides, the layer formed in the treatment solution including cobalt and fluoride contained clearly more fluorine than the one prepared by the fluoride-containing solution without cobalt (Figure 5.9(b)). Large negative values of the free enthalpy of formation of CrF_3 (-1088.0 kJ/mol) [175] and former XPS investigations that found CrF_3 in the TCC coating [176] suggest that a part of chromium is bonded with fluoride. Moreover, cobalt was detected in the coatings formed in the treatment solution containing cobalt. The Co concentration was calculated with the Co1 $\sim$ 705 eV (Figure 5.9 (c)) as well as the Co2 $\sim$ 772 eV (Figure 5.9 (d)). In good agreement with ICP-OES results, the cobalt-fluoride-containing sample contained significantly less cobalt compared with the sample formed in the treatment solution containing oxalate and cobalt (Figure 5.9 (c) and (d)).

When the level of Cr in the TCC coating on Zn and on the Al are compared, it can be seen that the level of Cr in the TCC coating was quite high (40-50 at%). This is significantly higher than the Cr levels in the TCC coatings (ca. 10 at%) formed on aluminium [41, 43, 44]. The underlying reason might be that the TCC process is closely related to the dissolution of the substrate. The K_{sp} of $Zn(OH)_2$ at 25°C is 3×10^{-17} [175] and the one for ZnO is 3.86×10^{-10} [177], while, the K_{sp} of $Al(OH)_3$ is 3×10^{-34} [175], and aluminium oxide is insoluble in water [178]. Consequently, the solubility of zinc coating in an aqueous solution and especially in an acidic medium is higher than the solubility of aluminium layer. Therefore, as discussed in Section 2.6, the formulation of a conversion coating varies depending on

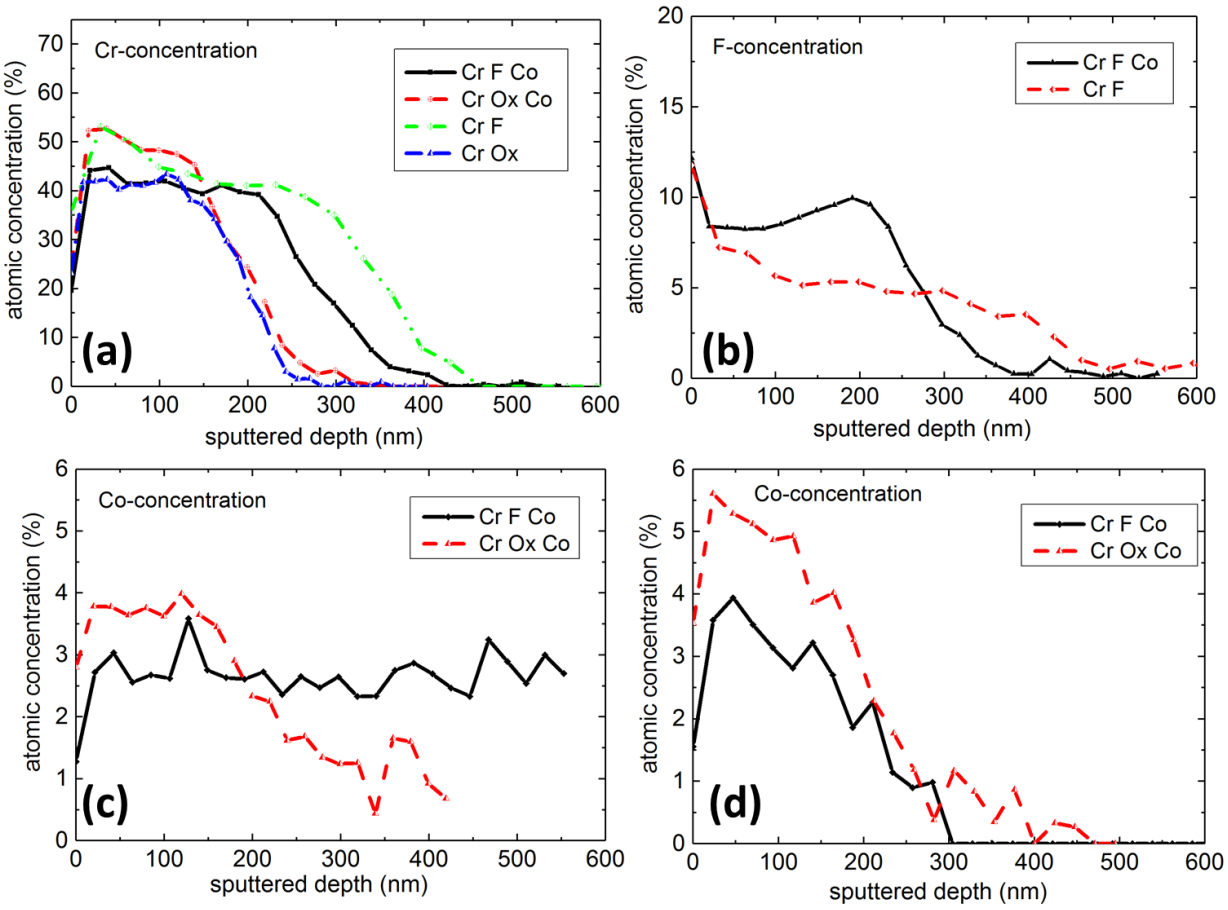

Figure 5.9 Quantitative Auger depth profiles of (a) Cr concentration, (b) F concentration, (c) Co concentration evaluated with the Co1 $\sim$ 705 eV peak, (d) Co concentration evaluated with the Co2 $\sim$ 772 eV peak

the substrate used. The TCC bath designed for the Al substrate is usually based on zirconium (Zr) and/or titanium (Ti) [33, 38, 90, 179], which is why there is less Cr in the resulting layer. Basically, the level of Cr in the TCC coating is proportional to the Cr concentration in the treatment solution. However, finding the proportional relationship between the amount of Cr in the treatment solution and that of deposited on the substrate in the literature is not easy. The reason is that many researchers investigated proprietary passivating baths [36, 40–44]. The drawback of the research on commercial TCC coatings is that the exact composition and especially the amount of Cr in the passivating bath are usually unknown. Moreover, immersion time also has a large effect on the Cr content in the layer. As an illustration, the Cr 2p3/2 spectrum fitting for the chromate layer on the Zn substrate of a previous study showed that the atomic percentage of Cr in the layer with a CCC processing time of 30 to 60s was increased [180].

Comparing the Cr and Co concentration in the treatment solution to the measured atomic concentration of these elements from AES, it is visible that the ratio of Cr concentration (0.08 mol/L) to the Co concentration (0.004 mol/L) in the treatment solution, is comparable to the ratio of detected Cr (40-50 at%) to that of cobalt ($\sim$ 5 at%) in the formed layer.

5.4 Discussion

Considering the FIB-SEM (Figure 5.1) and AFM (Figure 5.2) images, the TCC conversion coating formed in different passivating baths showed that specifically adding cobalt to the treatment solution reduced the density of microstructural defects. Moreover, the film formed in the fluoride-containing solution, and without cobalt, had the highest thickness and number of micropores. Furthermore, oxalate-containing treatment solutions produced uniform films. ICP-OES results indicated higher incorporation of chromium for films formed in fluoride-containing solutions and more cobalt incorporation for the layers produced by the oxalate-containing solutions (Table 5.5). A higher amount of Co in the layer formed in the Ox-containing solution was also proven by AES (Figure 5.9). Thus, the ingredients of the treatment

solution play a crucial role in the formation mechanism plus film composition and subsequently its structure.

Formation of the TCC coatings: Previous studies have suggested that when the zinc electroplated part is immersed in a Cr(III)-based passivation bath, the substrate starts to dissolve, zinc oxidation (reaction 5.1), and the cathodic reduction of hydrogen (reaction 5.2) and nitrate occur [24, 29, 102, 181, 182].
Zinc Oxidation:

$$\mathrm{Zn\,(s)} \rightleftarrows \mathrm{Zn^{2+}\,(aq)} + 2\,\mathrm{e^-} \tag{5.1}$$

E = 0.834 V, T = 40°C , E° = -0.76 vs NHE/V [96]
Hydrogen evolution:

$$2\,\mathrm{H^+(aq)} + 2\,\mathrm{e^-} \rightleftarrows \mathrm{H_2\,(g)} \tag{5.2}$$

E = -0.111 V, T = 40°C, E° = 0 vs NHE/V [96]

The standard potentials of the reactions involved during the cathodic reduction of nitrate ion vs SCE in acidic solutions range from +0.775 to +1.246 V (Table 5.7) [96, 183], which are much more noble than the reversible potential for the Hydrogen evolution reaction (HER). Therefore, it can be deduced that nitrate is a stronger oxidizing agent and from a thermodynamic point of view, the cathodic reduction of nitrate would be preferred compared to hydrogen evolution in an acidic electrolyte.

However, the standard potentials of the reduction of nitrate ion vs the SCE in alkaline solutions were reported as less noble than (Reaction 5.3) or almost the same as (Reaction 5.4) the reversible potential for the HER. Nevertheless, the extent of hydrogen evolution is also governed by the kinetics of the hydrogen reduction reaction on the substrate [184].

$$2\,\mathrm{NO3^-(aq)} + 2\,\mathrm{H_2O} + 2\,\mathrm{e^-} \rightleftarrows \mathrm{N_2O_4(g)} + 4\,\mathrm{OH^-(aq)} \tag{5.3}$$

E° = -0.806 vs SCE/V

$$\mathrm{NO3^-(aq)} + \mathrm{H_2O} + 2\,\mathrm{e^-} \rightleftarrows \mathrm{NO2^-(aq)} + 2\,\mathrm{OH^-(aq)} \tag{5.4}$$

$E^\circ = +0.01$ vs SCE/V

Table 5.7 Standard potentials vs SCE/V for the reduction of nitrate in acid solutions

No.	Possible reduction of nitrate reactions	E° vs SCE/V
1	$NO3^- + 10H^+ + 8e^- \rightleftarrows NH4^+ + 3H2O$	+0.875
2	$2NO3^- + 12H^+ + 10e^- \rightleftarrows N2\,(g) + 6H2O$	+1.246
3	$2NO3^- + 10H^+ + 8e^- \rightleftarrows N2O\,(g) + 5H2O$	+1.116
4	$NO3^- + 4H^+ + 3e^- \rightleftarrows NO\,(g) + 2H2O$	+0.957
5	$NO3^- + 3H^+ + 2e^- \rightleftarrows HNO2 + H2O$	+ 0.94
6	$NO3^- + 2H^+ + e^- \rightleftarrows NO2(g) + H2O$	+0.775
7	$2NO3^- + 4H^+ + 2e^- \rightleftarrows NO2O4(g) + 2H2O$	+0.803

All the cathodic reactions (including nitrate and hydrogen reductions) induce a local pH increase at the surface [39, 185, 186]. A previous study [185] exhibited 2-6 units of interfacial pH rise depending on the coating system. Therefore, due to the consumption of protons at the surface or the formation of hydroxide ions, precipitation of metal hydroxide on the substrate is facilitated.

To shed light on the possible composition of the TCC layer formed on the Zn substrate, the chemical speciation of the system with pH ranging from 0.0 to 14.0 was calculated using Visual MINTEQ software (version 3.1, Stockholm, Sweden, model by KTH, Jon Petter Gustafsson). First of all, it is worth to study the components that are probable to deposit from the relative bath. The kinetic of deposition depends on wetting, supersaturation, and temperature [187]. In chemical thermodynamics, a solid phase (A_aB_b) dissolves or precipitates according to the reaction Equation 5.5 (the law of mass action [188]).

$$A_aB_b \rightleftarrows aA + bB \tag{5.5}$$

This relationship (Reaction 5.5) determines the activities at the state of equilibrium at the given temperature. Therefore, the equilibrium constant in terms of activities of reactants and products at equilibrium is expressed as Equation 5.6:

$$K_{\mathrm{sp}} = \{A\}^{\mathrm{a}}{}_{\mathrm{eq}}\{B\}^{\mathrm{b}}{}_{\mathrm{eq}} \tag{5.6}$$

However, a real solution may not be in equilibrium. This non-equilibrium state is described by the Ion activity product (IAP), which is the same form as the equilibrium constant (K_{sp}), but involves the actual(measured) activities of species (effective concentrations), as follows in Equation 5.7:

$$IAP = \{A\}^{\mathrm{a}}{}_{\mathrm{actual}}\{B\}^{\mathrm{b}}{}_{\mathrm{actual}} \tag{5.7}$$

The ratio between the solubility products at the relevant temperature and the activity product of ions enters the definition of the Saturation Index (SI) (Equation 5.8) [189–191].

$$SI = \log(\frac{IAP}{K_{\mathrm{sp}}}) \tag{5.8}$$

The SI, which also derives from the change in the Gibbs free energy (ΔG) during the reaction, is used as an indicator of deposition (or corrosion) feasibility. If SI is positive, the component is supersaturated and may deposit. When SI is equal to zero the reaction is in equilibrium (saturated), and a negative value of SI indicates the undersaturated condition. For the calculations of this software, the Debye-Hueckel model was chosen to provide an approximation for the activity coefficients in solutions. The SI distribution of Cr(III), Co(II), and Zn(II) deposition species in Cr + Ox + Co and Cr + F + Co treatment solution for pH between 0 to 14 at temperature 40°C is shown in Figure 5.10. As can be seen from the (SI vs pH) plots, crystalline Cr_2O_3 and amorphous $Cr(OH)_3$ start to deposit between pH 4 to 5 in both TCC solutions. The rest of the components seems to start to deposit in the fluoride-containing solution slightly earlier in compared with the oxalate-containing one.

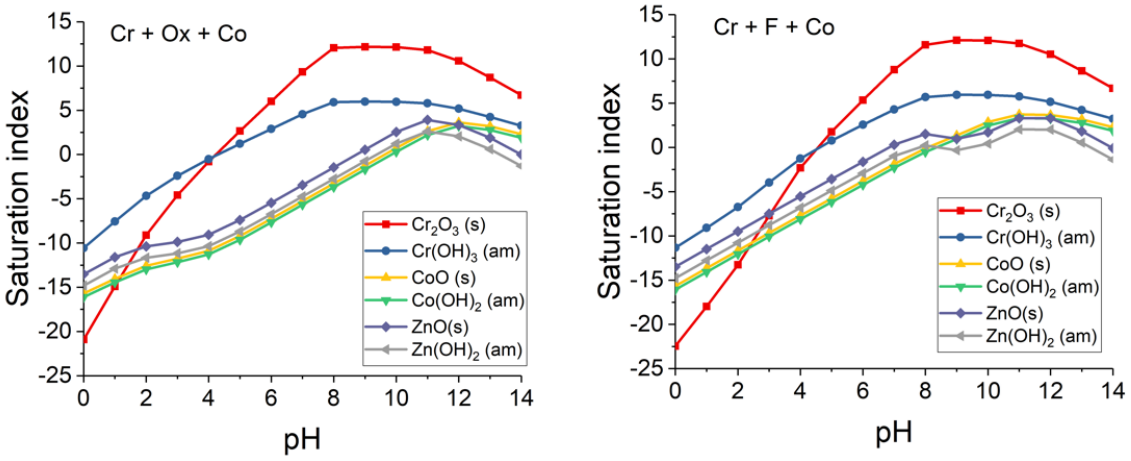

Figure 5.10 The saturation index distribution of Cr(III), Co(II), and Zn(II) deposition species in Cr + Ox + Co, and Cr + F + Co treatment solution for pH between 0 to 14 and T = 40 °C using VISUAL MINTEQ software

Figure 5.11 indicates the distribution of Cr(III), Co(II), and Zn(II) species in each TCC treatment solution for pH between 0 to 14 and at T = 40 °C that was also calculated using Visual MINTEQ software. Figure 5.11 (a) and (b) show that in both fluoride- and oxalate-containing solutions, $Cr(OH)_3$ starts to form at a pH level above 5. Cr may also be present as chromium trifluoride (CrF_3) in the fluoride-containing solution, at a pH value lower than 4 (Figure 5.11 (b)). The plots in Figure 5.11 suggest that increasing local pH aids the formation of $Cr(OH)_3$, $Co(OH)_2$, and $Zn(OH)_2$ during the TCC conversion coating process for solutions with both type of complexing agents (Ox and F).

Based on (XPS) results, it is proposed that the identified Cr(III) in the TCC coating is mainly representative of an amorphous hydrated $Cr(OH)_3$ rather than a crystalline Cr_2O_3 [29, 180]. In brief, the chemical state of Cr(III) in the coating, according to XPS analysis of some studies, mainly revealed as hydroxide [27, 29, 91, 119, 180, 192], oxide [27, 29, 180, 192] and fluoride [91]. In contrast to some studies [25, 29], cobalt was detected in the layers. Given that cobalt oxalate CoC_2O_4($K_sp = 2.9 \times 10^{-9}$) [175] and cobalt hydroxide ($Co(OH)_2$)($K_sp = 5.9 \times 10^{-15}$) [175] both have a low solubility product, the precipitation of these compounds in the layer formed in the cobalt-containing electrolyte is foreseeable. Figure 5.11 (c) shows that in the case of oxalate-containing solutions, cobalt oxalate and cobalt hydroxide

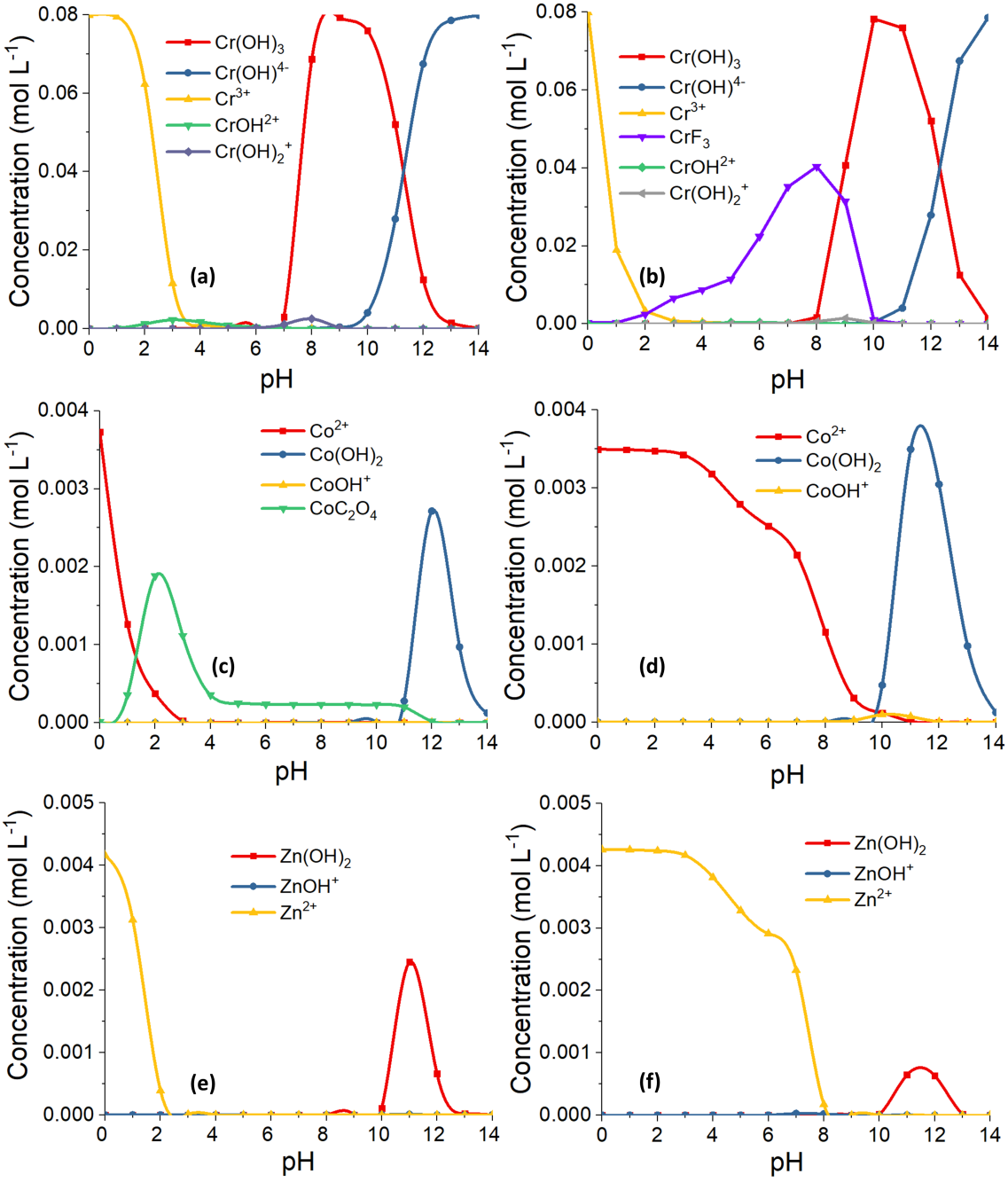

Figure 5.11 The distribution of metal species in each treatment solution for pH between 0 to 14 and at T = 40 °C using VISUAL MINTEQ software (a) Cr(III) species in Cr + Ox + Co, (b) Cr(III) species in Cr + F + Co, (c) Co(II) species in Cr + Ox + Co, (d) Co(II) species in Cr + F + Co, (e) Zn(II) species in Cr + Ox + Co, (f) Zn(II) species in Cr + F + Co

begin to form at a pH level above 1 and above 11, respectively. Figure 5.11 (e) and (f) indicate that zinc hydroxide starts to deposit at pH values above 10 in the oxalate-containing solution and above 8 in the fluoride-containing solution.

For nitrate reduction to happen, water in an alkaline media (Reactions 5.3 and 5.4) and proton in acidic solutions has to be supplied (Reactions in Table 5.7) [193]. It was shown that the potential of nitrate reduction becomes more positive in the presence of a metal ion because it is suggested that the metal ion acts as an intermediary for charge transfer from the electrode to the nitrate ion [194]. Liu et al. [195] by employing the I–V curves of the ZnO films, electrodeposited from nitrate aqueous solution with different Zn^{2+} concentrations and the same $NO3^-$ concentration (1.0 M), showed that the reduction of nitrate was enhanced upon increasing the Zn^{2+} concentration. Moreover, it is suggested that the rate of the nitrate reduction reaction in an electrolyte is increased by the addition of a metal ion which can be precipitated as hydroxide (i.e. Cr^{3+},Co^{2+}, and Zn^{2+}). This was attributed to the hydrolysis of metal ions which breaks the O-H bond in water and releases a proton [96]. The reaction of Cr(III) hydrolysis is as follows (Reaction 5.9) [196, 197].

$$[Cr(H_2O)_6]^{3+} + H_2O \rightleftharpoons Cr(H_2O)_5\,(OH)^{2+} + H_3O^+ \qquad pK_a = 4.0 \qquad (5.9)$$

Ogawa et al. [193] performed alternating current (ac) polarography on nitrate reduction in the presence of various metals and discovered a linear shift of the reduction potential correlated to the logarithm of the stability constants for the first hydration of the added metal cations. The results were interpreted as indicating that hydrolysis of metal ion supplied protons to the nitrate ion throughout the reduction process. Figure 5.10 showed that for both fluoride and oxalate solutions, Cr precipitates on the substrate at much lower pH values (around 4) in comparison with Co and Zn (above 8). Figure 5.12 displays the distribution of first hydration of Cr, Zn, and Co for both Ox- and F-containing TCC solution. It appears that at pH levels below 9 for oxalate-containing solution and below 7 for fluoride-containing solution, the highest stability constants for the first hydration of the metal belongs to Cr. Thus, it is suggested that in the related pH range for each treatment solution,

the hydroxide ions which were produced by the excess nitrate reduction due to the addition of Co^{2+}(first hydration of Co) was used by Cr. Taking the ICP-OES results (Table 5.5) and the deposited Cr amount from EDXRF for 18 and 40°C (Figure 5.7) into account, that might be the reason for the higher deposition of chromium in the films formed by the cobalt-containing treatment solution. It is suggested that the addition of cobalt to the electrolyte provided more protons, due to the hydrolysis of an extra metal ion (generation of H_3O^+ the same as in Reaction 5.9), and thus accelerated the rate of nitrate reduction (due to the more available protons (Table 5.7)). When nitrate is reduced, the interfacial pH value is increased (Reactions 5.3 and 5.4, and Table 5.7) and subsequently the precipitation of metal hydroxides is facilitated (Figure 5.10)

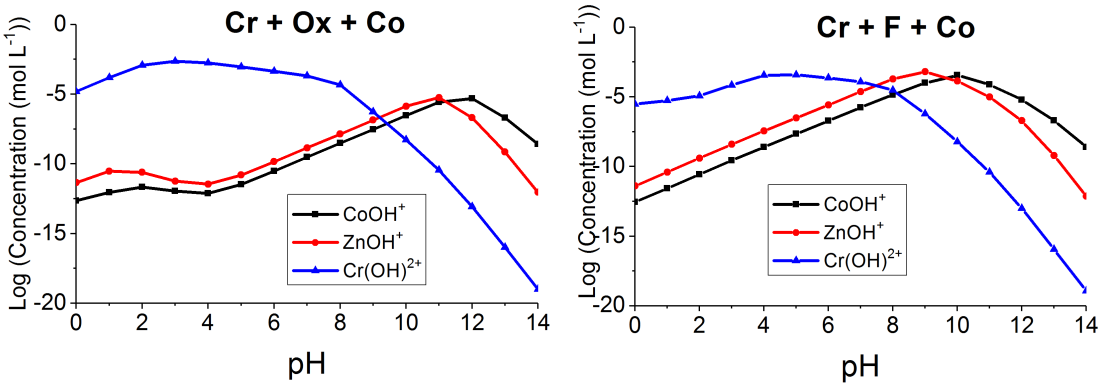

Figure 5.12 The distribution of first hydration of Cr, Zn, and Co for (a) Cr + Ox + Co solution, (b) Cr + F + Co solution for pH between 0 to 14 and T =40°C using VISUAL MINTEQ software

The exponential fit for the layer thicknesses that were formed during 60s of immersion time (deposition rate) versus the reciprocal of absolute temperature (1/T, when T is the passivating bath temperatures; 3, 18, and 40°C) for each TCC treatment solution is shown in Figure 5.13. Employing this graph as an Arrhenius plot and assuming $Cr(OH)_3$ as the main component of the layer, bring about the activation energy attributed to the formation of this compound (Reaction 5.10). As can be seen from Table 5.8, the values indicate that the type of complexing agents

influences the film growth by influencing the activation energy. As an illustration, the activation energy of Cr + Ox + Co sample (21 ± 3 kJ/mol) was higher than the sample produced by a passivating bath with the same amount of Cr and Co, with fluoride complexing agents (14 ± 3 kJ/mol for sample Cr + F + Co). Furthermore, adding cobalt to the oxalate-containing treatment solution did not lower the activation energy associated with the layer formation (comparing 22 ± 4 kJ/mol for Cr + Ox to 21 ±3 kJ/mol for Cr + Ox + Co), as much as it did for fluoride-containing solution (comparing 18 ± 4 to 14 ± 3 kJ/mol). The lower activation energy of fluoride-containing TCC process in comparison to the oxalate one implies the faster growth (i.e. higher thickness) of the film during the same processing time.

$$Cr^{3+} + 3\,(OH)^{-} \rightleftharpoons Cr(OH)_3\,(ppt) \tag{5.10}$$

$K_{sp} = 10^{-30}$, ΔG° = -858 kJ/mol [96]

Table 5.8 Activation energy of the film growth produced by the TCC treatment solution is presented as the average ± standard error obtained by linear regression of Originlab software 2017

Passivation	**Activation energy (kJ/mol)**
Cr + Ox	22 ± 4
Cr + Ox + Co	21 ± 3
Cr + F	18 ± 4
Cr + F + Co	14 ± 3

The presence of fluoride ions in the treatment solution is reported to activate the surface [66, 198], besides dissolving the zinc substrate during the film formation [66, 134, 198]. Based on the representative data (Table 5.5), the films formed in fluoride-containing treatment agents are around 100-200 nm thicker than those formed in the oxalate-containing solution. This effect relates to the nature of the ligands. In a Cr(III)-based passivating bath, adding complexing agents disassembles the stable Cr(III) aqua complex structure and increases the electrochemical activity by forming $[Cr(H_2O)_{6-n}L_n]^{3-n}$ (L, complexing agents) [199]. Thus, the lability of the ligand with the metal ion defines the rate of Cr(III) ions precipitation on the substrate. The order of the ligand replacement lability decreases as the ligand field stabilization increases [30]. For a metal ion, the ligand field strength increases

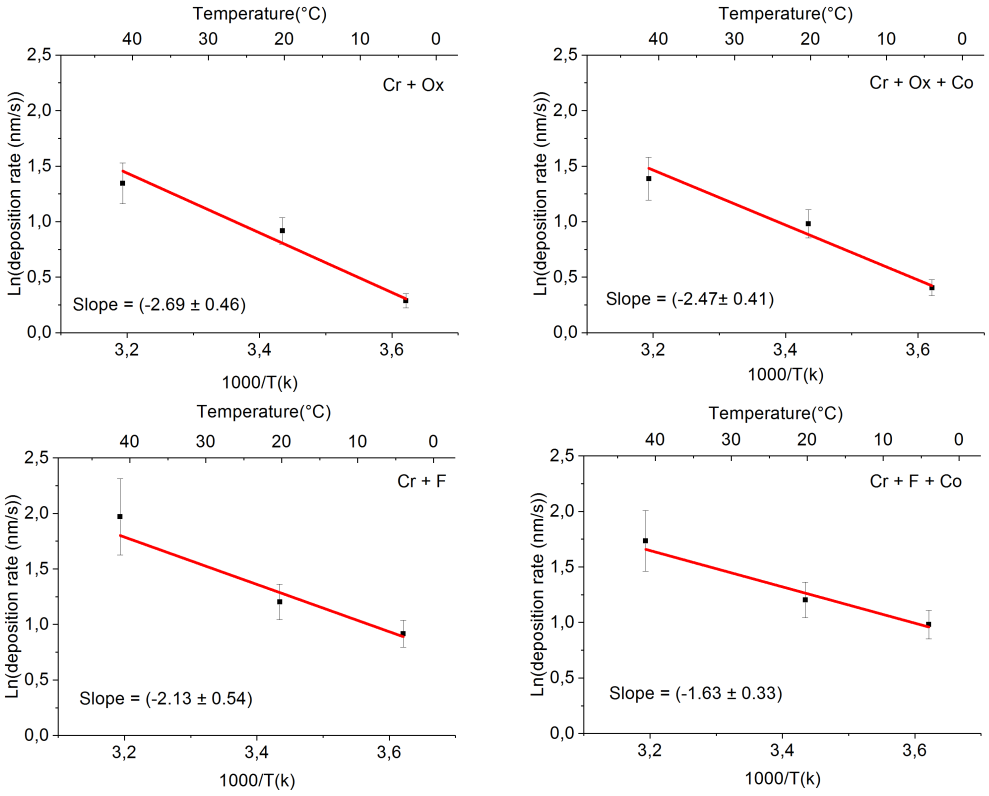

Figure 5.13 Arrhenius plots of TCC coatings (a) Cr + Ox, (b) Cr + Ox + Co (c) Cr + F (d) Cr + F + Co

according to the spectrochemical series [200]. According to the spectrochemical series [200] and comparing fluoride and oxalate as the complexing agent, the field strength of the ligand which Cr(III) ion is coordinated to is weaker when fluoride is the complexant. Therefore, at a given time, more Cr(III) ions by the fluoride-containing solution are deposited onto the substrate. That might be the reason for the higher incorporation of chromium and consequently higher thickness of the film produced by the fluoride-containing bath. Moreover, the presence of fluorine in the AES depth profiling data might imply the formation of compounds such as ZnF_2 (ΔG° = -713 kJ/mol [96]) and CrF_3 (ΔG° = -1088 kJ/mol [96]). Nevertheless, less cobalt was detected by AES and ICP-OES for the fluoride-containing sample. Since ZnF_2 and CoF_2 are slightly soluble in water [201], the deposited form of these compounds was possibly dissolved from the treated surface during water rinsing and resulted in a lower cobalt content and the formed cavities.

In general, defects (micro-voids) can be produced when evolved gases try to leave the layer during the deposition process, resulting in tensile stress [202]. It is reported that the formation of bubbles that cling to the surface throughout the deposition process may result in voids [203], this process often interferes with film growth and may lead to porous or spongy deposits [204]. It was also addressed that evolved gases can produce a non-uniform porous layer by sticking at the surface, concealing the underneath layer [205, 206].

The reduction of nitrate to gaseous products was reported for various materials in the literature [207–209]. The gaseous products formed during nitrate and nitrite reduction reactions were analysed using the gas detector tube method and gas chromatography-mass spectrometry and found to contain NH_3, NO_2, and NO [207]. Additionally, it was shown that the possibility of nitrate reduction reactions strongly depends on the pH of the solution. For instance, at pH 4, the reduction of nitrate to N_2, N_2O, and NO was possible while hydrogen evolution was not possible [207].

As soon as the zinc-plated part is immersed in the treatment solution, a variety of reactions including anodic dissolution, nitrate, and H^+ reduction, adsorption-desorption of metal-oxide/hydroxide reactions may take place at the interface between the electrolyte and the substrate. While the zinc-plated part is still immersed in the bath, different types of gases may form at the substrate surface, either as the result

of nitrate reduction or hydrogen evolution. During the conversion process, the gas bubbles may interfere with the film deposition, locally inhibit mass transfer, and form pores as they are leaving the TCC layer.

It is reported that adding surfactants to the passivating bath results in better wetting of the zinc surface and producing a more uniform film [102]. Moreover, adding a substance to the treatment solution which acts as a surfactant, permits the free evolution of entrapped gases [210]. It was reported that in the binary liquid mixture of water and oxalic acid increasing the mole fraction (x_i = 0.004, 0.010, 0.043, 0.128) decreased the surface tension (σ = 70.3, 68.6, 66.5, 65,8 mN/m) (the values of mole fractions (x_i) and surface tensions (σ) are connected respectively) [211]. This indicates that oxalic acid is enable to function as a surfactant in a water-based solution. Oxalate ions were shown to act as a surfactant also in another study [212]. Therefore, it can be suggested that in the oxalate-containing treatment solution, the oxalate ions acted as a surfactant which facilitates the free evolution of formed gases. Consequently, fewer micropores and cavities were observed for the film produced by the oxalate-containing electrolyte. Based on previous studies [39, 43], cracks, detachment, and delamination were also observed on TCP coatings on aluminium alloys produced by fluoride-containing proprietary treatment solution.

A schematic illustration of the layer formation process by the TCC treatment solution is suggested in Figure 5.14. During the conversion coating process, a mixture of the above-mentioned gases (e.g. N_2 and NO_2) may form in the reaction layer between the substrate (zinc) and the bulk electrolyte (Figure 5.14 (a)). The formed gases may hinder the smooth deposition of metal hydroxide/oxide on the substrate. Throughout the TCC process, in the regions in which the deposition reactions are taking place, there are forces parallel to the substrate, due to the surface tension (vertical blue arrows); there are normal forces caused by the agitation perpendicular to the zinc substrate (green arrows); and there is the internal pressure of the formed bubbles (black arrows). As the bubble expands, its internal pressure decreases [213], and the resultant forces cause the bubble to detach from the reaction layer. After detachment of a bubble, the gas region consists of disjoint volumes. However, the TCC process duration might not be long enough to fill the gap with metal hydroxide/oxide depositions. As a result, microstructural defects are formed in the

TCC layer. A previous study indicated that water was entrapped through the formed micropores in the layer [214]. The ultimate morphology of a TCC coating exhibits a duplex structure (Figure 5.14 (b)); a thick barrier layer with microstructural defects (micropore and voids) is formed on the Zn substrate and a thin layer on top of that. It is not clear why and when the second layer is formed. Considering the AES depth profiling of the TCC coating, the outer layers (first 20-40 nm of the coating) consist of C, Zn, F and Co for those samples which had these elements in their passivating solution. Cr and O seem to increase as the inner TCC layer is reached. It may also be that the top layer was formed after withdrawing the samples from the passivating bath because of exposure to oxygen or humidity in the air. Therefore, the film (inner layer) was reacted with ambient oxygen and humidity and as a result, a dense continuous barrier (outer) layer was formed on top of that. Besides, the coating morphology was clearly influenced by adding cobalt to the treatment solution, in a way which favours the production of a smoother film.

Influence of immersion time: As the film forms, the reaction layer occludes the zinc surface and the reaction between the zinc surface and the Cr^{3+} ions continues by diffusion of the active constituents through the film. It might be that the layer is thickened until the substrate is protected from the oxidizing agent in the passivation solution. In other words, during the TCC treatment process, when nitrate (oxidant) ions in the treatment solution no longer contact the zinc/zinc oxide interface to be able to oxidize (dissolve) it, the film thickness reaches a limiting value.

It was shown that increasing immersion time did not necessarily lead to an increased thickness of the film. Figure 5.11 (a) and (b) also indicate that for pH values higher than 9 in oxalate-containing solution or higher than 10 in fluoride-containing solution, solubility increases due to the formation of a more soluble complex, $[Cr(OH)_4]^-$. Therefore, it is suggested that by increasing the immersion time from 60 to 80s, due to an increased interfacial pH, a part of the deposited $Cr(OH)_3$ was dissolved and $[Cr(OH)_4]^-$ was formed (Reaction 5.11).

$$Cr(OH)_3\,(ppt) + OH^-\,(aq) \rightleftharpoons [Cr(OH)_4]^-\,(aq) \tag{5.11}$$

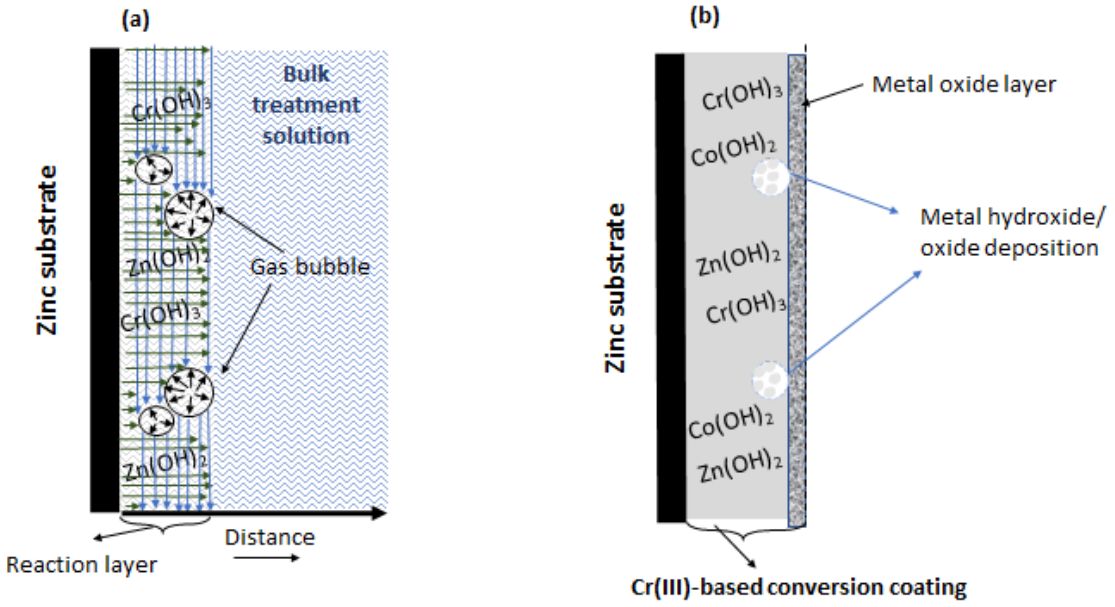

Figure 5.14 A schematic illustration of (a) TCC coating formation during immersion time, the vertical blue arrows show the forces due to surface tension, acting along the direction parallel to the interface; the horizontal green arrows indicate the normal tension perpendicular to the zinc substrate due to the agitation (manual shaking) throughout the immersion time; the black arrows show the force due to the internal pressure of the formed bubbles. The reaction layer is the area between the substrate and the bulk treatment solution, in which during the TCC process the deposition reactions are taking place. (b) A schematic illustration of the ultimate morphology of the formed TCC layer

$K = 10^{-0.4}$ [96]

Gigandet et al. [215] showed that in the CCC process, the chromate film reaches a limiting thickness at a specific immersion time attributable to the dissolution/deposition mechanism of the film formation. It is suggested that as the immersion time increases initially, the coating gets thicker until the path from the substrate through reaching the treatment solution is closed [198]. Afterwards, the film thickening ceases. Subsequently, the metal oxidation stops until some of the formed films are dissolved again; therefore, the resistivity drops, and oxidation starts again. It is also reported that for TCC coating, the zinc substrate becomes passive as the layers are deposited, and this process retards its oxidation [199]. Hence, although various reaction species can still access the Zn substrate via diffusion through the porous passive layer, the passivation of the substrate decelerates the pH increase near the surface of the growing film. Thereafter, the formed layer re-dissolves into the solution as proton concentration along the surface is restored via diffusion from the bulk. Therefore, it is suggested that increasing immersion time does not necessarily lead to a thicker layer. The limiting thickness is probably influenced by the passivation bath processing parameters, immersion time plus temperature and pH of the solution, as well as its composition.

6 Characterization of the Corrosion Behaviour of Trivalent Chromium-based Conversion Coatings

6.1 Neutral salt spray test

The corrosion resistance of the coatings (samples 1 to 6 in Table 3.2) was evaluated by NSS testing [48]. The NSS tests were discontinued when white rust covered 80% of the surface. The coating resistance duration to white rust propagation by exposing the samples in a salt spray chamber is listed in Table 6.1. The results indicate that the layers formed in a Co-containing Cr(III)-based treatment solution are more durable than those formed in an electrolyte without this ion, when both are in the same corrosive environment (e.g. ∼120 hours for Cr + Ox + Co sample in comparison with ∼72 hours for Cr + Ox). This can be attributed to the smaller number of micropores in the film. The microstructural defects might act as favourable paths for chloride ions to penetrate the film and cause corrosion in the layer. Also, the reduction of the layer thickness following annealing might be the reason for the degradation of the protective layer after heating. However, it is worth mentioning that a higher thickness of the layer does not necessarily result in better corrosion protection.

Table 6.1 The corrosion resistance duration, up to 80% white rust coverage for TCC coatings in NSS chamber

	Corrosion test resistance hours	
Specimen	**As prepared**	**Heated**
Cr + Ox	~72	~48
Cr + Ox + 1/2Co	~90	~60
Cr + Ox + Co	~120	~80
Cr + F	~60	~48
Cr + F + 1/2Co	~72	~60
Cr + F + Co	~90	~72

6.2 Potentiodynamic polarization measurements

The anodic sweep polarization curves of Zn and TCC coated Zn surfaces (samples 1 to 6 in Table 3.2) in 3.5 wt% NaCl solution are shown in Figure 6.1.

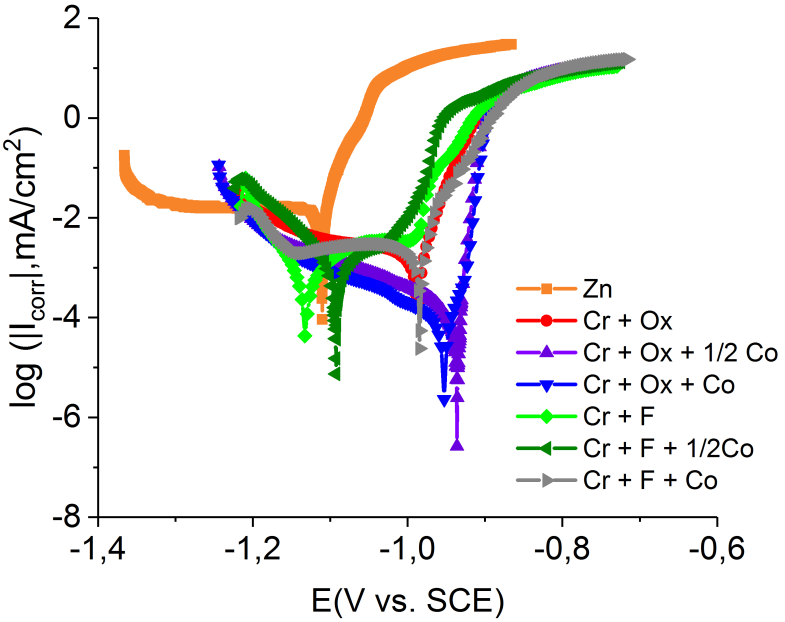

Figure 6.1 Potentiodynamic polarization curves of zinc surface and passivated specimens (samples 1 to 6 in Table 3.2) with 60s immersion time in 3.5 wt% NaCl solution

Values for j_{corr} and E_{corr}, for each TCC coating, were obtained by the Tafel line extrapolation of the anodic j-E curve and are listed in Table 6.2. Comparing the corrosion potential of the bare zinc surface (-1.111 V) to the TCC passivated surfaces (e.g. -0.989 V for Cr + Ox), it is obvious that the TCC coatings shifted the corrosion potential towards less negative (less cathodic) values. Except for the case of Cr + F, it is proposed that TCC coatings provided corrosion protection to the zinc substrate by increasing the corrosion potential. A substantial change in corrosion potential can be seen in the case of oxalate-containing solutions. It was observed that by addition of Co to the Ox-containing solution, the corrosion potential of the sample Cr + Ox was increased from -989 to -954 and -971 mV for samples Cr + Ox + 1/2Co and Cr + Ox + Co, respectively. Among TCC layers, the Cr + F sample had the least noble potential, which can be due to the high density of pores in this sample (Figure 5.1 (c) and Figure 5.2 (c)) that forms a pathway for the penetration of chloride ions. Moreover, breakdown potential (localized corrosion) was only observed in the polarization curve of this sample (Cr + F). Despite a porous structure, even for this sample, the corrosion current density was lower ($1.66\,\mu A\,cm^{-2}$) than the value that was observed for the Zn surface ($2.28\,\mu A\,cm^{-2}$). The decrease in the corrosion current density is related to the thickness of the TCC layer on the Zn surface. The corrosion current density was decreased significantly for oxalate-containing samples; in particular, when the layer was formed in the Co-containing solution ($1.46\,\mu A\,cm^{-2}$ for Cr + Ox in compared with $0.14\,\mu A\,cm^{-2}$ for Cr + Ox + 1/2Co, and $0.05\,\mu A\,cm^{-2}$ for Cr + Ox + Co). The good corrosion protection properties of the coatings formed in the oxalate- and cobalt-containing treatment solution can be ascribed to their denser and less defective morphology (as observed in Figures 5.1 (b) and 5.2 (b)). Also in the case of fluoride containing solution, the corrosion potentials of the surfaces coated in cobalt-containing treatment solutions were more noble. As an illustration, the corrosion potential of the fluoride-containing layer was increased from -1.129 V (Cr + F) to -0.986 V (Cr + F + Co) by adding cobalt to the treatment solution. The corrosion current density was decreased as well from $1.66\,\mu A\,cm^{-2}$ for Cr + F to $1.46\,\mu A\,cm^{-2}$ for Cr + F + Co. This is assigned to the less porous morphology of the Co-containing conversion coatings, plus the role of Co ions at low concentrations in the formed layer as a corrosion inhibitor [216]. Nevertheless, the corrosion current density of the oxalate-containing TCC coatings was less than the corresponding for the fluoride-containing films. It was suggested that fluoride enrichment at the

coating/substrate interface, can promote substrate dissolution around the cathodic sites [115]. Dissolution of zinc is the reaction that takes place in the anodic branch and oxygen and/or hydrogen ion or water reduction occurs in the cathodic branch. The results of Table 6.2 shows a considerable reduction in corrosion current density and an increase in corrosion potential for TCC coated samples. This might suggest the effectiveness of TCC coatings to retard oxidation of zinc by decelerating oxygen and chloride transfer to the zinc substrate.

Table 6.2 Corrosion potential (E_{corr}(V vs SCE)) and corrosion current density (j_{corr} ($\mu A\,cm^{-2}$)) values of polarization tests of TCC coatings (samples 1 to 6 in Table 3.2 with 60s immersion time) in 3.5 wt% NaCl solution, data are presented as the average ± standard error of ten measurements

Specimen	**E_{corr}(V vs SCE)**	**j_{corr} ($\mu A\,cm^{-2}$)**
Zn	-1.111 ± 0.005	2.28 ± 0.43
Cr + Ox	-0.989 ± 0.009	1.46 ± 0.51
Cr + Ox + 1/2Co	-0.954 ± 0.010	0.14 ± 0.02
Cr + Ox + Co	-0.971 ± 0.009	0.05 ± 0.01
Cr + F	-1.129 ± 0.004	1.66 ± 0.83
Cr + F + 1/2Co	-1.015 ± 0.027	1.52 ± 0.07
Cr + F + Co	-0.986 ± 0.011	1.46 ± 0.55

Samples 7 and 8 in Table 3.2 were produced at different immersion times of 40, 60, and 80 s. Afterwards, their corrosion resistance was assessed by potentiodynamic polarization measurements in 3.5 wt% NaCl in a region of -50 mV to +25 mV of the OCP. Figure 6.2 shows the outcome for different immersion time. As can be seen for the TCC layers formed for any immersion time, the Co-containing samples show a more noble E_{corr}. Moreover, the j-E curves in Figure 6.2 indicate a notable reduction of the anodic and cathodic branch for the layers formed in the cobalt-containing treatment solution for any immersion time. That is due to the decrease of both dissolution and reduction reactions, and is ascribed to the more homogenous film that was formed in the treatment solution containing Co (Figures 5.4 and 5.5).

Related j_{corr} and E_{corr} values, for the above-mentioned TCC coatings are listed in Table 6.3. The TCC coatings with higher Cr content as well as the samples shown in Table 6.1 shifted the corrosion potential of the Zn surface to less cathodic values (e.g. E_{corr} for the Zn surface is -1.111 V, from Table 6.2, while the one for

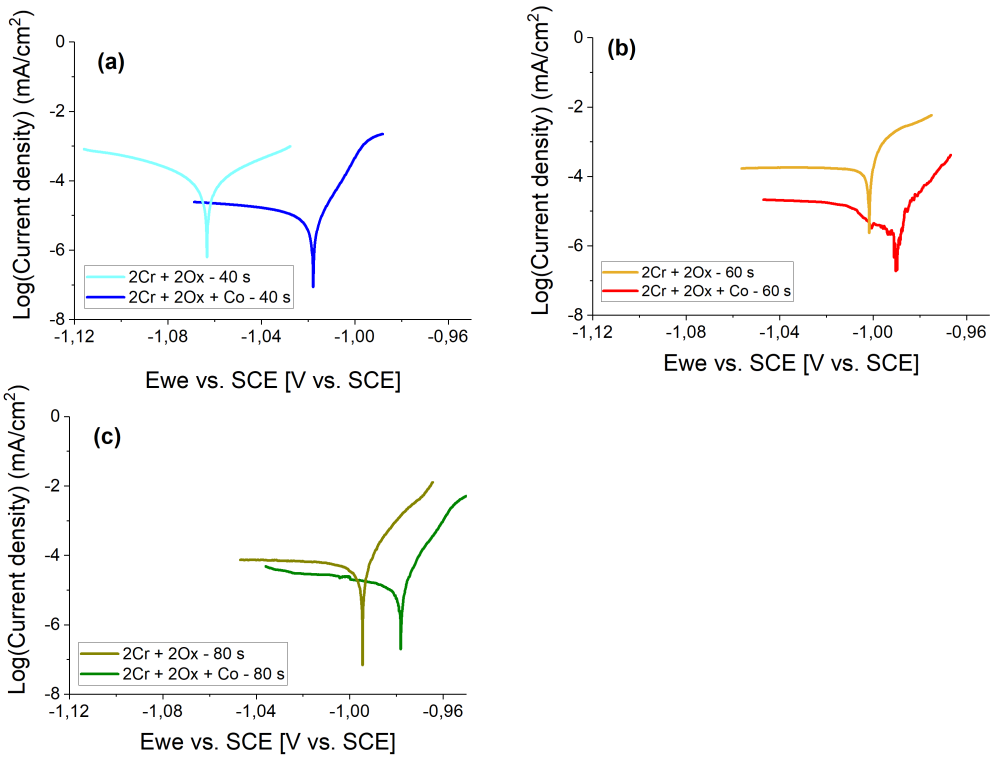

Figure 6.2 Potentiodynamic polarization curves of the Zn-passivated surfaces, samples 7 and 8 in Table 3.2), with the immersion time of (a) 40s, (b) 60s, (c) 80s in 3.5 wt% NaCl solution

2Cr + 2Ox + Co is -0.978 mV). Moreover, the current density of these layers also was reduced one to two orders of magnitude compared to that of the Zn surface ($2.28\,\mu A\,cm^{-2}$). For instance, the current density was $0.20\,\mu A\,cm^{-2}$ for the 2Cr + 2Ox sample with an immersion time of 40s and $0.01\,\mu A\,cm^{-2}$ for the 2Cr + 2Ox + Co sample with 80s of immersion time. Among the studied TCC layers shown in Table 6.3, the sample formed in 2Cr + 2Ox treatment solution after 40s of immersion time had the most cathodic corrosion potential (-1.051 mV), and the highest current density ($0.20\,\mu A\,cm^{-2}$), while the layer formed in the 2Cr + 2Ox + Co treatment solution with the same immersion time has more noble corrosion potential (-1.018 mV) and much lower current density ($0.06\,\mu A\,cm^{-2}$). The results listed in Table 6.3 indicate that the films formed in cobalt-containing treatment solutions for each immersion time had more anodic corrosion potentials. Furthermore, the corrosion current density of the layer formed with the same immersion time was reduced when Co was added to the treatment solution. This finding is consistent with the results discussed in Table 6.2, regarding the effectiveness of Co presence in the corrosion protection properties of the TCC layer. Comparing the j_{corr} and E_{corr} values related to sample Cr + Ox (Table 6.2) with that of 2Cr + 2Ox (Table 6.3), it can be seen that although the j_{corr} of 2Cr + 2Ox is 20 mV less noble, its corrosion current density is almost 10 times less ($1.46\,\mu A\,cm^{-2}$ for Cr + Ox, and $0.15\,\mu A\,cm^{-2}$ for 2Cr + 2Ox). This might be due to the higher thickness of the 2Cr + 2Ox film (Thickness of 2Cr + 2Ox was 290 nm, while the one for Cr + Ox was 230 nm).

Table 6.3 Corrosion potential (E_{corr} (V vs SCE)) and corrosion current density (j_{corr} ($\mu A\,cm^{-2}$)) values of polarization tests of TCC coatings (samples 7 and 8 in Table 3.2) with different immersion times in 3.5 wt% NaCl solution, data are presented as the average ± standard error of ten measurements

Specimen	**Immersion time**	**E_{corr} (V vs SCE)**	**j_{corr} ($\mu A\,cm^{-2}$)**
2Cr + 2Ox	40s	-1.051 ± 0.008	0.20 ± 0.01
2Cr + 2Ox + Co	40s	-1.018 ± 0.008	0.06 ± 0.02
2Cr + 2Ox	60s	-1.009 ± 0.003	0.15 ± 0.06
2Cr + 2Ox + Co	60s	-0.989 ± 0.006	0.01 ± 0.01
2Cr + 2Ox	80s	-0.991 ± 0.004	0.05 ± 0.01
2Cr + 2Ox + Co	80s	-0.978 ± 0.006	0.01 ± 0.01

In summary, when the corrosion current density and the corrosion potential of the TCC layers (Tables 6.3 and 6.2) are compared with that of the Zn layer (Table 6.2), it can be clearly seen that the formed layer protects the zinc from the corrosive environment by reducing the j_{corr} and shifting the E_{corr} towards more anodic values. It can be concluded that the addition of cobalt to the TCC treatment solutions retards the oxidation of Zn and the extent of oxygen or hydrogen reduction.

Moreover, with the aid of polarization curves, the corrosion resistance of the TCC layers with higher Cr content (samples 7 and 8 in Table 3.2) following the heat treatment (kept in the oven for 6 hours and 210 °C) was evaluated. The corresponding j_{corr} and E_{corr} values are listed in Table 6.4. As can be seen, the value of the corrosion current density was increased following the heat treatment of the TCC layers. This effect was more pronounced for the samples formed in the treatment solution without Co. For instance, the j_{corr} of the 2Cr +2Ox sample with 40s immersion time was increased from $0.20\,\mu A\,cm^{-2}$ (Table 6.3) to $1.79\,\mu A\,cm^{-2}$ (Table 6.4), after heat treatment. This can be attributed to the degradation and thinning of the formed layers induced by elevated temperatures. However, it is worth mentioning that the formed layers in the treatment solution containing Co still showed a lower corrosion current density and consequently, better corrosion protection. It can be seen as an example that the j_{corr} of the 2Cr +2Ox + Co sample with 40s immersion time was increased from $0.01\,\mu A\,cm^{-2}$ (Table 6.3) to $0.06\,\mu A\,cm^{-2}$ (Table 6.4), after heat treatment. Moreover, comparing the corrosion current density and corrosion potential values of the heated TCC coatings and that of Zn substrate (e.g. the Zn surface with E_{corr} of -1.111 V and j_{corr} of $2.28\,\mu A\,cm^{-2}$ from Table 6.2 in comparison with 2Cr +2Ox + Co sample with 60s immersion time and E_{corr} of -0.997 V and j_{corr} of 0.01 $\mu A\,cm^{-2}$ from Table 6.4), it can be concluded that these layers are still protective against corrosion, even after heat treatment. This outcome is in good agreement with the previous studies which suggests that TCC coatings maintain up to 70% of their original protective properties even after heat treatment [15, 78].

Table 6.4 Corrosion potential (E_{corr} (V vs SCE)) and corrosion current density (j_{corr} ($\mu A\,cm^{-2}$)) values of the heated TCC coatings (samples 7 and 8 in Table 3.2) with different immersion times in 3.5 wt% NaCl solution, data are presented as the average ± standard error of ten measurements

Specimen	**Immersion time**	**E_{corr} (V vs SCE)**	**j_{corr} ($\mu A\,cm^{-2}$)**
2Cr + 2Ox	40s	-1.061 ± 0.006	1.79 ± 0.02
2Cr + 2Ox + Co	40s	-1.025± 0.007	0.06 ± 0.02
2Cr + 2Ox	60s	-1.013 ± 0.005	0.96 ± 0.02
2Cr + 2Ox + Co	60s	-0.997 ± 0.014	0.01 ± 0.02
2Cr + 2Ox	80s	-1.005 ± 0.006	0.44 ± 0.01
2Cr + 2Ox + Co	80s	-1.004 ± 0.007	0.05 ± 0.02

6.3 Electrochemical impedance spectroscopy analysis

In order to better characterize the electrochemical behaviour of Zn-plated samples passivated with the TCC treatment solutions, EIS measurements were done at OCP. Nyquist plots of EIS analysis for the Zn and TCC coated Zn surfaces (samples 1 to 6 in Table 3.2) in 3.5 wt% NaCl solution, with high- and lower ranges of x- and y-axis are depicted in Figures 6.3 and 6.4, respectively. Figure 6.4(b) shows one semicircle (time constant) for the Zn surface. The impedance spectra of samples Cr + Ox + Co and Cr + Ox + 1/2Co are the broadest in Figure 6.3(a) with the x-y axis ranges up to 35 $k\Omega cm^2$. The Nyquist plots of samples Cr + F + Co and Cr + F + 1/2 have x-y axis range up to 5 $k\Omega cm^2$ (Figure 6.3(b)), and that of samples Cr + Ox and Cr + F have x-y axis ranges up to 2.5 $k\Omega cm^2$ (Figure 6.4 (a)). As can be seen for all the TCC coated samples, their spectra indicate two semicircles (i.e. two time constants). Comparing the Nyquist plot of sample Cr + Ox in Figure 6.4(a) and the corresponding for samples Cr + Ox + 1/2Co and Cr + Ox + Co in Figure 6.3(a), it is obvious that adding Co to the TCC treatment solution increased the Z_{real} (the x-axis of Nyquist plot, which is measured by the total diameter of the semicircle) by 15 and 30 factors, respectively.

Figure 6.5 shows the evolution of the impedance and the phase angle on frequency for the Zn surface in the non-coated condition and after TCC treatment in NaCl

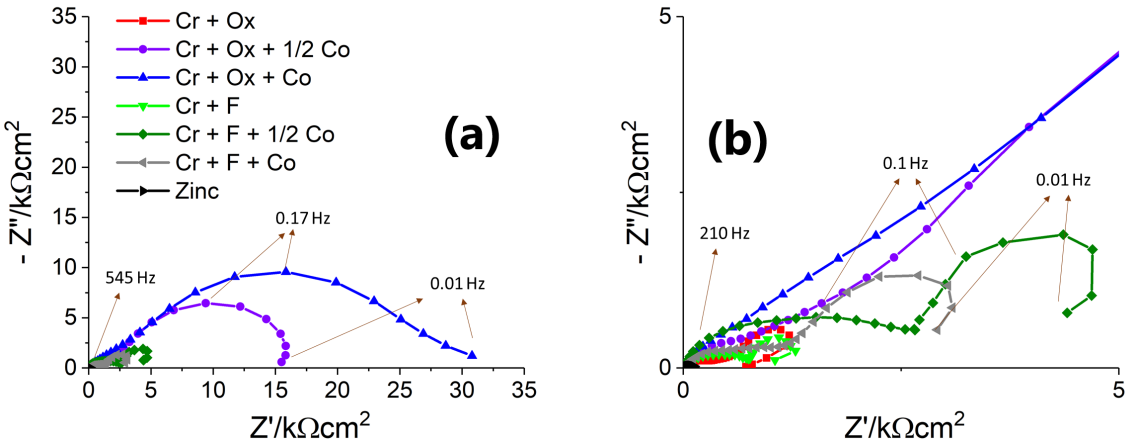

Figure 6.3 Nyquist plots of EIS data for the Zn and TCC-passivated-Zn surfaces (samples 1 to 6 in Table 3.2) with the immersion time of 60s in 3.5 wt% NaCl solution, (a) shows impedance spectra in their highest range (up to 35 kΩcm^2), (b) is a zoom-in of impedance spectra (Z_{real} and $Z_{imaginary}$) up to 5 kΩcm^2

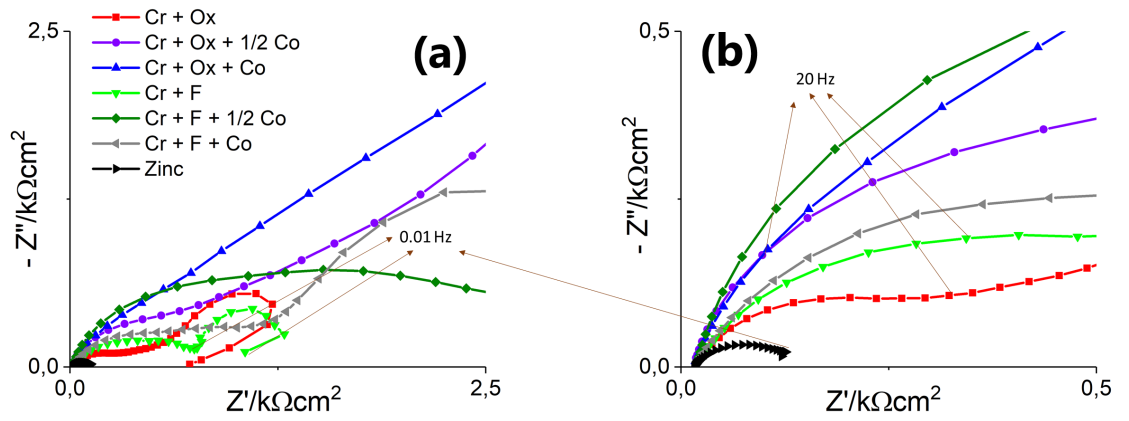

Figure 6.4 Nyquist plots of EIS data for the Zn and TCC-passivated-Zn surfaces (samples 1 to 6 in Table 3.2) with the immersion time of 60s in 3.5 wt% NaCl solution, a zoom-in of impedance spectra, (Z_{real} and $Z_{imaginary}$), (a) up to 2.5, (b) up to 0.5 kΩcm^2

solution. In Bode plots, a lower value of impedance at low frequencies represent a poorer coating protection [217, 218]. It can be clearly seen that TCC coatings improve the corrosion resistance of the zinc surface (e.g. from 0.1 $k\Omega cm^2$ for zinc surface to almost 1 $k\Omega cm^2$ for Cr + Ox and Cr + F samples). The Bode plots of TCC coatings show at least two time constants at high- and low frequencies that were attributed to the change in morphology of the layer [80, 122]. It is reported that the time constant at high frequencies is related to pores and defects in the film [68, 126], and is independent of the kinetics of the Faradaic process at the electrode [219]. The low-frequency time constant is determined by the Faradaic kinetics [219] and is ascribed to the charge transfer reaction dealing with TCC conversion coatings [41, 67, 68, 126]. Two RC elements were also interpreted as the outer and inner layers of the conversion coating [68]. In Section 5.1.1, it was shown that TCC coatings were composed of an outer thin barrier layer plus an inner thicker layer with a porous structure (Figures 5.1 and 5.4). Therefore, in this study, the higher frequency time constant in the Bode plots is attributed to the porous outer TCC layer, and the one for lower frequencies is ascribed to the inner TCC layer.

It is reported that the phase angle in the Bode plot at high frequencies correlate the roughness of the electrode surface, in a way that the lower phase angle in this region suggests a higher surface roughness of the outer layer [220]. Figure 6.5(b) shows higher (absolute) phase angles for the layers formed in the Co-containing treatment solution (e.g. Cr + Ox + 1/2Co, Cr + F + 1/2Co, and Cr + Ox + Co), which implies a lower roughness value for these films. This outcome is matching the roughness values which were obtained by AFM (Section 5.1.2).

In Figure 6.5(b), all phase angles are below 90°, such behaviour suggests a deviation from the behaviour of an ideal capacitor [122]. That is ascribed to the inhomogeneity of the film and distributed values for diffusion coefficients [219]. Using a Constant phase element (CPE) is suggested as considering the heterogeneities of systems (i.e. porosity or defects of the layers and interfaces) [221]. Therefore, a CPE was used for fitting the electrochemical impedance spectra with a non-ideal behaviour of capacitance [222]. The impedance of a CPE is given by

$$Z = \frac{1}{(j\omega)^{\mathrm{n}} Q} \tag{6.1}$$

In Equation 6.1, Q is the CPE parameter, ω is the angular frequency (rad/s), j^2 = -1 is the imaginary number, and n is the intensity of deviation from an ideal system and is the CPE exponent [223, 224].

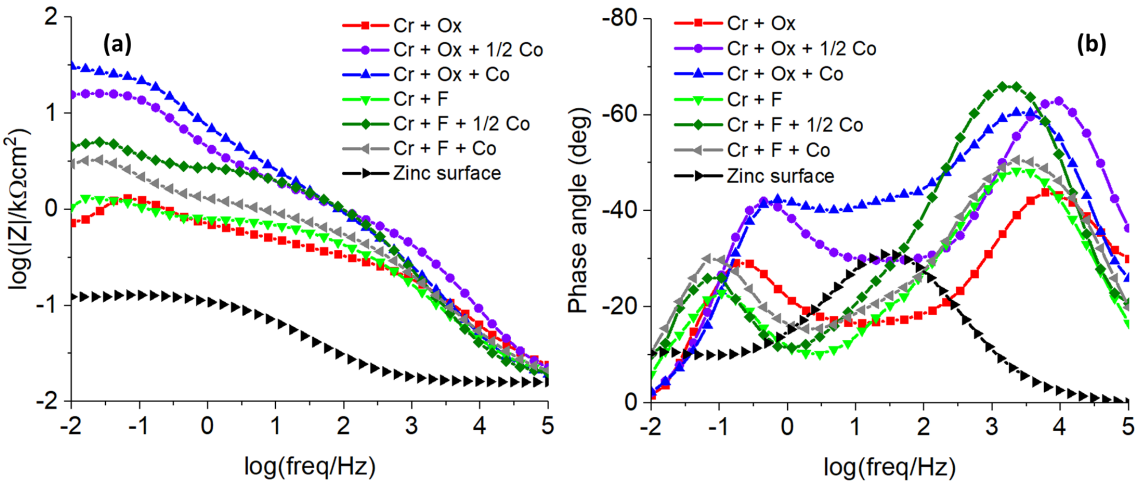

Figure 6.5 Bode plots of Zn and TCC passivated specimens (samples 1 to 6 in Table 3.2) with the immersion time of 60s in 3.5 wt% NaCl solution shows the dependence of (a) impedance and (b) phase angle versus frequency

One of the main challenges in EIS data analysis is to find a suitable Electrochemical equivalent circuit (EEC), and parameters that represent the analysed system. The EEC has to be coherent with the morphological information. The physical model and corresponding electrochemical equivalent circuit models that formed the basis of this analysis are shown in Figure 6.6. In the case of a zinc surface, the characteristic shape of the Bode diagram suggests that the corrosion of Zn-plated steel is a charge transfer-controlled reaction (one time-constant model) [225]. Therefore, the data for the (bare) zinc surface was fitted using a simple EEC (Figure 6.6 (a)) consisting of ohmic resistance in the bulk solution (R_e), and a parallel combination of a CPE (Q_{dl}), and the charge transfer resistance (R_{ct}). R_{ct} and Q_{dl} illustrate the corrosion process taking place at the metal (Zn) substrate/electrolyte interface [82, 226].

The EEC for the TCC coated specimens (Figure 6.6 (b)) included an additional pore resistance of the coating ($R_{coating}$) and a CPE ($Q_{coating}$) that represents the coating (outer layer)/solution interface, while the metal (Zn) substrate/coating (inner layer) interface is represented by a parallel combination of Q_{dl} and R_{ct} [217, 227].

Electrical parameters obtained by fitting the experimental results of EIS analysis to the EEC shown in Figure 6.6 are listed in Table 6.5. As can be seen, the solution resistance, R_e is almost the same for all the samples. $R_{coating}$ represents the resistance of the solution down the pores of an outer TCC layer (the corrosion protection of the outer layer of TCC film). When the values of $R_{coating}$ for samples Cr + Ox and Cr + Ox + 1/2Co in Table 6.5 are compared, it can be seen that the addition of Co improved the $R_{coating}$ from 0.53 to 3.61 kΩcm^2. Besides, R_{ct} that is ascribed to the corrosion resistance of the inner TCC layer was increased from 1.67 (for Cr + Ox) to 26.90 (for Cr + Ox + Co) kΩcm^2. In addition, for all TCC coatings except for the Cr + F, $R_{coating}$ is significantly less than the corresponding values for the resistance of the inner TCC layer (R_{ct}) (e.g. for Cr + F + Co, $R_{coating}$ is 0.93 kΩcm^2 and R_{ct} is 3.04 kΩcm^2). This finding is consistent with the fact that except for the sample Cr + F, which had a relatively porous structure of the inner and outer layer, the inner layer of TCC coatings were thicker with fewer defects (Figures 5.1 and 5.4). Furthermore, considering the AES depth profiling images (Figure 5.8), it can be noticed that in the first 20-40 nm of a TCC coating, the amount of Cr is low. The Cr content is the highest in a distance between 20-200 nm for Ox-containing samples, and 20-300 nm for F-containing samples from the surface. In general, Cr species in a TCC layer contribute to the corrosion protection properties of the film. Therefore, it is obvious that the inner layer played the major role in the protective properties of the coatings [39]. In general, for layers formed in TCC treatment solutions with the same complexing agent, those containing Co have higher $R_{coating}$ and R_{ct} values. This suggests fewer defects in the films formed in the Co-containing solution.

In Equation 6.1, when n<1, the system behaviour is representative of a heterogeneous surface [224, 228]. In this case, the CPE parameter (Q) cannot be regarded as the capacitance. Studies showed that when the local resistivity varies noticeably over the thickness of a film, the effective capacitance can be derived by Brug formulas [222, 224, 228] (Equation 6.2).

$$C_{\text{eff}} = Q^{1/n}\left(\frac{R_e R_t}{R_e + R_t}\right)^{(1-n)/n} \tag{6.2}$$

In Equation 6.2, R_e is the global Ohmic resistance and R_t, Q, and n are global properties of the (under study) time constant [224].

Using Equation 6.2, the effective capacitance values for the low-frequency process (C_{dl}), and that for the high-frequency time constant ($C_{coating}$) were calculated (Table 6.6). The results show that the $C_{coating}$ values of the Zn-electroplated samples passivated in different TCC solutions are in general low, of the order of $\mu F/cm^2$. This was attributed to the presence of a thin TCC film [122, 229], here the outer TCC layer. The values associated with the double layer capacitance (C_{dl}) at the substrate/coating (inner layer) interface are of the order of mF/cm^2, which was attributed to the interfacial corrosion process [230], and the mass transport across the porous film [229]. It is reported that the corrosion products increase the interface area of the electrode, which results in larger values of C_{dl} [230, 231]. Furthermore, on heterogeneous surfaces of coated metals, water penetration, even at lower rates, leads to the change in the electrical constant of the layer, which also causes the increase of C_{dl} [219]. Therefore, for samples Cr + Ox + 1/2Co and Cr + Ox + Co with relatively packed film, and probably fewer corrosion products, the C_{dl} values are smaller in comparison to the corresponding for the other TCC coatings.

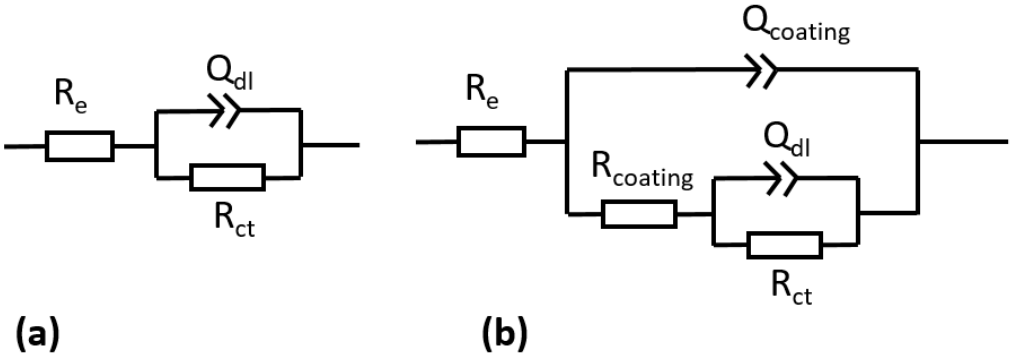

Figure 6.6 Electrochemical equivalent circuit used for (a) Zn surface, (b) TCC-passivated Zn surface, $R_e(Q_{coating}(R_{coating}(R_{ct}Q_{ct})))$

Taking the R_{ct} values from EIS analysis (Table 6.5) and I_{corr} values from Tafel extrapolation of polarization tests (Table 6.2) into account, it can be seen that the layers that formed in oxalate- and cobalt-containing solutions have the lowest corrosion current density (I_{corr}) and the highest charge transfer resistance (R_{ct}). Therefore, both polarization and EIS measurements suggest that these layers have a higher barrier effect of conversion coating compared with the other TCC films. The Stern-Geary equation (Equation 6.3) introduces the direct relationship between

Table 6.5 Parameters of TCC coating/Zn systems obtained from fitting EIS data using a R(Q(R(QR))) equivalent circuit for the passivation of Zn for 60s, data are presented as the average ± standard error of ten measurements

	R_e	$R_{coating}$	R_{ct}	$Q_{coating}$	Q_{dl}	$n_{coating}$	n_{dl}
		($k\Omega cm^2$)		($\mu F.s\widehat{}(n-1)/cm^2$)			
Zn	0.017 ± 0.003		0.14 ± 0.01		$(4.89 \pm 1.64)\times10^{2}$		0.67 ± 0.05
Cr + Ox	0.018 ± 0.002	0.53 ± 0.01	1.67 ± 0.04	7.50 ± 0.65	$(1.62 \pm 0.43)\times10^{3}$	0.60 ± 0.04	0.79 ± 0.08
Cr + Ox + 1/2 Co	0.017 ± 0.002	3.61 ± 0.09	20.20 ± 1.06	6.95 ± 0.74	$(5.30 \pm 0.90)\times10^{1}$	0.68 ± 0.07	0.81 ± 0.07
Cr + Ox + Co	0.016 ± 0.003	1.27 ± 0.13	26.90 ± 0.99	4.04 ± 0.73	$(4.30 \pm 0.62)\times10^{1}$	0.74 ± 0.03	0.85 ± 0.02
Cr + F	0.017 ± 0.001	0.84 ± 0.05	0.69 ± 0.12	$(1.20 \pm 0.31)\times10^{1}$	$(2.74 \pm 0.14)\times10^{3}$	0.61 ± 0.03	0.64 ± 0.04
Cr + F + 1/2 Co	0.016 ± 0.003	2.26 ± 0.21	2.50 ± 0.19	3.82 ± 0.72	$(6.39 \pm 1.35)\times10^{2}$	0.79 ± 0.03	0.83 ± 0.11
Cr + F + Co	0.017 ± 0.002	0.93 ± 0.05	3.04 ± 0.28	$(1.14 \pm 0.48)\times10^{1}$	$(2.87 \pm 1.49)\times10^{3}$	0.67 ± 0.05	0.78 ± 0.12

Table 6.6 Effective capacitance calculated for the constant phase element values in Table 6.5

	$C_{coating}$	C_{dl}
	($\mu F/cm^2$)	
Zn		$(1.82 \pm 0.99) \times 10^3$
Cr + Ox	2.34 ± 0.32	$(4.08 \pm 1.38) \times 10^3$
Cr + Ox + 1/2 Co	2.54 ± 0.08	$(5.16 \pm 1.07) \times 10^1$
Cr + Ox + Co	1.73 ± 0.27	$(4.08 \pm 0.68) \times 10^1$
Cr + F	4.04 ± 1.71	$(2.26 \pm 0.18) \times 10^4$
Cr + F + 1/2 Co	2.24 ± 0.49	$(1.19 \pm 0.3) \times 10^3$
Cr + F + Co	5.09 ± 2.48	$(9.27 \pm 3.67) \times 10^3$

the steady-state corrosion current (I_{corr}) and the DC polarization resistance (R_{pol}), across the interface [219].

$$R_{pol} = \frac{1}{2.303 I_{corr}} \frac{\beta_a \beta_c}{\beta_a + \beta_c} \tag{6.3}$$

In Equation 6.3, β_a and β_c are the Tafel coefficients for the anodic and cathodic partial reactions. In the case of steady-state corrosion (when the rate of corrosion does not change with time), the polarization resistance is identical to the charge-transfer resistance [219]. Subsequently, I_{corr} can be identified at the low-frequency range of the impedance spectrum. In this study, the I_{corr} calculated from EIS data at low frequencies was not the same as the I_{corr} that were obtained from Tafel extrapolation (Table 6.2), although the trend was the same. This might relate to the fact that the electrochemical reaction of the low-frequency time constant was not solely kinetically-controlled. The most common complications were reported as followings: (1) oxidation or reduction of some other electroactive species besides the corroding metal, (2) a change in the open-circuit or corrosion potential throughout the time taken to perform the measurement, (3) both the anodic and cathodic reactions are not charge transfer-controlled processes [232].

6.4 Composition of corrosion products

Figure 6.7 shows a SEM micrograph of a TCC treated sample (Cr + Ox + Co) after 48 hours exposed in the NSS chamber with 5 wt% of NaCl. This figure indicates the initiation of white rust on a micro-scale. The image exhibits the beginning of corrosion with the formation of the flower-like microstructures (possibly ZnO). The EDXS analysis was performed to identify the composition of these microstructures. Table 6.7 lists the composition of a flower-like microstructures at two different positions (spot 1 and spot 2 in Figure 6.7), and the composition of a point outside of a flower-like microstructures (spot 3 in Figure 6.7). These spots are mainly composed of Zn, Cr, O, and C. However, the amount of Zn is lower on the flower-like microstructures, while its oxygen amount is higher in comparison to the composition of spot 3 in Figure 6.7.

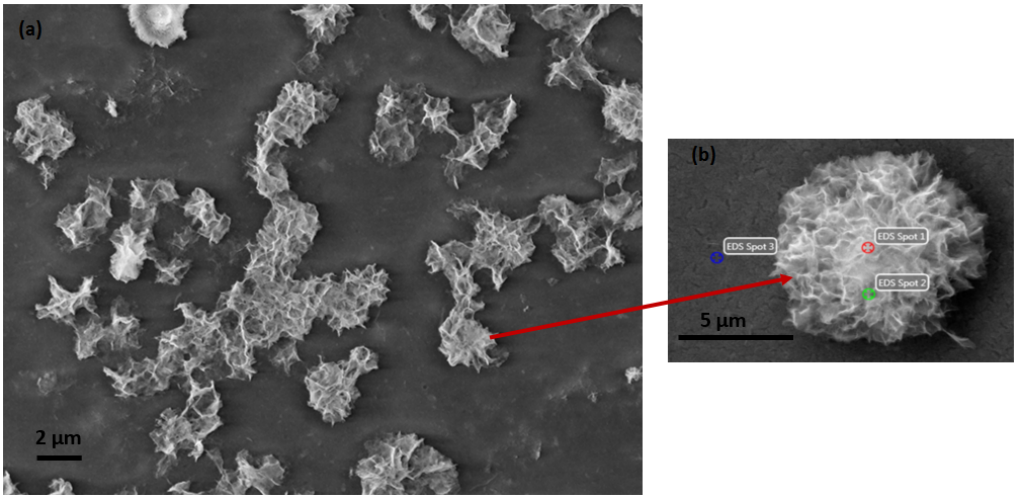

Figure 6.7 Top surface view of a TCC treated sample (Cr + Ox + Co) taken by SEM with (a) lower and (b) higher magnification after 48 hours exposed in NSS chamber with 5 wt% of NaCl

6.5 Contact angle

Surface wetting behaviour can conventionally be broken into two regimes based on the value of the water contact angle. The contact angle of $10° < \theta_a < 90°$ is

Table 6.7 EDXS analysis of (a) a flower structure on the TCC surface (spot 1 and 2 shown in Figure 6.7) and a spot outside of a flower-like structure on the TCC surface (spot 3 shown in Figure 6.7)

	Atom%		
Element	**Spot 1**	**Spot 2**	**Spot 3**
Zn	26	34	71
Cr	1	1	1
O	52	49	17
C	21	17	11

defined as hydrophilic, and $90° < \theta_a < 150°$ as the hydrophobic regimes. Increasing surface hydrophobicity reduces the corrosion rate of the metal by restricting their interactions with corrosive compounds like water and various ions. Hydrophobic coatings used in many engineering applications because they retard the diffusion of water into the coating [233].

Table 6.8 lists the contact angle values of water drop on TCC coatings formed in different treatment solution (sample 1 to 8 in Table 3.2) after immersion time of 60 s. The same water contact angle for right and left denotes a homogenous TCC film surface. Moreover, the results showed that the water contact angle of the samples 1 to 8 varied from 99 to 107 °. Therefore, all contact angles are $\theta_a > 90°$, implying a hydrophobic surface. Figure 6.8 shows a side view of a water droplet on a TCC film while fitting with the sessile drop method the contact angle which represents a hydrophobic surface.

Corrosion protection offered by a coating depends on its composition, structure, and thickness of the film, which principally affect oxygen and water permeability, as well as bonds between the coating and substrate. The formation of a close-packed, thick and hydrophobic film on a metal substrate can hinder corrosion by retarding the transport of uncharged compounds (i.e. water and oxygen) and charged species (ions) [234, 235].

Table 6.8 Contact angle of water drop on films formed in different TCC treatment solution after an immersion time of 60 s

No.	Specimen	Theta(M)[deg]	System	Theta(L)[deg]	Theta(R)[deg]
1	Cr + Ox	103.0 ± 0.1	Water	103.0 ± 0.1	103.0 ± 0.1
2	Cr + Ox + 1/2Co	104.7 ± 0.7	Water	104.7 ± 0.7	104.7 ± 0.7
3	Cr + Ox + Co	100.3 ± 0.6	Water	100.3 ± 0.6	100.3 ± 0.6
4	Cr + F	100.7 ± 1.2	Water	100.7 ± 1.2	100.7 ± 1.2
5	Cr + F + 1/2Co	101.2 ± 1.0	Water	101.2 ± 1.0	101.2 ± 1.0
6	Cr + F + Co	99.0 ± 0.2	Water	99.0 ± 0.2	99.0 ± 0.2
7	2Cr + 2Ox	105.1 ± 0.2	Water	105.1 ± 0.2	105.1 ± 0.2
8	2Cr + 2Ox + Co	107.3 ± 0.4	Water	107.3 ± 0.4	107.3 ± 0.4

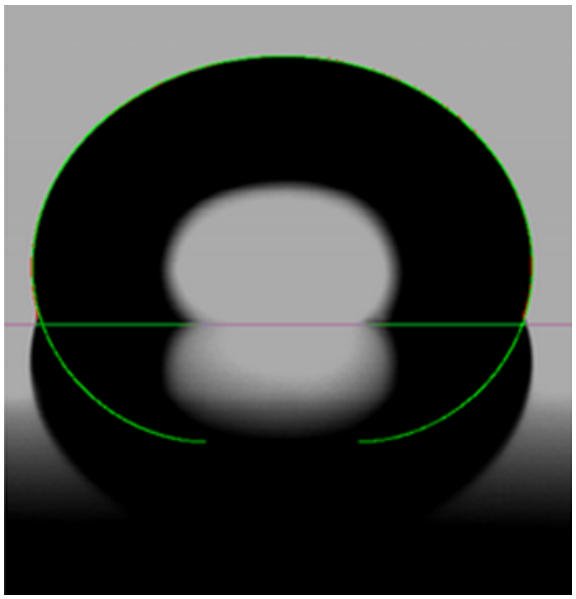

Figure 6.8 Side view of a drop of water on a TCC film

7 Formation of Cr(VI) in the Layers Produced in Cr(III)-based Treatment Solution Containing Cobalt

7.1 Introduction

As it was mentioned earlier, the oxidation of Cr(III) to Cr(VI) in the TCC films causes a lot of controversy surrounding these layers as being compatible with the European directives (Section 2.1). In this chapter, the formation of Cr(VI) in the TCC layers will be discussed.

The potentially occurring half-reactions influencing the formation of Cr(VI) that were suggested in the literature [45] with their standard potentials in an alkaline environment [96] are as follows;

$$O_2 + 2H_2O + 4e^- \rightleftarrows 4OH^- \qquad E^\circ = 0.401\,V \tag{7.1}$$

$$CrO4^{2-} + 4H_2O + 3e^- \rightleftarrows Cr(OH)4^- + 4OH^- \qquad E^\circ = -0.13\,V \tag{7.2}$$

$$CrO_4{}^{2-} + 4H_2O + 3e^- \rightleftarrows Cr(OH)_3\,(ppt) + 5OH^- \qquad E^\circ = -0.11\,V \qquad (7.3)$$

Obviously, the standard potential of oxygen reduction (Reaction 7.1) is higher than the oxidation potential of Cr(III) to Cr(VI) (Reaction 7.2 and 7.3). This suggests that Cr(III) can be oxidized to Cr(VI) in the presence of oxygen and water in alkaline conditions.

The proposed reason [47] behind the enhancement of Cr(III) oxidation in the presence of cobalt is that, under certain circumstances, divalent cobalt is oxidized to the trivalent state (Reaction 7.4), at a more cathodic potential compared with the oxygen reduction potential [96].

$$Co(OH)3 + e^- \rightleftarrows Co(OH)2 + OH^- \qquad E^\circ = 0.17\,V \qquad (7.4)$$

Besides, because Co(III) is not stable in an aqueous solution, it may take electrons from Cr(III) and this leads to the oxidation of Cr(III) to Cr(VI). However, the problem associated with this hypothesis is that all the reactions are assumed to take place in an alkaline environment. It is noteworthy that the above-mentioned arguments are only based on thermodynamics and kinetics was not considered. To shed some light on the formation of Cr(VI) in TCC coatings, the following steps were accomplished.

7.2 Preparation of samples

For these measurements, the model solutions 1, 3, 4, and 6 in Table 3.2 were chosen. The zinc electroplated steel parts were immersed in these TCC treatment solutions at 40°C for 60 seconds. Conversion coatings might be used in areas where elevated temperatures close to 200°C are expected. Therefore, to examine the formation of

Cr(VI) in heat-treated coatings, the as-prepared specimens were heat-treated for 6 hours at 210°C.

7.3 Experimental techniques

To be able to determine whether a TCC coating contains hexavalent chromium, it is necessary to apply methods that are sensitive to the oxidation state of Cr(III). One of the suggested methods (so-called boiling test) is where the piece is extracted for a defined time in DI water at its boiling point temperature [236]. Another method is to expose the sample in an accelerated corrosion test condition in the absence of a strong oxidizing agent [46, 47]. Therefore, to extract the possible formed hexavalent chromium in the TCC coatings, the boiling test (Section 7.3.1) and accelerated corrosion test in a NSS chamber (Section 7.3.2) were performed.

7.3.1 Screening boiling test

The pieces with a surface area of (50 ± 5) cm^2, were extracted in DI water at its boiling point temperature. The sample was placed on a bed of anti-bumping granules inside a graduated beaker filled with 100 ml water (Figure 7.1). The beaker was covered with a watch glass, and the sample was boiled for 10 minutes. Then, the beaker was removed from the hot plate and kept at ambient temperature to cool down. To determine Cr(VI) in the extracted solution, the colorimetric method using UV-VIS following DIN EN 15205 [237] was performed. Solutions were transferred to a 100 ml volumetric flask to be prepared for the UV-VIS measurements (Section 7.3.3.1). Besides, with the same procedure for the preparation of samples, the total chromium amount in the extracted solutions was measured using ICP-OES (Section 7.3.3.2).

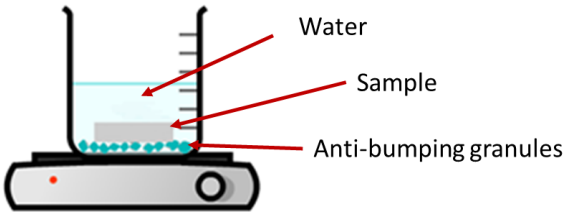

Figure 7.1 Schematic representation of screening boiling test, the samples were placed on anti-bumping granules and extracted for 10 minutes at the boiling point of water

7.3.2 Corrosion test

To investigate the influence of the NSS cabinet environment on the formation of hexavalent chromium in TCC treated samples, a NSS cabinet (according to ASTM-B117 [48]) was used. The TCC passivated samples were placed above a funnel mounted on a 100 ml Erlenmeyer flask and the assemblies were kept in the salt spray cabinet (Figure 7.2) for 24 hours. The extracted solutions from the surfaces of specimens that were collected in each Erlenmeyer flask during this time were examined for the presence of hexavalent chromium with UV-VIS (Section 7.3.3.1).

With the same procedure for the preparation of samples, the total chromium amount of the collected solutions was detected with ICP-OES (Section 7.3.3.2).

7.3.3 Analytical methods used for the determination of hexavalent chromium

7.3.3.1 Ultraviolet-visible spectrophotometry

In order to determine Cr(VI) in the extracted solutions, UV-VIS was used according to the description that was explained in Section 3.2.2.5. Diphenyl carbazide solution, Cr(VI) standard solution, and ortho-phosphoric acid (85%) were all prepared following DIN EN 15205 [237]. All chemicals were reagent grade and were obtained from Carl Roth GmbH + Co KG. Calibration solutions were prepared from different concentrations of Cr(VI) standard solution (0.02, 0.04, 0.06, 0.08, 0.1, 0.12) mg/l in a 100 ml volumetric flask, adding 1 ml phosphoric acid, 1 ml of diphenyl carbazide

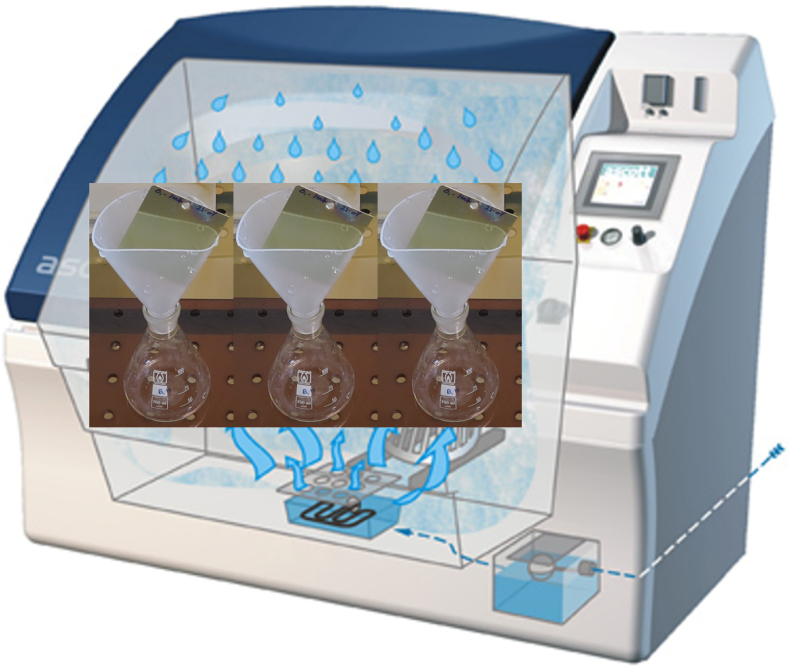

Figure 7.2 Schematic representation of specimen assembly inside the NSS cabinet, samples were placed above a funnel mounted on a 100 ml Erlenmeyer flask inside the NSS cabinet

solution, and mixed thoroughly. After 10 minutes the reaction was complete and the values required for the absorbance-concentration calibration curve were measured. The above-mentioned procedures also were accomplished for the test solutions, and their Cr(VI) concentration was measured interpolating from the calibration curve. An obtained value higher than $0.1\,\mu g\,cm^{-2}$ is an indication of hexavalent chromium in the solution. As a control experiment, a non-passivated zinc layer was also boiled in water and no hexavalent chromium was detected when its extracted solution was tested.

7.3.3.2 Inductively coupled plasma optical emission spectroscopy

The ICP-OES (as described in Section 3.2.2.2) was used to calculate Cr amount in the extracted solutions obtained by screening boiling (Section 7.3.1) test and corrosion test (Section 7.3.2) for the heat-treated TCC passivated samples. The

results presented herein are for total Cr, because this technique cannot distinguish between the oxidation states of an analyte species (here Cr(III) and Cr(VI)) [238].

7.4 Determination of Cr(VI) species

7.4.1 Ultraviolet-visible spectrophotometry

The absorbance-concentrations calibration curve was plotted with a correlation coefficient, $R^2 = 0.999 \pm 0.001$ (Figure A.1 in Appendix, Section 2). Next, the hexavalent chromium concentration in solutions was determined, interpolating from the calibration curve. Figure 7.3 shows the results of UV-VIS for extracted solutions prepared by screening boiling test (described in Section 7.3.1) for the as-prepared and heated TCC passivated samples. It can be seen that the Cr(VI) content in the solution obtained from all as-prepared TCC coatings was less than $0.1\,\mu g\,cm^{-2}$. This implies that Cr(VI) was not detected in these layers. This observation also goes for the extracted solutions obtained from heat-treated samples, formed in oxalate-containing TCC solution (Cr + Ox and Cr + Ox + Co). Nevertheless, Cr(VI) was detected in the extracted solutions from the layers that were formed in fluoride-containing electrolytes and were heat-treated (heated Cr + F and Cr + F + Co in Figure 7.3, with Cr(VI) amount $> 0.1\,\mu g\,cm^{-2}$).

Figure 7.4 indicates the UV-VIS results for condensate solutions from as-prepared and heated samples after keeping specimens in the NSS cabinet for 24 hours (preparation was described in Section 7.3.2). It is obvious that the level of hexavalent chromium in the extracted solutions from the as-prepared and heated samples formed in oxalate-containing TCC solution (as-prepared and heated Cr + Ox and Cr + Ox + Co) was less than $0.1\,\mu g\,cm^{-2}$. Therefore, in good agreement with results that were seen in Figure 7.3, Cr(VI) was not found in these layers. For the obtained solutions from the as-prepared samples formed in fluoride-containing TCC electrolytes (as-prepared Cr + F and Cr + F + Co in Figure 7.4), the same result was yielded. However, Cr(VI) was clearly observed in the obtained solution from heat-treated TCC layers formed in the fluoride-containing treatment solution (detected Cr(VI) amount was $> 0.1\,\mu g\,cm^{-2}$) (heated Cr + F and Cr + F + Co in Figure 7.4). These

results were in accordance with the results gained from the screening boiling test (Figure 7.3).

Consequently, the sharp increases in the concentration of Cr(VI) for the TCC layers formed in fluoride-containing treatment solutions were ascribed to the heat treatment procedure. Whereas, the process of heat treatment seems to have no influence on the formation of Cr(VI) in TCC layers formed in oxalate-containing treatment solutions.

In both cases of extraction of solutions by screening boiling test (Figure 7.3) and corrosion test (Figure 7.4), a less amount of Cr(VI) was observed when the layer was formed in the TCC solution containing cobalt and fluoride (Cr + F + Co in Figures 7.3 and 7.4).

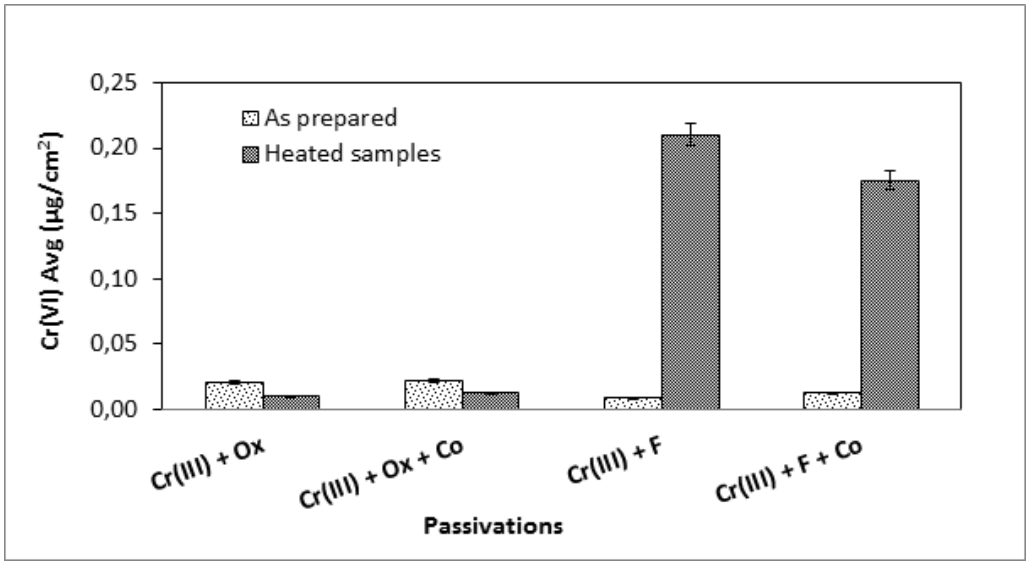

Figure 7.3 Determination of Cr(VI) via UV-VIS for the extracted solutions from screening boiling test (preparation was described in Section 7.3.1) for as-prepared and heated TCC-treated samples

7.4.2 Inductively coupled plasma optical emission spectroscopy analysis

Total chromium amount in the extracted solutions obtained by screening boiling test (described in Section 7.3.1) and corrosion test (described in Section 7.3.2) was

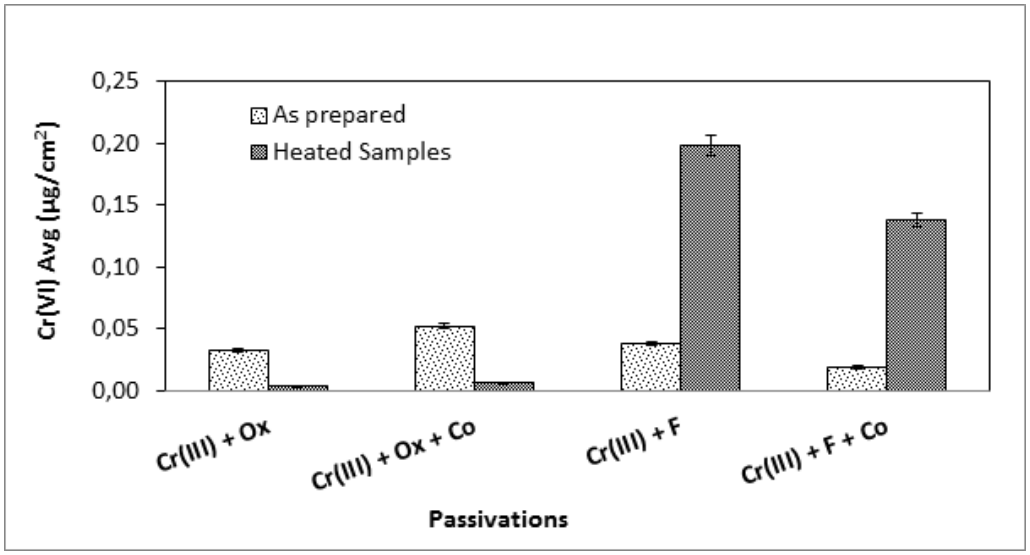

Figure 7.4 Determination of Cr(VI) via UV-VIS for the extracted solutions from as-prepared and heated samples after keeping samples in the NSS cabinet after 24 hours (preparation was described in Section 7.3.2)

analysed using ICP-OES for the TCC treated samples that were heated in the forced air convection oven (MEMMERT oven (Memmert GmbH + Co. KG)). Table 7.1 lists the total amount of Cr(III) and Cr(VI) for the extracted solutions. For either of the extraction methods (screening boiling test and corrosion test), the total Cr amount that was detected in obtained solutions from heat-treated layers formed in oxalate-containing TCC solutions (Cr + Ox and Cr + ox + Co) was lower than the limit of detection. Nevertheless, traces of chromium were found in obtained solutions from heat-treated TCC coatings formed in fluoride-containing treatment solutions. The outcome of ICP-OES measurements demonstrated that in both cases of screening boiling test (Table 7.1 (a)) and corrosion test (Table 7.1 (b)), a less amount of chromium was detected in the extracted solution from the coating that was formed in the TCC treatment solution including cobalt (Cr + F + Co). This result was also demonstrated by UV-VIS results (Cr + F + Co in Figures 7.3 and 7.4).

Table 7.1 Total chromium amount in the extracted solutions obtained by (a) screening boiling test, (b) corrosion test analysed via ICP-OES for the TCC passivated samples that were heated in the forced convection oven

	Detected Cr ($\mu g\,cm^{-2}$)	
Specimen	**(a)**	**(b)**
Cr + Ox	<LOD	<LOD
Cr + Ox + Co	<LOD	<LOD
Cr + F	0.29	0.26
Cr + F + Co	0.18	0.14

Remark: Limit of detection (LOD) is $0.05\,\mu g\,cm^{-2}$

7.4.3 Influence of oxygen on the formation of Cr(VI) in TCC coatings

The results (Section 7.4.1 and Section 7.4.2) relate the presence of hexavalent chromium in TCC coatings to the composition of the treatment solution and the process of heat treatment.

Referring to the Section 7.1, and comparing the standard reduction potential of Reactions 7.1 to 7.2 and 7.3, the more positive value of E° for the $O_2\backslash H_2O$ couple in comparison to the reduction of Cr(VI) to Cr(III) suggests that the presence of water and oxygen may facilitate the oxidation of Cr(III) to Cr(VI).

To assess the role of oxygen in the oxidation of Cr(III) to Cr(VI), the heat-treatment process was carried out in the absence of oxygen using a nitrogen-purged oven (VACUCELL MMM Group). Afterwards, the screening boiling test (Section 7.3.1) and the corrosion test (Section 7.3.2) were performed to prepare the required solutions for the rest of the examinations. The presence of Cr(VI) in the obtained solutions were determined using UV-VIS. Table 7.2 lists the results. As can be seen, Cr(VI) was not detected in any of the extracted solutions from TCC layers that were heated in a nitrogen-purged oven. This outcome clearly proved that O_2 presence influenced the oxidation of Cr(III) species.

Moreover, for the specimens passivated with fluoride-containing TCC treatment solution, a discolouration was observed after heat treatment in the forced air convec-

Table 7.2 Determination of Cr(VI) by UV-VIS for extracted solutions obtained by (a) screening boiling test (b) corrosion test for the heat-treated TCC layers, when the heat treatment was done in nitrogen-purged oven

	Avg Cr ($\mu g\,cm^{-2}$)	
Specimen	**(a)**	**(b)**
Cr + Ox	<LOD	<LOD
Cr + Ox + Co	<LOD	<LOD
Cr + F	<LOD	<LOD
Cr + F + Co	<LOD	<LOD

Remark: Limit of detection (LOD) is $0.1\,\mu g\,cm^{-2}$

tion oven, while no colour change was noticed when heat treatment was done in the nitrogen-flushed oven (Figure 7.5). This suggests that oxygen as an oxidizing agent played the role in the discolouration of the TCC film during heat treatment.

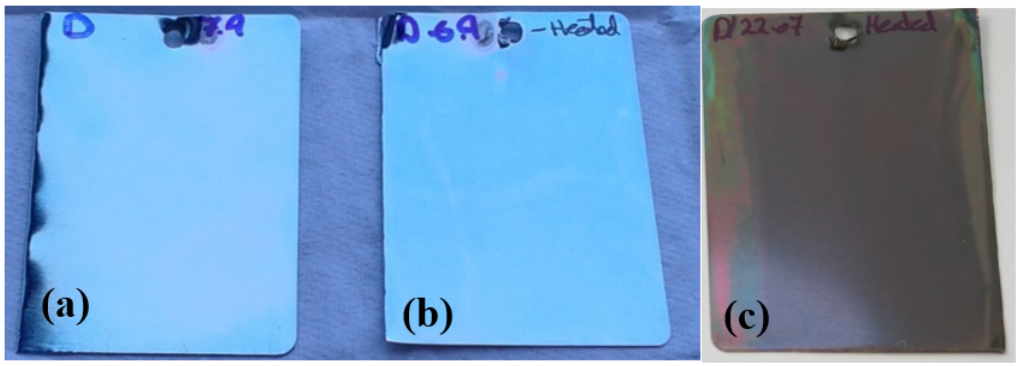

Figure 7.5 Images of TCC layers formed in Cr + F + Co treatment solution, (a) as-prepared, (b) Heat-treated in N_2 purge oven (c) Heat-treated in airflow oven

7.5 Water content of coatings

For oxygen reduction to take place, water is needed (Reaction 7.1). To determine trace amounts of water in the TCC layers, cKFT analysis was used. Table 7.3 lists the water contents of the specimens. It can be observed that more amount of water was captured in the layers formed in the fluoride-containing TCC treatment solutions. As it is listed, Cr + F with 225 $mg\,m^{-2}$ and Cr + F + Co with 162

$mg\,m^{-2}$ had a higher water content in comparison to the one for layers formed in the oxalate-containing TCC treatment solution (e.g. 140 $mg\,m^{-2}$ for Cr + Ox with a higher amount of water). Additionally, for each of the complexing agents, the water content is less when Co was also present in the TCC bath (Cr + Ox + Co and Cr + F + Co with 117 and 162 $mg\,m^{-2}$ respectively).

Table 7.3 Water contents of the different TCC coatings

Specimen	**Water content**($mg\,m^{-2}$)
Cr + Ox	140
Cr + Ox + Co	117
Cr + F	225
Cr + F + Co	162

7.6 Morphology of coatings

Morphology and structure of TCC layers were discussed already in Sections 5.1.1 and 5.1.2. It was shown that the type of complexing agents as well as the presence of cobalt in the TCC treatment solution, had a great impact on the formation of a TCC layer (Section 5.4).

Figure 7.6 shows the FIB-SEM micrographs corresponding to the TCC layers studied in this part (chapter 7). As can be seen, in good agreement with the previous results (Section 5.1.1), the layers formed in the oxalate-containing treatment solutions (Figures 7.6 (a), (b)) show a uniform and relatively pore-free structure. In contrast, a non-uniform and porous morphology can be seen for the TCC coatings formed in the fluoride-containing treatment solutions (Figures 7.6 (c) and (d)).

Comparing Figure 7.6 (c) with (d), or (a) with (b), it is obvious that a significant improvement in the microstructure was obtained by adding cobalt to the treatment solution (as it was also observed in Section 5.1.1). The size and number of pores in the layers were diminished when the coating was formed in the Co-containing TCC treatment solution.

It is concluded that water was penetrated in the microstructural defects (micropores and voids) and was stored there until it evaporated at elevated temperatures. That is why, particularly for the coatings formed in TCC treatment solutions containing Co, a smaller amount of water was observed (Table 7.3). Hence, the higher number of microstructural defects filled with water increased the probability of oxygen reduction and Cr(III) oxidation. Therefore, a smaller amount of Cr(VI) was detected in the layer which was formed in the Co-containing TCC treatment solution (sample Cr + F + Co in Figures 7.3 and 7.4). Consequently, oxygen diffusion into the micropores filled with water promoted Cr(VI) formation. The higher number of micropores in TCC coatings formed in fluoride-containing solutions (Cr + F and Cr + F + Co) increased the interaction of water and oxygen in these layers that resulted in the formation of Cr(VI).

7.7 Discussion

The above-mentioned results in this chapter provided evidence that the formation of Cr(VI) does not depend on the presence of cobalt in the TCC treatment solution. Seemingly, what plays the role is the coating microstructure that varies based on the composition of the TCC treatment solution. The standard potentials of the probable half-reaction occurring on the TCC coating at high pH were depicted in the Reactions 7.1 to 7.3. The standard potentials of the probable half-reaction occurring on the TCC coating at low pH are as follows [96]:

$$HCrO_4^- + 7H^+ + 3e^- \rightleftarrows Cr^{3+} + 4H_2O \qquad E^\circ = +1.38\,V \tag{7.5}$$

$$Cr_2O_7^- + 14H^+ + 6e^- \rightleftarrows 2Cr^{3+} + 7H_2O \qquad E^\circ = +1.386\,V \tag{7.6}$$

$$O_2 + 4H^+ + 4e^- \rightleftarrows 2H_2O \qquad E^\circ = +1.23\,V \tag{7.7}$$

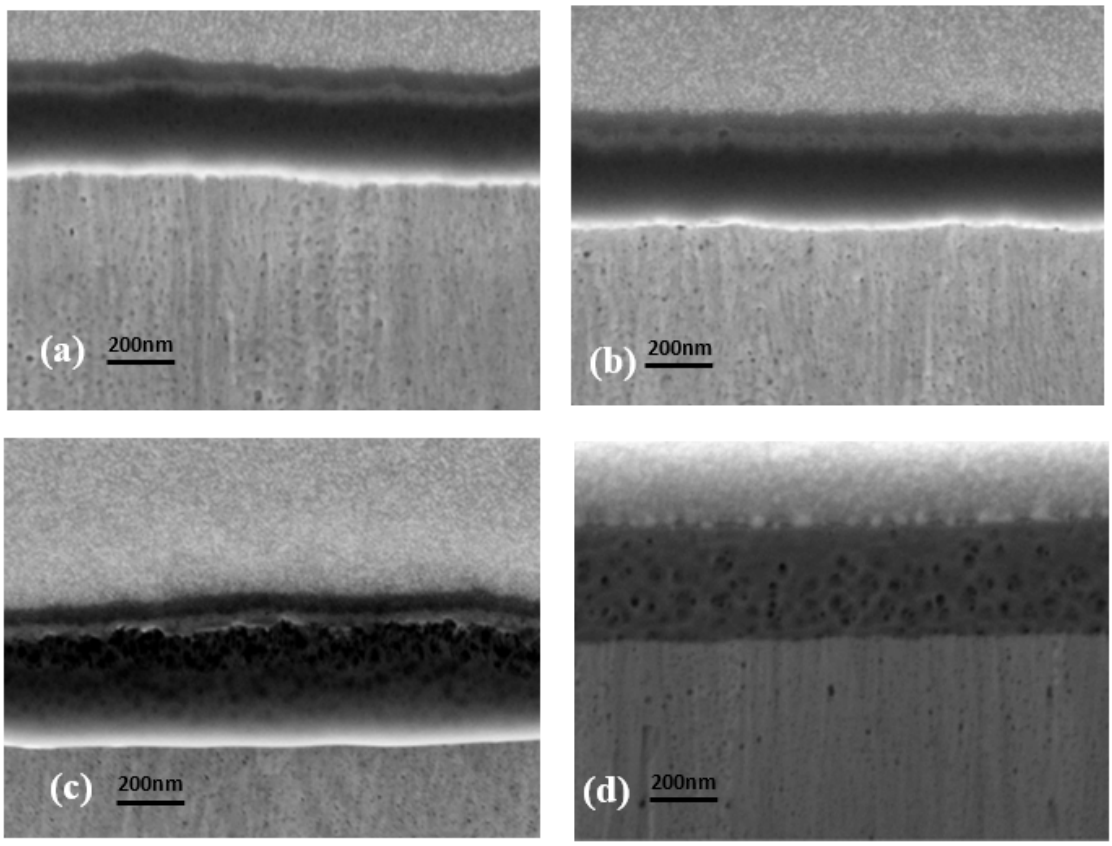

Figure 7.6 FIB-SEM images of the TCC coatings formed in the treatment solution with (a) Cr + Ox , (b) Cr + Ox + Co (c) Cr + F (d) Cr + F + Co, water traces were most likely entrapped in the microstructural defects

Figure 7.7 depicts the standard potential versus pH for oxygen reduction and chromium oxidation. As can be seen, the intersection of the lines for Cr and O_2 occurs around the pH value of 3. Consequently, above this pH value, the oxidation of Cr(III) to Cr(VI) by oxygen is thermodynamically possible.

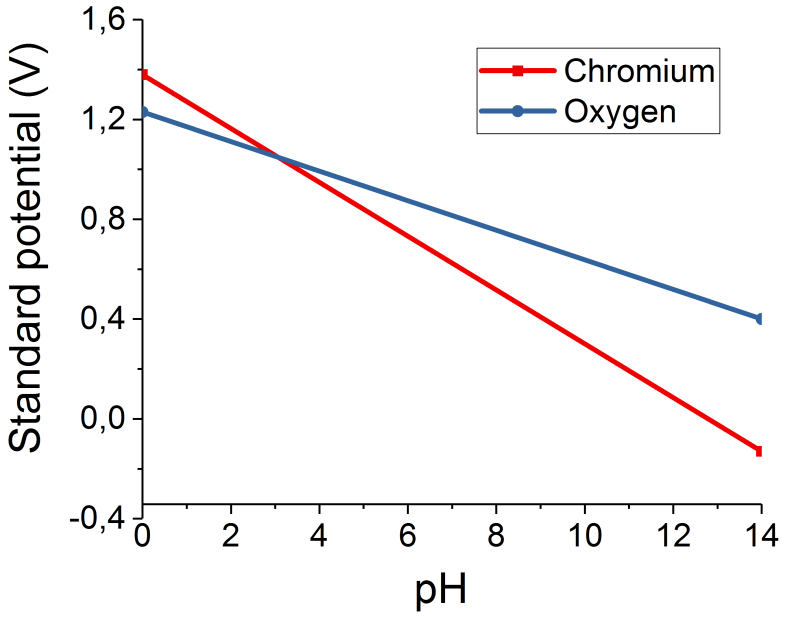

Figure 7.7 Standard potentials (V) of Chrome and Oxygen versus pH

The main compositions of the TCC treatment solutions are Cr(III) and the oxidizer which is mostly $NO3^-$. When the zinc-plated part is immersed in the TCC treatment solution, zinc oxidation (Reaction 5.1) and reduction of oxidizing agent (reactions shown in Table 5.7) can take place. These cathodic reactions (including nitrate reduction and possibly HER, as it was discussed in Section 5.4) induce a local pH rise. Studies exhibited 2-6 units' increase of interfacial pH depending on the coating system [185].

In addition, the AES results proved the deposition of Cr(III) on the Zn electroplated steel surface for all TCC treatment solutions (Figure 5.8). It was shown that a TCC coating is formed on the zinc surface by precipitation of Cr^{3+} and Zn^{2+} (free or complexed) ions present in the TCC solution (Section 5.3.2). Furthermore, as it was discussed in Section 5.4, Cr(III) ions start to deposit on the Zn surface when SI value

exceeds zero, and that would be at a pH around 4 as it was demonstrated in Figure 5.10.

Consequently, despite the fact that the TCC treatment solution had a pH value of 1.8 at the process commencement, a localized pH increase is expected during the TCC formation process. Therefore, it is very likely that the pH value in the microstructural pores of a TCC layer is above 3.1, which is the intersection point of the standard potential versus pH for Cr and O_2 lines in Figure 7.7.

In summary, taking the FIB-SEM images (Figure 7.6) into account, it is apparent that the composition of the treatment solution influenced the morphology and structure of the coating. During the heat-treatment process in a forced air convection oven, oxygen penetrated into the porous layers that were formed in the fluoride-containing TCC treatment solutions. Because these micropores were filled with water, the oxygen reduction that occurred there, facilitated the oxidation of Cr(III) to Cr(VI).

It can be concluded that the formation of Cr(VI) relates to the structure of the TCC layer rather than the presence of Co ion in the TCC solution. Therefore, the oxidation of Cr(III) to Cr(VI) in these layers seems to be independent of the presence of Co in the treatment solution.

8 Summary and Suggestions for Further Work

8.1 Summary of results

This thesis was aimed at understanding the role of constituents in the trivalent chromium-based conversion treatment solution on the formation of the film produced on the zinc-plated steel. A matrix of eight Cr(III)-based conversion model solutions with two different complexing agents, fluoride and oxalate, including and excluding Co was designed and applied on the zinc electroplated steel. One of the main goals of this work was to express the role of cobalt in the Cr(III)-based conversion treatment solution on the produced layers.

The first contribution of this work was to give an overview regarding the state of the art and the research that was already done surrounding Cr(III)-based conversion coatings (Chapter 2). After describing the material and methods that were used (Chapter 3), a short introduction was given on the structure and composition of the Zn-electroplated layer (Chapter 4). Then, the structure of formed layers was observed by a focused ion beam assisted with scanning electron microscope and an atomic force microscope (Sections 5.1.1 and 5.1.2). A comparison of the morphology and structure of the trivalent chromium-based conversion coatings formed in the treatment solutions, including and excluding Co, was performed (Section 5.1). Results obtained in the present study imply that the Cr(III)-based conversion coating is deposited in a layered structure, which is thinned through heat treatment. It was shown that the treatment solution composition (i.e. complexing agents used and the presence of Co) influences the formation of Cr(III)-based conversion coatings (Chapter 5). The

fluoro ligand produced a porous layer that was thicker, while oxalate made a thinner and yet more uniform film. The type of complexing agent plays an essential role in Cr(III) ions lability in the bath, and therefore, the deposition of this ion on the zinc surface (Section 5.4). Furthermore, the structure and corrosion protective properties of the film are influenced by the type of complexing agent used. Based on inductively coupled plasma atomic emission spectroscopy measurements, when fluoride was the complexing agent, more Cr was deposited on the zinc substrate; while, when oxalate was the complexant, more cobalt was incorporated into the coating (Section 5.3.1). The addition of cobalt to the Cr(III)-based treatment solution with either of the complexing agents resulted in a smoother layer. Cobalt might affect the kinetics of the film deposition throughout the conversion coating process (Section 5.4).

Moreover, microstructural defects in the layer formed in the fluoride-containing treatment solution were ascribed to the formation of gas bubbles (e.g. N_2O, N_2), locally interfering coating precipitation and prohibiting uniform deposition of metal hydroxides on the substrate. In contrast, oxalate ions act as a surfactant that improves wetting over the zinc substrate and prevents gas bubbles to adhere on the surface. It was also found that the thickness of the trivalent chromium conversion coatings increases with increasing immersion time to the point at which the competition between the growth of trivalent chromium conversion coating and Zn dissolution leads to an optimal film thickness (Section 5.4). In general, to produce a Cr(III)-based conversion coating, a competing substrate dissolution/film formation situation has to be established. Moreover, with the aid of a thermodynamic model, the pH at which the Cr(III), Co(II), and Zn(II) start to deposit was calculated (Figure 5.10).

Another contribution relies on the corrosion characteristics of the TCC films, in particular, those produced in the Co-containing TCC treatment solution, as discussed in Chapter 6. It was observed that the thicker coating does not necessarily better protect the film against corrosion. In general, TCC coatings protected the zinc substrate by reducing the cathodic and anodic current density, and shifting the corrosion potential (E_{corr}) to less cathodic values. Furthermore, it was also shown that adding Co to the TCC treatment solution resulted in the reduction of anodic (Zn dissolution) and cathodic reactions (oxygen or hydrogen reduction) on the Zn substrate. It is proposed that the formation of a dense layer with fewer cavities,

which is influenced by the type of anions in the treatment solution, is crucial for the corrosion resistance [239]. The corrosion properties of the layer was also evaluated using EIS. The advantage of EIS compared to polarization measurements is to obtain information about TCC layer properties, such as the presence of defects and reactivity of the interface. EIS analysis (Section 6.3) showed change in the morphology of a layer, which might suggest that the TCC coatings have layered structure (i.e. inner and outer layer). The inner layer of oxalate-containing TCC films are observed as less defective (Figure 5.1). The EIS analysis clearly indicated the protective properties of layers that were formed in Ox- and Co-containing TCC treatment solutions. Therefore, due to the less porous inner layer, the values of R_{ct} were higher for films formed in Ox-containing solutions.

After all, the influence of Co on the formation of Cr(VI) species in the trivalent chromium conversion coatings was studied (Chapter 7). It was shown that the formation of Cr(VI) in these layers was influenced by factors such as composition and operating conditions (e.g. temperature, and pH) of the passivating bath. Nevertheless, the stable valence state of chromium ions seemed to be independent of the cobalt presence. The microstructure of the TCC layer played a crucial role. Correspondingly, acquiring few microstructural defects, less porous morphology, and thinner TCC coating decreased in the susceptibility towards hexavalent chromium formation [214].

8.2 Future works

Future work related to the TCC coatings should address a deeper analysis of film formation mechanism and new suggestions to apply different characterization techniques. The matrix of treatment solutions can be varied and further developed to better understand the role of different constituents on the formation of TCC layers. In this respect, their structure and corrosion properties can be evaluated. The following ideas could be tested:

- Most of the published articles on the TCC coatings have been done on proprietary products. Therefore, fundamental understanding of the formation and compo-

sition of the TCC coatings on different substrates, e.g. Zn and Zn alloys or Al and Al alloys, with the aid of model solutions is suggested.

- Most of the published studies were done on the Al alloy substrate. Further investigations on various substrates, e.g. Zn electroplated steel or Mg alloy shall be carried out.

- Model solutions with different complexing agents, oxidants, additional metal, and nano-crystalline particles can be investigated.

- The dynamics of the TCC formation process can be studied by means of in situ analysis techniques, such as difference viewer imaging technique (DVIT) [240], which might be useful to observe the nucleation and growth of a conversion layer.

- Advanced surface analysis of the TCC layer with the aid of methods with higher resolution and chemical sensitivity compared to XPS and AES, such as nanoscale secondary ion mass spectroscopy (NanoSIMS) and ion beam analysis (IBA) can be considered [241].

- The kinetics of the TCC film formation with the aid of simulations could be studied.

- Research can be done to compare the morphology and corrosion protection of the TCC coatings with the other type of chromium-free conversion coatings, for example on Zn [241] or Al [68, 69] substrates.

- TCC coating might be often used where the main function of the treatment is to improve the adhesion of paints or polymer coatings [180], studies can be done to achieve a compatible TCC formulation with polymer coatings with synergistic effects.

- The corrosion initiation and propagation in the TCC coatings can be studied with the aid of methods such as scanning reference electrode technique (SRET) and scanning vibrating electrode technique (SVET) [242], to map the current density around the scratches (artificial defects).

Bibliography

[1] WE John. 'Method of Coating Zinc or Cadmium base Metals'. Patent US2035380A (US). May 1933.

[2] X Zhang, W Sloof, A Hovestad, EV Westing, H Terryn, and JD Wit. 'Characterization of Chromate Conversion Coatings on Zinc using XPS and SKPFM'. In: *Surface and Coatings Technology* 197.2-3 (2005), pp. 168–176.

[3] L Xia. 'Chemistry of a Chromate Conversion Coating on Aluminium Alloy AA2024-T3 Probed by Vibrational Spectroscopy'. In: *Journal of The Electrochemical Society* 145.9 (1998), p. 3083.

[4] J Zhao, L Xia, A Sehgal, D Lu, R Mccreery, and G Frankel. 'Effects of Chromate and Chromate Conversion Coatings on Corrosion of Aluminium Alloy 2024-T3'. In: *Surface and Coatings Technology* 140.1 (2001), pp. 51–57.

[5] N Zaki. 'Chromate Conversion Coatings'. In: *Met. Finish.* 105.10 (2007), pp. 413–424.

[6] FW Eppensteiner and MR Jenkins. 'Chromate Conversion Coatings'. In: *Met. Finish.* 99.1 (2001), pp. 494–506.

[7] A Hughes, T Harvey, N Birbilis, A Kumar, and R Buchheit. 'Coatings for Corrosion Prevention based on Rare Earths'. In: *Rare Earth-based Corrosion Inhibitors* (2014), pp. 186–232.

[8] M Kendig, S Jeanjaquet, R Addison, and J Waldrop. 'Role of Hexavalent Chromium in the Inhibition of Corrosion of Aluminium Alloys'. In: *Surface and Coatings Technology* 140.1 (2001), pp. 58–66.

[9] XB Chen, N Birbilis, and AT B. 'Review of Corrosion-Resistant Conversion Coatings for Magnesium and Its Alloys'. In: *CORROSION* 67 (2011), pp. 0350051–03500516.

[10] RL Twite and GP Bierwagen. 'Review of Alternatives to Chromate for Corrosion Protection of Aluminum Aerospace Alloys'. In: *Progress in Organic Coatings* 33 (1988), pp. 91–100.

[11] "DSDM Stearns". 'The Role of chromium(V) in the Mechanism of Chromate-Induced Oxidative DNA Damage and Cancer'. In: *J Environ Pathol Toxicol Oncol* 19.3 (2000), pp. 215–230.

[12] HJ Gibb, PSJ Lees, PF Pinsky, and BC Rooney. *Lung Cancer Among Workers in Chromium Chemical Production*. July 2000.

[13] PL Hagans and CM Haas. 'Chromate Conversion Coatings'. In: *Surface Engineering* 5 (1994), pp. 405–411.

[14] KA Korinek. *Chromate Conversion Coatings*. Vol. 13. ASM International. Metals Handbook, 1987, pp. 389–395.

[15] N Zaki. 'Trivalent Chrome Conversion Coating for Zinc and Zinc Alloys'. In: *Metal Finishing* 79 (2007), pp. 428–437.

[16] M Sahre, RM Souto, and W Kautek. 'Chromate-free Zinc Conversion Coatings Characterised by Grazing Incidence X-Ray Diffractometer'. In: *Mikrochim. Acta* 133.1-4 (2000), pp. 137–142.

[17] C Gensch, Y Baron, and K Moch. *8 th Adaptation to Scientific and Technical Progress of Exemptions 2(c), 3 and 5 of Annex II to Directive 2000/53/EC (ELV)*. en. Tech. rep. 2016.

[18] C Gensch and Y Baron. *Assistance to the Commission on Technological Socio-Economic and Cost-Benefit Assessment Related to Exemptions from the Substance restrictions in Electrical and Electronic Equipment (RoHS Directive)*. en. Tech. rep. 2014.

[19] G Dehoust and D Schueler. *Life cycle assessment of the Treatment and Recycling of Refrigeration Equipment Containing CFCs and Hydrocarbons (Final report)*. en. Tech. rep. 2007.

[20] B Dingwerth. 'The Second Conversion Coating - Final Finishing Black Passivates with Trivalent Chromium based Post-dip Solutions'. In: *Galvanotechnik* 5 (2008), pp. 1080–1096.

[21] A Gardner and J Scharf. 'High Performance Alternative to Hexavalent Chromium Passivation of Plated Zinc and Zinc Alloys'. In: *Trans. Inst. Met. Finish.* 81.B107 (2003).

[22] PH Patricia Preikschat Rolf Jansen. 'Chromate-free Conversion Layer and Process for Producing the same'. Patent US6287704B1 (US). Sept. 2001.

[23] J Bento Da Fonte. 'Trivalent Chromium Passivate Solution and Process for Yellow Passivate Film'. Patent US4359346A (US). Apr. 1981.

[24] V Dikinis, V Rezaite, I Demcenko, A Seiskis, T Bernatavicius, and R Sarmaitis. 'Chracterization of Zinc Corrosion and Formation of Conversion Films on the Zinc Surface in Acidic Solutions of Cr(III) Compounds'. In: *Trans Inst Metal Finishing* 82.3-4 (2004), pp. 98–104.

[25] CR Tomachuk, CI Elsner, ARD Sarli, and OB Ferraza. 'Corrosion Resistance of Cr(III) Conversion Treatments Applied on Electrogalvanised Steel and Subjected to Chloride Containing Media'. In: *Materials Chemistry and Physics* 119 (2010), pp. 19–29.

[26] M Mouanga, Ricq, and P Bercot. 'Electrodeposition and Characterization of Zinc–Cobalt Alloy from Chloride Bath; Influence of Coumarin as Additive'. In: *Surface and Coatings Technology* 202 (2008), pp. 1645–1651.

[27] ARD Sarli, JD Culcasi, CR Tomachuk, CI Elsner, JM Ferreira-Jr, and I Costa. 'A Conversion Layer based on Trivalent Chromium and Cobalt for the Corrosion Protection of Electrogalvanized Steel'. In: *Surface and Coatings Technology* 258 (2014), pp. 426–436.

[28] CR Tomachuk, CI Elsner, ARD Sarli, and OB Ferraz. 'Morphology and Corrosion Resistance of Cr(III)-based Conversion Treatments for Electrogalvanized Steel'. In: *Coating Technology* 7.4 (2010), pp. 493–502.

[29] R Chapaneri. 'A Study of Hexavalent and Trivalent Chromium Conversion Coatings on Zinc Surfaces'. An optional note. PhD thesis. UK: Loughborough University, Oct. 2010.

[30] C Rollinson, J Bailar, H Emelus, and R Nyholm. *The Chemistry of Chromium, Molybdenum and Tungsten: Pergamon International Library of Science, Technology, Engineering and Social Studies*. Pergamon Texts in Inorganic Chemistry. Elsevier Science, 2015.

[31] M Schlesinger and M Paunovic. *Modern Electroplating*. The ECS Series of Texts and Monographs. Wiley, 2011.

[32] MA Dominguez-Crespo, E Onofre-Bustamante, AM Torres-Huerta, and FJ Rodriguez-Gomez. 'Morphology and Corrosion Performance of Chromate Conversion Coatings on Different Substrates'. In: *J. Mex. Chem. Soc.* 52.4 (2008), pp. 235–240.

[33] I Milosev and GS Frankel. 'Review—Conversion Coatings based on Zirconium and/or Titanium'. In: *Journal of The Electrochemical Society* 165.3 (2018), pp. C127–C144.

[34] GJ X Cui, MD E Liu, QL Wang, and F. 'Influence of Substrate Composition on the Formation of Phytic Acid Conversion Coatings'. In: *Materials and Corrosion* 63.3 (2012).

[35] J Qi and GE Thompson. 'Comparative Studies of Thin Film Growth on Aluminium by AFM, TEM and GDOES Characterization'. In: *Applied Surface Science* 377 (2016), pp. 109–120.

[36] X Dong, P Wang, S Argekar, and DW Schaefer. 'Structure and Composition of Trivalent Chromium Process (TCP) Films on Al Alloy'. In: *Langmuir* 26.13 (2010), pp. 10833–10841.

[37] Y Guo. 'A Study of Trivalent Chrome Process Coatings on Aluminium Alloy 2024-T3'. Thesis. 2011.

[38] Y Guo and GS Frankel. 'Active Corrosion Inhibition of AA2024-T3 by Trivalent Chrome Process Treatment'. In: *Corrosion Science* 68.4 (2012).

[39] JT Qi, T Hashimoto, JR Walton, X Zhou, P Skeldon, and GE Thompson. 'Trivalent Chromium Conversion Coating Formation on Aluminium'. In: *Surface and Coatings Technology* 280 (2015), pp. 317–329.

[40] A Iyer, W Willis, S Frueh, and SL Suib. 'Characterization of NAVAIR Trivalent Chromium Process (TCP) Coatings and Solutions'. In: *Plating and Surface Finishing* 97.4 (2010).

[41] L Li, GP Swain, A Howell, D Woodbury, and GM Swain. 'The Formation, Structure, Electrochemical Properties and Stability of Trivalent Chrome Process (TCP) Coatings on AA2024'. In: *Journal of The Electrochemical Society* 158.9 (2011), pp. C274–C283.

[42] L Li, DY Kim, and GM Swain. 'Transient Formation of Chromate in Trivalent Chromium Process (TCP) Coatings on AA2024 as Probed by Raman Spectroscopy'. In: *Journal of The Electrochemical Society* 159.8 (2012), pp. C326–33.

[43] CA Munson and GM Swain. 'Structure and Chemical Composition of Different Variants of a Commercial Trivalent Chromium Process (TCP) Coating on Aluminium Alloy 7075-T6'. In: *Surface and Coatings Technology* 315 (2017), pp. 150–162.

[44] M Ely, J Swiatowsk, A Seyeux, S Zanna, and P Marcusa. 'Role of Post-Treatment in Improved Corrosion Behaviour of Trivalent Chromium Protection (TCP) Coating Deposited on Aluminium Alloy 2024-T3'. In: *Journal of The Electrochemical Society* 164.6 (2017), pp. C276–C284.

[45] J Li, C Yao, Y Liu, D Li, B Zhou, and W Cai. 'The Hazardous Hexavalent Chromium Formed on Trivalent Chromium Conversion Coating'. In: *Journal of Hazardous Materials* 221– 222 (2012), pp. 56–61.

[46] Z Rochester and ZW Kennedy. 'Unexpected Results from Corrosion Testing of Trivalent Passivates'. In: *Plating and Surface Finishing* (2007), pp. 14–18.

[47] ZW Kennedy. 'Behaviour of Trivalent Passivates in Accelerated Corrosion Tests'. In: *Electroplat. Finish* 27 (2009), p. 23.

[48] A B117-16. *Standard Practice for Operating Salt Spray (Fog) Apparatus*. Tech. rep. ASTM International, West Conshohocken, PA, USA, 2016.

[49] R Revie and H Uhlig. *Uhlig's Corrosion Handbook*. Electrochemical Society Series. Wiley, 2011.

[50] P Philip A. Schweitzer. *Fundamentals of Metallic Corrosion: Atmospheric and Media Corrosion of Metals*. Corrosion Engineering Handbook, Second Edition. CRC Press, 2006.

[51] R Kelly, J Scully, D Shoesmith, and R Buchheit. *Electrochemical Techniques in Corrosion Science and Engineering*. Corrosion Technology. CRC Press, 2002.

[52] V Cicek and B Al-Numan. *Corrosion Chemistry*. Wiley, 2011.

[53] Y Waseda and S Suzuki. *Characterization of Corrosion Products on Steel Surfaces*. Advances in Materials Research. Springer Berlin Heidelberg, 2006.

[54] J Davis. *Surface Engineering for Corrosion and Wear Resistance*. ASM International, 2001.

[55] D Landolt. *Corrosion and Surface Chemistry of Metals*. Engineering Sciences. Materials. EPFL Press, 2007.

[56] H Kanematsu and D Barry. *Corrosion Control and Surface Finishing: Environmentally Friendly Approaches*. Springer Japan, 2016.

[57] R Revie. *Corrosion and Corrosion Control: An Introduction to Corrosion Science and Engineering*. Wiley, 2008.

[58] P Philip A. Schweitzer. *Corrosion of Linings and Coatings: Cathodic and Inhibitor Protection and Corrosion Monitoring*. Corrosion Engineering Handbook, Second Edition. CRC Press, 2006.

[59] MC Cotell. *Surface Engineering*. 5. ASM International, 1994.

[60] T Fuller and J Harb. *Electrochemical Engineering*. Wiley, 2018.

[61] N Kanani. *Electroplating: Basic Principles, Processes and Practice*. Elsevier Science, 2004.

[62] M Tencer. 'Electrical Conductivity of Chromate Conversion Coating on Electrodeposited Zinc'. In: *Applied Surface Science* 252 (2006), pp. 8229–8234.

[63] D Gabe and D Hopkins. *Principles of Metal Surface Treatment and Protection: Pergamon International Library of Science, Technology, Engineering and Social Studies: International Series on Materials Science and Technology*. International Series on Materials Science and Technology. Elsevier Science, 2014.

[64] TSNS Narayanan. 'Surface Pretreatment by Phosphate Conversion Coatings - A Rewiew'. In: *Rev.Adv.Mater.Sci.* 9 (2005), pp. 130–177.

[65] Y Matsushima and T Matsumura. 'Oxalate Conversion Coating Method for Stainless Steel'. Patent US3632452A (US). Apr. 1972.

[66] HA Katzman and GM Malouf. 'Corrosion Protective Chromate Coatings on Aluminium'. In: *Applications of Surface Science* 2 (1979), pp. 416–432.

[67] R Saillard, B Viguier, G Odemer, A Pugliara, B Fori, and C Blanc. 'Influence of the Microstructure on the Corrosion Behaviour of 2024 Aluminium Alloy Coated with a Trivalent Chromium Conversion Layer'. In: *Corrosion Science* 142 (2018), pp. 119–132.

[68] Q Boyera, MRO Vega, CdF Malfattib, S Duluarda, and F Ansarta. 'Correlation Between Morphology and Electrochemical Behaviour of chromium-free Conversion Coatings for Aluminium Alloys Corrosion Protection'. In: *Surface and Coatings Technology* 351 (2018), pp. 115–127.

[69] RL Twite and GP Bierwagen. 'Review of Alternatives to Chromate for Corrosion Protection of Aluminium Aerospace Alloys'. In: *Progress in Organic Coatings* 33.2 (1998), pp. 91–100.

[70] D U.S. Department of Labor Washington. *Occupational Exposure to Hexavalent Chromium*. USA. Tech. rep. 2006.

[71] DM Johnson. 'Zinc and Cadmium Passivating Bath'. Patent US2559878A (US). July 1951.

[72] T Letcher. *Thermodynamics, Solubility and Environmental Issues*. Elsevier Science, 2007.

[73] O Gharbi, S Thomas, C Smith, and N Birbilis. 'Chromate replacement: what does the future hold?' In: *npj Materials Degradation* 12 (2018).

[74] X Zhang, S Boehm, AJ Bosch, EPM van Westing, and JHW de Wit. 'Influence of Drying Temperature on the Corrosion Performance of Chromate Coatings on Galvanized Steel'. In: *Materials and Corrosion* 55.7 (2004), pp. 501–510.

[75] A Matsuzaki, M Nagoshi, H Noro, M Yamashita, and N Hara. 'Self-Healing Effect by Zinc Phosphate and Calcium Silicate Included in Organic-Inorganic Composite Coating on 55% Al-Zn Coated Steel Sheet'. In: *MATERIALS TRANSACTIONS* 52.6 (2011), pp. 1244–1251.

[76] L Grasso, AS Fantoli, MG Ienco, A Parodi, MR Pinasco, E Angelini, and F Rosalbino. 'Corrosion Resistance of Cr (III)-based Conversion Layer on Zinc Coatings in Comparison with a Traditional Cr (VI)-based Passivation Treatment'. In: *la metallurgia italiana* (2006), pp. 31–39.

[77] DE Walker. 'Enhanced Molybdate Conversion Coatings'. Thesis. 2012.

[78] A Gardner and J Scharf. 'Trivalent Passivation of Plated Zinc and Zinc Alloys - Alternatives to Hexavalent based Systems'. In: *TIMF* 81.6 (2003), pp. 107–111.

[79] A Gardner and J Scharf. *High Performance Alternative to Hexavalent Chromium Passivation of Plated Zinc and Zinc Alloys*. Tech. rep. SAE 2001 World Congress, 2001.

[80] T Bellezze, G Roventi, and R Fratesi. 'Electrochemical Study on the Corrosion Resistance of Cr(III)-based Conversion Layers on Zinc Coatings'. In: *Surface and Coatings Technology* 155 (2002), pp. 221–230.

[81] L Fedrizzi, H Terryn, and A Simoes. *Innovative Pre-Treatment Techniques to Prevent Corrosion of Metallic Surfaces*. European Federation of Corrosion (EFC) Series. Elsevier Science, 2014.

[82] CR Tomachuk, ARD Sarli, and CI Elsner. 'Anti-Corrosion Performance of Cr^6 free Passivating Layers Applied on Electrogalvanized'. In: *Materials Sciences and Applications* 1 (2010), pp. 202–209.

[83] P Maass, P Peissker, and C Ahner. *Handbook of Hot-dip Galvanization*. Wiley, 2011.

[84] P Marcus. *Corrosion Mechanisms in Theory and Practice*. Corrosion Technology. CRC Press, 2002.

[85] M Wen and K Dusek. *Protective Coatings: Film Formation and Properties*. Springer International Publishing, 2017.

[86] F Defloriana, S Rossia, L Fedrizzib, and PL Bonoraa. 'EIS Study of Organic Coating on Zinc Surface Pretreated with Environmentally friendly Products'. In: *Progress in Organic Coatings* 52 (2005), pp. 271–279.

[87] L Li, KP Doran, and GM Swaina. 'Electrochemical Characterization of Trivalent Chromium Process (TCP) Coatings on Aluminium Alloys 6061 and 7075'. In: *Journal of The Electrochemical Society* 160.8 (2013), pp. C396–C401.

[88] P Puomi, HM Fagerholm, JB Rosenholm, and K Jyrkaes. 'Comparison of Different Commercial Pretreatment Methods for Hot-dip Galvanized and Galfan Coated Steel'. In: *Surface and Coatings Technology* 115 (1999), pp. 70–78.

[89] V Cicek and B Al-Numan. *Corrosion Engineering and Cathodic Protection Handbook: With Extensive Question and Answer Section*. Wiley, 2017.

[90] Y Guo and GS Frankel. 'Characterization of Trivalent Chromium Process Coating on AA2024-T3'. In: *Surface and Coatings Technology* 206 (2012), pp. 3895–3902.

[91] J Qi, T Hashimoto, J Walton, X Zhou, P Skeldon, and G EThompson. 'Formation of a Trivalent Chromium Conversion Coating on AA2024-T351 Alloy'. In: *Journal of The Electrochemical Society* 163.2 (2016), pp. C25–C35.

[92] J Qi, L Gao, Y Liu, B Liu, T Hashimoto, Z Wang, and GE Thompson. 'Chromate Formed in a Trivalent Chromium Conversion Coating on Aluminium'. In: *Journal of The Electrochemical Society* 164.7 (2017), pp. C442–C449.

[93] T Wanotayan, Y Boonyongmaneerat, Y Boonyongmaneerat, J Panpranot, and A Nishikata. 'Electrochemical Evaluation of Corrosion Resistance of Trivalent Chromate Conversion Coatings with Different Organic Additives'. In: *ISIJ International* 58.7 (2018), pp. 1316–1323.

[94] BW Whitman, L Li, and GM Swaina. 'Anti-Corrosion Properties of a TCP Pretreatment Conversion Coating on Aluminium Alloy 2024-T3 during Moist SO_2 Atmospheric Testing: Effects of Galvanic Coupling'. In: *Journal of The Electrochemical Society* 164.4 (2017), pp. C135–C147.

[95] OO Knudsen and A Forsgren. *Corrosion Control Through Organic Coatings*. Corrosion Technology. CRC Press, 2017.

[96] A Bard, R Parsons, and J Jordan. *Standard Potentials in Aqueous Solution*. Monographs in Electroanalytical Chemistry and Electrochemistr. Taylor and Francis, 1985.

[97] P Brown and C Ekberg. *Hydrolysis of Metal Ions*. Hydrolysis of Metal Ions v. 1. Wiley, 2016.

[98] L Thiery and N Pommier. *Hexavalent Chromium-free Passivation Treatments in the Automative Industry*. Tech. rep. Coventya SAS - Lionel Thiery and Nicolas Pommier, 2004.

[99] KO Legg. 'DoD Metal Finishing Workshop Chromate Alternatives for Metal Treatment and Sealing'. In: *Hazmat Alternatives*. Rowan Technology Group.

[100] A Martell and R Hancock. *Metal Complexes in Aqueous Solutions*. Modern Inorganic Chemistry. Springer US, 2013.

[101] HA Ramezani Varzaneh, SR Allahkaram, and M Isakhani Zakaria. 'Effects of Phosphorus Content on Corrosion Behaviour of Trivalent Chromium Coatings in 3.5 wt% NaCl Solution'. In: *Surface and Coatings Technology* 244 (2014), pp. 158–165.

[102] C Barnes, JJB Ward, TS Sehmbhi, and VE Carter. 'Non-Chromate Passivation Treatments for Zinc'. In: *Transactions of the IMF* 60.1 (1982).

[103] CR Tomachuk, CI Elsner, and ARD Sarli. 'Behaviour of Electro-galvanized Steel Pre-Treated with Cr(III)-based Baths and Exposed to 0.5 M Na_2SO_4 Solution'. In: *Portugaliae Electrochimica Acta* 30.3 (2012), pp. 145–162.

[104] NT Wen, FJ Chen, MD Ger, YN Pan, and CS Lin. 'Microstructure of Trivalent Chromium Conversion Coating on Electrogalvanized Steel Plate'. In: *Electrochemical and Solid-State Letters* 11.8 (2008), pp. C47–C50.

[105] X Zhang, Cvd Bos, WG Sloof, H Terryn, A Hovestad, and JHWd Wit. 'Investigation of Cr(III) based Conversion Coatings on Electrogalvanized Steel'. In: *Surface Engineering* 20.4 (2004).

[106] NT Wen, CS Lin, CY Bai, and MD Ger. 'Structures and Characteristics of Cr(III)-based Conversion Coatings on Electro-galvanized Steels'. In: *Surface and Coatings Technology* 203 (2008), pp. 317–323.

[107] ARD Sarli, CI Elsner, and CR Tomachuk. 'Characterization and Corrosion Resistance of Galvanized Steel/Passivation Composite/ Polyurethane Paint Systems'. In: *British Journal of Applied Science and Technology* 4.6 (2014), pp. 853–878.

[108] F Pearlstein and VS Agarwala. 'Trivalent Chromium Solutions for Applying Chemical Conversion Coatings to Aluminium Alloys or for Sealing Anodised Aluminium'. In: *Plat. Surf. Finish.* 81 (1994), pp. 50–55.

[109] F Pearlstein and VS Agarwala. 'Trivalent Chromium Conversion Coatings for Aluminium'. Patent US5304257 A (US). July 1994.

[110] DB Mitton, A Carangelo, A Acquesta, T Monetta, M Curioni, and F Bellucci. 'Selected Cr(VI) Replacement Options for Aluminium Alloys: A Literature Survey'. In: *CORROSION REVIEWS* 35.6 (2017), pp. 365–381.

[111] F Pearlstein and VS Agarawala. *Trivalent Chromium Conversion Coatings for Aluminium.* Apr. 1994.

[112] S Dardona, L Chen, M Kryzman, D Goberman, and M Jaworowski. 'Polarization Controlled Kinetics and Composition of Trivalent Chromium Coatings on Aluminium'. In: *Anal. Chem.* 83 (2011), pp. 6127–6131.

[113] R Berger, U Bexell, TM Grehk, and SE Hoernstroem. 'A Comparative Study of the Corrosion Protective Properties of Chromium and Chromium free Passivation Methods'. In: *Surface and Coatings Technology* 202 (2007), pp. 391–397.

[114] SL Manchet, D Verchere, and J Landoulsi. 'Effects of Organic and Inorganic Treatment Agents on the Formation of Conversion Layer on Hot-dip Galvanized Steel: An X-ray Photoelectron Spectroscopy Study'. In: *Thin Solid Films* 520 (2012), pp. 2009–2016.

[115] J Qi, L Gao, Y Li, Z Wang, GE Thompson, and P Skeldon. 'An Optimized Trivalent Chromium Conversion Coating Process for AA2024-T351 Alloy'. In: *Journal of The Electrochemical Society* 164.7 (2017), pp. C390–C395.

[116] B Ramezanzadeh, MM Attar, and M Farzam. 'Corrosion Performance of a Hot-dip Galvanized Steel Treated by Different Kinds of Conversion Coatings'. In: *Surface and Coatings Technology* 205 (2010), pp. 874–884.

[117] J Qi, B Zhanga, Z Wanga, Y Lib, P Skeldon, and GE Thompson. 'Effect of an Fe(II)-modified Trivalent Chromium Conversion Process on Cr(VI) Formation during Coating of AA 2024 Alloy'. In: *Electrochemistry Communications* 92 (2018), pp. 1–4.

[118] K Cho, VS Rao, and H Kwon. 'Microstructure and Electrochemical Characterization of Trivalent Chromium based Conversion Coating on Zinc'. In: *Electrochimica Acta* 52 (2007), pp. 4449–4456.

[119] J Qi, J Walton, GE Thompsona, SP Albu, and J Carra. 'Spectroscopic Studies of Chromium VI formed in the Trivalent Chromium Conversion Coatings on Aluminium'. In: *Journal of The Electrochemical Society* 163.7 (2016), pp. C357–C363.

[120] BD BARKER. 'ELECTROLESS DEPOSITION OF METALS'. In: *Surface Technology* 12 (1981), pp. 77–88.

[121] J Qi, T Hashimoto, GE Thompson, and J Carrb. 'Influence of Water Immersion Post-Treatment Parameters on Trivalent Chromium Conversion Coatings Formed on AA2024-T351 Alloy'. In: *Journal of The Electrochemical Society* 163.5 (2016), pp. C131–C138.

[122] JG Anton, RMF Domene, RS Tovar, CE Cerdan, RL Garcia, V Garcia, and A Urtiaga. 'Improvement of the Electrochemical Behaviour of Zn-electroplated Steel using Regenerated Cr(III) Passivation Baths'. In: *Chemical Engineering Science* 111 (2014), pp. 402–409.

[123] SdS Borges, M Korn, and JLFdC Lima. 'Chromium(III) Determination with 1,5-Diphenylcarbazide based on the Oxidative Effect of Chlorine Radicals Generated from CCl4 Sonolysis in Aqueous Solution'. In: *Analytical Sciences* 18 (2002), pp. 1361–65.

[124] SL Suib and JJL Scala. 'Determination of Hexavalent Chromium in NAVAIR Trivalent Chromium Process (TCP) Coatings and Process Solutions'. In: *Metal Finishing* 107.2 (2009), pp. 28–34.

[125] J Qi, Y Miao, Z Wang, Y Li, X Zhang, P Skeldon, and GE Thompson. 'Influence of Copper on Trivalent Chromium Conversion Coating Formation on Aluminium'. In: *Journal of The Electrochemical Society* 164.12 (2017), pp. C611–C617.

[126] L Li and GM Swain. 'Effects of Ageing Temperature and Time on the Corrosion Protection Provided by Trivalent Chromium Process Coatings on AA2024-T3'. In: *ACS Appl. Mater. Interfaces* 5 (2013), pp. 7923–7930.

[127] L Zahner. *Aluminum Surfaces: A Guide to Alloys, Finishes, Fabrication and Maintenance in Architecture and Art.* Architectural Metals Series. Wiley, 2019.

[128] CR Tomachuk, CI Elsnerb, and ARD Sarli. 'Electrochemical Characterization of Chromate Free Conversion Coatings on Electro-galvanized Steel'. In: *Materials Research.* 17.1 (2014), pp. 61–68.

[129] C Stromberg, P Thissen, I Klueppel, N Fink, and G Grundmeier. 'Synthesis and Characterisation of Surface Gradient Thin Conversion Films on Zinc Coated Steel'. In: *Electrochimica Acta* 52.3 (2006), pp. 804–815.

[130] T Lostak, A Maljusch, B Klink, S Krebs, M Kimpel, J Flock, S Schulz, and W Schuhmann. 'Zr-based Conversion Layer on Zn-Al-Mg Alloy Coated Steel Sheets: Insights into the Formation Mechanism'. In: *Electrochimica Acta* 137 (2014), pp. 65–74.

[131] X Zhanga, Cvd Bosa, WG Sloofa, A Hovestadb, H Terrync, and JHWd Wit. 'Comparison of the Morphology and Corrosion Performance of Cr(VI)- and Cr(III)-based Conversion Coatings on Zinc'. In: *Surface and Coatings Technology* 199 (2005), pp. 92–104.

[132] I Schoukens, I Vandendael, JD Strycker, AA Saleh, H Terryn, and ID Graeve. 'Effect of surface Composition and Microstructure of Aluminised Steel on the Formation of a Titanium-based Conversion Layer'. In: *Surf. Coat. Technol.* 235 (2013), p. 628.

[133] J Cerezo, I Vandendael, R Posner, K Lill, JHWd Wit, JMC Mol, and H Terryn. 'Initiation and Growth of Modified Zr-based Conversion Coatings on Multi-Metal Surfaces'. In: *Surf. Coat. Technol.* 236.284 (2013).

[134] P Taheri, K Lill, JHWd Wit, JMC Mol, and H Terryn. 'Effects of Zinc Surface Acid-based Properties on Formation Mechanisms and Interfacial Bonding Properties of Zirconium-based Conversion Layers'. In: *The journal of Physical Chemistry* 116.15 (2012), pp. 8426–8436.

[135] H Fujiwara. *Spectroscopic Ellipsometry: Principles and Applications*. Wiley, 2007.

[136] S Dardona and M Jaworowski. 'In situ Spectroscopic Ellipsometry Studies of Trivalent Chromium Coating on Aluminium'. In: *Applied Physics Letters* 97.181908 (2010).

[137] G Fragneto-Cusani. 'Neutron Reflectivity at the Solid/Liquid Interface: Examples of Applications in Biophysics'. In: *J. Phys.: Condens. Matter* 13 (2001), pp. 4973–4989.

[138] X Dong, S Argekar, P Wang, and DW Schaefer. 'In situ Evolution of Trivalent Chromium Process Passive Film on Al in a Corrosive Aqueous Environment'. In: *ACS Appl. Mater. Interfaces* 3.11 (2011), pp. 4206–4214.

[139] A B201-80. *Standard Practice for Testing Chromate Coatings on Zinc and Cadmium Surfaces*. Tech. rep. ASTM International, West Conshohocken, PA, 2000.

[140] L Giannuzzi and N University. *Introduction to Focused Ion Beams: Instrumentation, Theory, Techniques and Practice*. Springer US, 2006.

[141] R Wirth. 'Focused Ion Beam (FIB) combined with SEM and TEM: Advanced Analytical Tools for Studies of Chemical Composition, Microstructure and Crystal Structure in Geomaterials on a Nanometre Scale'. In: *Chemical Geology* 261.3-4 (2009), pp. 217–229.

[142] G Friedbacher and H Bubert. *Surface and Thin Film Analysis: A Compendium of Principles, Instrumentation, and Applications*. Wiley, 2011.

[143] P Holloway and P Vaidyanathan. *Characterization of Metals and Alloys*. Materials characterization series. Momentum Press, 2009.

[144] G Haugstad. *Atomic Force Microscopy: Understanding Basic Modes and Advanced Applications*. Wiley, 2012.

[145] P Eaton and P West. *Atomic Force Microscopy*. OUP Oxford, 2010.

[146] 'NanoScope Software 6.13 User Guide'. In: *Veeco Instruments Inc* (2004), pp. 134–137.

[147] M Yao, D Wang, and M Zhao. 'Element Analysis based on Energy-Dispersive X-Ray Fluorescence'. In: *Advances in Materials Science and Engineering* (2015).

[148] X Hou and BT Jones. *Encyclopedia of Analytical Chemistry; Inductively Coupled Plasma/Optical Emission Spectrometry*. John Wiley and Sons Ltd, Chichester, 2000. 2000.

[149] G McGuire. *Auger Electron Spectroscopy Reference Manual: A Book of Standard Spectra for Identification and Interpretation of Auger Electron Spectroscopy Data*. Springer US, 2013.

[150] S Hofmann. *Auger- and X-Ray Photoelectron Spectroscopy in Materials Science: A User-Oriented Guide*. Springer Series in Surface Sciences. Springer Berlin Heidelberg, 2012.

[151] F Settle. *Handbook of Instrumental Techniques for Analytical Chemistry*. Handbook of Instrumental Techniques for Analytical Chemistry v. 1. Prentice Hall PTR, 1997.

[152] DH Naroumand and KD Childs. 'Auger Spectrometers: A Tutorial Review'. In: *Applied Spectroscopy Reviews* 34.3 (1999), pp. 139–158.

[153] D Lee and E Scholz. *Karl Fischer Titration: Determination of Water*. Chemical Laboratory Practice. Springer Berlin Heidelberg, 2012.

[154] S Ahuja and S Scypinski. *Handbook of Modern Pharmaceutical Analysis*. Separation Science and Technology. Elsevier Science, 2001.

[155] P Worsfold, A Townshend, C Poole, and M Miro. *Encyclopedia of Analytical Science*. Elsevier Science, 2019.

[156] U Sahoo, AK Seth, and R Chawla. *Uv/ Visible Spectroscopy*. Lap Lambert Academic Publishing GmbH KG, 2012.

[157] HH Perkampus, HC Grinter, and TL Threlfall. *UV-VIS Spectroscopy and Its Applications*. Springer Lab Manuals. Springer Berlin Heidelberg, 2013.

[158] *Course In Chem For Iit-Jee 2010*. McGraw-Hill Education (India) Pvt Limited.

[159] B Michalke. *Metallomics: Analytical Techniques and Speciation Methods*. Wiley, 2016.

[160] W Williams. *Handbook of Anion Determination*. Elsevier Science, 2013.

[161] R Kohli and K Mittal. *Developments in Surface Contamination and Cleaning - Vol 2: Particle Deposition, Control and Removal*. Elsevier Science, 2009.

[162] RG Buchheit, M Cunningham, H Jensen, MW Kendig, and MA Martinez. 'A Correlation Between Salt Spray and Electrochemical Impedance Spectroscopy Test Results for Conversion-Coated Aluminium Alloys'. In: *CORROSION* 54.1 (1998), pp. 61–72.

[163] F Altmayer. 'Critical Aspects of the Salt Spray Test'. In: *Plating and Surface Finishing* 72 (1985), pp. 36–40.

[164] DEI 9227. *Spruehnebelpruefungen mit verschiedenen Natriumchlorid-Loesungen*. Tech. rep. Deutsches Institut fur Normung E.V. (DIN), 1988.

[165] BR Appleman. 'Survey of Accelerated Test Methods for Anti-Corrosive Coating Performance'. In: *J. Coatings Tech.* 62.787 (1990), pp. 57–67.

[166] K Law and H Zhao. *Surface Wetting: Characterization, Contact Angle, and Fundamentals*. Springer International Publishing, 2015.

[167] V Kulkarni and C Shaw. *Essential Chemistry for Formulators of Semisolid and Liquid Dosages*. Elsevier Science, 2015.

[168] L Wu. 'Investigation of Zinc Whisker Growth from Electro-deposits Produced using Commercial Electroplating Baths'. Thesis. 2016.

[169] L WU, MA ASHWORTH, and GD WILCOX. 'Zinc Whisker Growth from Electroplated Finishes - a Review'. In: *Transactions of the Institute of Metal Finishing* 93.2 (2015), pp. 66–73.

[170] JMC Anaya. 'Growth of Zinc Whiskers'. Thesis. 2014.

[171] A Etienne, E Cadel, A Lina, L Cretinon, and P Pareige. 'Crystallographic Characterization of an Electroplated Zinc Coating Prone to Whiskers'. In: *IEEE Transactions on Components, Packaging and Manufacturing Technology* 2.11 (Nov. 2012), pp. 1928–1932.

[172] R Lahtinen and T Gustafsson. 'The Driving Force Behind Whisker Growth - An Investigation on What Triggers this Phenomenon in Hot-dip Galvanized Zinc Coating (Part 1)'. In: *Metal Finishing* 103.11 (), pp. 25–29.

[173] HF McMurdie, MC Morris, EH Evans, B Paretzkin, W Wong-Ng, L Ettlinger, and CR Hubbard. 'Standard X-Ray Diffraction Powder Patterns from the JCPDS Research Associateship'. In: *Powder Diffraction* 1.2 (1986), pp. 64–77.

[174] A Soudavar. *Mithraic Societies: From Brotherhood to Religions Adversary*. Lulu.com, 2018.

[175] 'CRC Handbook of Chemistry and Physics, 88th ed Editor-in-Chief: David R. Lide (National Institute of Standards and Technology) CRC Press/Taylor and Francis Group: Boca Raton, FL. 2007. 2640 pp. $139.95. ISBN 0-8493-0488-1.' In: *Journal of the American Chemical Society* 130.1 (2008), pp. 382–382.

[176] J Qi. 'Trivalent Chromium Conversion Coatings on Al and Al-Cu Alloys'. An optional note. PhD thesis. Manchester, UK: University of Manchester/School of Materials / Corrosion and Protection Centre, Nov. 2015.

[177] P Somasundaran and D Wang. *Solution Chemistry: Minerals and Reagents*. Developments in Mineral Processing. Elsevier Science, 2006.

[178] A Fullick and P Fullick. *Chemistry for Aqa Co-Ordinated Award*. Coordinated award. Pearson Education, 2001.

[179] Z Feng, J Boerstler, GS Frankel, and CA Matzdorf. 'Effect of Surface Pretreatment on Galvanic Attack of Coated Al Alloy Panels'. In: *Corrosion Science* 71.6 (2015), pp. 771–783.

[180] X Zhang. 'Cr(VI) and Cr(III)-based Conversion Coatings on Zinc'. An optional note. PhD thesis. Delft, Netherlands: Technische Universiteit Delft, July 2005.

[181] LL Diaddario and JM Marzano. 'Trivalent Chromate Conversion Coating'. Patent US7029541B2 (US). Apr. 2006.

[182] DE Crotty. 'Non-peroxide Trivalent Chromium Passivate Composition and Process'. Patent US4578122A (US). Mar. 1986.

[183] JW Schultze. 'A. J. Bard (Ed.): Encyclopedia of Electrochemistry of the Elements, Vol. 4, Marcel Decker Inc., New York and Basel 1975, 465 Seiten, Preis: 300,– DM.' In: *Berichte der Bunsengesellschaft fuer physikalische Chemie* 80.11 (), pp. 1249–1249.

[184] R White. *Modern Aspects of Electrochemistry 45*. Modern Aspects of Electrochemistry. Springer New York, 2009.

[185] L Li, AL Desouzac, and GM Swain. 'In situ pH Measurement during the Formation of Conversion Coatings on an Aluminium alloy (AA2024)'. In: *Analyst* 138 (2013), pp. 4398–4402.

[186] SA Kulinich and AS Akhtara. 'On Conversion Coating Treatments to Replace Chromating for Al Alloys'. In: *Russian Journal of Non Ferrous Metals* 53.2 (2012), pp. 176–203.

[187] AN Chen, MM Scanlan, and SE Skrabalak. 'Surface Passivation and Supersaturation: Strategies for Regioselective Deposition in Seeded Syntheses'. In: *ACS Nano* 11 (2017), pp. 12624–12631.

[188] R Holyst and A Poniewierski. *Thermodynamics for Chemists, Physicists and Engineers*. SpringerLink : Buecher. Springer Netherlands, 2012.

[189] C Clauser and J Bartels. *Numerical Simulation of Reactive Flow in Hot Aquifers: Shemat and Processing Shemat*. Springer Berlin Heidelberg, 2003.

[190] E Bardal. *Corrosion and Protection*. Engineering Materials and Processes. Springer London, 2007.

[191] L Melo, T Bott, and C Bernardo. *Fouling Science and Technology*. Nato Science Series E: Springer Netherlands, 2012.

[192] L Li. 'Corrosion Protection Provided by Trivalent Chromium Process Conversion Coatings on Aluminium Alloys'. An optional note. PhD thesis. USA: Michigan State University, July 2013.

[193] N OGAWA, R KIKUCHI, A NAKAMURA, H AIZAWA, and S IKEDA. 'Effects of Non-aqueous Solvents on the Polarographic Reduction of Nitrate Ion in the Presence of Zirconium(lV)'. In: *Analytical Sciences* 9.6 (1993), p. 847.

[194] M Sima, MN Grecu, M Sima, and I Enculescu. 'Growth and Characterization of ZnO:Mn Submicron Wires via Electrodeposition from Nitrate-Lactic Acid Solution'. In: *ECS Transactions, The Electrochemical Society* 25.27 (2010), pp. 163–171.

[195] Z Liu, Z Jin, J Qiu, X Liu, W Wu, and W Li. 'Preparation and Characteristics of Ordered Porous ZnO Films by a Electrodeposition Method using PS Array Templates'. In: *Semicond. Sci. Technol.* 21 (2006), pp. 60–66.

[196] G Wulfsberg. *Principles Of Descriptive Inorganic Chemistry*. University Science Books, 1991.

[197] D Rai, BM Sass, and DA Moore. 'Chromium(III) Hydrolysis Constants and Solubility of Chromium(III) Hydroxide'. In: *Inorganic Chemistry* 26.3 (1987), pp. 345–349.

[198] P Campestrini, EPMv Westing, A Hovestad, and JHWd Wit. 'Investigation of the Chromate Conversion Coating on Alclad 2024 Aluminium Alloy: Effect of the pH of the Chromate Bath'. In: *Electrochimica Acta* 47 (2002), pp. 1097–1113.

[199] Z Zeng, Y Zhang, W Zhao, and J Zhang. 'Role of Complexing Ligands in Trivalent Chromium Electrodeposition'. In: *Surface and Coatings Technology* 205 (2011), pp. 4771–4775.

[200] E Abel, T University, E Moore, and R Janes. *Metal-Ligand Bonding*. Royal Society of Chemistry, 2007.

[201] D Perry. *Handbook of Inorganic Compounds, Second Edition*. CRC Press, 2016.

[202] M Madou. *Fundamentals of Micro-fabrication: The Science of Miniaturization, Second Edition*. CRC Press, 2002.

[203] A Sammells and M Mundschau. *Non-porous Inorganic Membranes: For Chemical Processing*. Wiley, 2006.

[204] S Glasstone. *An Introduction to Electrochemistry*. Read Books Limited, 2013.

[205] M Kuhl, GM O Halloran, PTJ Gennissen, and PJ French. 'Formation of Porous Silicon using an Ammonium Fluoride based Electrolyte for Application as a Sacrificial Layer'. In: *J. Micromech. Microeng.* 8.4 (1998), pp. 317–322.

[206] KI Popov, NaD Nikolic, SS Djokic, and VD Jovic. *Morphology of Electrochemically and Chemically Deposited Metals*. Springer International Publishing, 2016.

[207] X Li, F Gui, H Cong, CS Brossia, and GS Frankel. 'Evaluation of Nitrate and Nitrite Reduction Kinetics Relatedto Liquid-Air-Interface Corrosion'. In: *Electrochimica Acta* 117 (2014), pp. 299–309.

[208] J Yu and MJ Kupferle. 'Two-stage Sequential Electrochemical Treatment of Nitratebrine Wastes, Water, Air, and Soil Pollution'. In: *Focus 8* (2008), p. 379.

[209] JD Genders, D Hartsough, and DT Hobbs. 'Electrochemical Reduction of Nitrates and Nitrites in Alkaline Nuclear Waste Solutions'. In: *J. Appl. Electrochem* 26.1 (1996), pp. 1–9.

[210] GM O Halloran, M Kuhl, PJ Trimp, and P French. 'The Effect of Additives on the Adsorption Properties Porous Silicon'. In: *Sensors Actuators* A.61 (1998), pp. 415–20.

[211] C Wohlfarth, M Lechner, and B Wohlfarth. *Surface Tension of Pure Liquids and Binary Liquid Mixtures*. Landolt-Boernstein: Numerical Data and Functional Relationships in Science and Technology - New Series. Springer Berlin Heidelberg, 1997.

[212] T Pinnavaia and M Thorpe. *Access in Nanoporous Materials*. Fundamental Materials Research. Springer US, 2006.

[213] C Brennen. *Cavitation and Bubble Dynamics*. Cambridge University Press, 2013.

[214] S Hesamedini and A Bund. 'Formation of Cr(VI) in Cobalt Containing Cr(III)-based Treatment Solution'. In: *Surface and Coatings Technology* 334.C (2018), pp. 444–449.

[215] MP Gigandet, J Faucheu, and M Tachez. 'Formation of Black Chromate Conversion Coatings on Pure and Zinc Alloy Electrolytic Deposits: Role of the Main Constituents'. In: *Surface and Coating Technology* 89 (1997), pp. 285–291.

[216] H Leidheiser and I Suzuky. 'Cobalt and Nickel Cations as Corrosion Inhibitors for Galvanized Steel'. In: *J. Electrochem. Soc.* 128 (1981), pp. 242–249.

[217] A Lasia. *Electrochemical Impedance Spectroscopy and its Applications*. SpringerLink : Buecher. Springer New York, 2014.

[218] M Orazem and B Tribollet. *Electrochemical Impedance Spectroscopy*. The ECS Series of Texts and Monographs. Wiley, 2011.

[219] V Lvovich. *Impedance Spectroscopy: Applications to Electrochemical and Dielectric Phenomena*. Wiley, 2015.

[220] H Cesiulis, N Tsyntsaru, A Ramanavicius, and G Ragoisha. 'The Study of Thin Films by Electrochemical Impedance Spectroscopy'. In: *Nanostructures and Thin Films for Multifunctional Applications. NanoScience and Technology*. Ed. by I Tiginyanu, P Topala, and V Ursaki. Springer, Cham, 2016.

[221] G Goeminne, H Terryn, and J Vereecken. 'Characterisation of Conversion Layers on Aluminium by means of Electrochemical Impedance Spectroscopy'. In: *Electrochimica Acta* 40.4 (1995), pp. 479–486.

[222] GJ Brug, ALGvd Eeden, JHM Sluyters Rehbach, and Sluyters. 'The Analysis of Electrode Impedances Complicated by the Presence of a Constant Phase Element'. In: *Journal of Electroanalytical Chemistry and Interfacial Electrochemistry* 176.1-2 (1984), pp. 275–295.

[223] E Barsoukov and JR Macdonald. *Impedance Spectroscopy: Theory, Experiment, and Applications*. Wiley, 2005.

[224] B Hirschorn, ME Orazema, B Tribollet, V Vivierb, I Frateur, and M Musiani. 'Determination of Effective Capacitance and Film Thickness from Constant-Phase-Element Parameters'. In: *Electrochimica Acta* 55 (2010), pp. 6218–6227.

[225] X Zhang. *Corrosion and Electrochemistry of Zinc*. Springer US, 2013.

[226] V Barranco and S Feliu. 'EIS study of the Corrosion Behaviour of Zinc-based Coatings on Steel in Quiescent 3% NaCl Solution. Part 1: Directly Exposed Coatings'. In: *Corrosion Science* 46.9 (2004), pp. 2203–2220.

[227] CC Lee and F Mansfeld. 'Automatic Classification of Polymer Coating Quality using Artificial Neural Networks'. In: *Corrosion Science* 41.3 (1998), pp. 439–461.

[228] B Hirschorn, ME Orazem, B Tribollet, V Vivier, I Frateur, and M Musiani. 'Constant-Phase-Element Behavior Caused by Resistivity Distributions in Films'. In: *Journal of The Electrochemical Society* 157.12 (2010), pp. C452–C457.

[229] AC Bastos, MGS Ferreira, and AM Simoes. 'Comparative Electrochemical Studies of Zinc Chromate and Zinc Phosphate as Corrosion Inhibitors for Zinc'. In: *Progress in Organic Coatings* 52 (2005), pp. 339–350.

[230] R Touir, N Dkhireche, ME Touhami, M Lakhrissi, B Lakhrissi, and M Sfaira. 'Corrosion and Scale Processes and their Inhibition in Simulated Cooling Water Systems by Monosaccharides Derivatives Part I: EIS study'. In: *Desalination* 249 (2009), pp. 922–928.

[231] R Touir, M Cenoui, ME Bakri, and ME Touhami. 'Sodium Gluconate as Corrosion and Scale Inhibitor of Ordinary Steel in Simulated Cooling Water'. In: *Corrosion Science* 50 (2008), pp. 1530–1537.

[232] R Baboian. *Corrosion Tests and Standards: Application and Interpretation*. ASTM manual series. ASTM, 1995.

[233] SO Pehkonen and S Yuan. *Tailored Thin Coatings for Corrosion Inhibition Using a Molecular Approach*. Interface Science and Technology. Elsevier Science, 2018.

[234] AW Neumann, R David, and Y Zuo. *Applied Surface Thermodynamics*. Surfactant Science. CRC Press, 2010.

[235] K Mittal. *Advances in Contact Angle, Wettability and Adhesion*. v. 3. Wiley, 2018.

[236] *Determination of Certain Substances in Electrotechnical Products –Part 7-2: Hexavalent Chromium – Determination of Hexavalent Chromium (Cr(VI)) in Polymers and Electronics by the Colorimetric Method*. International Standard. Geneva, CH: International Electrotechnical Commission, Mar. 2017.

[237] DE 15205. *Determination of Hexavalent Chromium in Corrosion Protection Layers - Qualitative Analysis*. Tech. rep. 2. An optional note. The address of the publisher: Deutsches Institut fuer Normung e. V., Feb. 2007.

[238] MO Montes-Holguin, JR Peralta-Videa, G Meitzner, A Martinez-Martinez, G de la Rosa, HA Castillo-Michel, and JL Gardea-Torresdey. 'Biochemical and Spectroscopic Studies of the Response of Convolvulus arvensis L. to Chromium(III) and Chromium(VI) Stress'. In: *Environmental Toxicology and Chemistry* 25.1 (2006), pp. 220–226.

[239] S Hesamedini, G Ecke, and A Bund. 'Structure and Formation of Trivalent Chromium Conversion Coatings Containing Cobalt on Zinc Plated Steel'. In: *Journal of The Electrochemical Society* 165.10 (2018), pp. C657–C669.

[240] RS Huang, CJ Lin, and HS Isaacs. 'A Difference-Imaging Technique Used to Study Streaking Corrosion of Aluminum Alloys AA7075 and AA8006 in Chloride Solution'. In: *Electrochemical and Solid-State Letters* 9.2 (2006), B11–B14.

[241] Z Gao, D Zhang, Zy Liu, X li, S Jiang, and Q Zhang. 'Formation Mechanisms of Environmentally Acceptable Chemical Conversion Coatings for Zinc: A

Review'. In: *Journal of Coatings Technology and Research* 16.1 (2019), pp. 1–13.

[242] AC Bastos, MC Quevedo, OV Karavai, and MGS Ferreira. 'Review—On the Application of the Scanning Vibrating Electrode Technique (SVET) to Corrosion Research'. In: *Journal of The Electrochemical Society* 164.14 (2017), pp. C973–C990.

Appendix

1 Alkaline Zn electroplating

1.1 Zn electrolyte

Commercial alkaline zinc electrolyte: was supplied by Atotech GmbH. Namely, Protolux 3000, is an alkaline, cyanide-free electroplating process for the deposition of bright zinc (Table A.1).

Table A.1 Alkaline zinc electrolyte formulation

Makeup of 1 Liter	**g/l or ml/l**
Zinc oxide, 99.5 % **	12.5 g/l
Sodium hydroxide	120 g/l
Protolux Modifier	30 ml/l
Protolux 3000 Additive	4 ml/l
Protolux 3000 Make up	3 ml/l
Protolux 3000 Brightener (BG)	15 ml/l

1.2 Calculations of Zn electro-deposition

Required current for Zn plating:

Total area of polished mild steel panel (half of hull cell panel and both sides):

Total area (mm^2) = Length (mm) x Width (mm) x 2
7500 = 50 x 75 x 2

Note: The operating current density of alkaline Zn plating was ranged from 1 to 3 A dm^{-2} in Atotech Protolux 3000 datasheet for rack plating. However, the recommended value was 2 A dm^{-2}.

Current density (A dm^{-2}) x Total area plated (dm^2) = Current (A)
2 x 0.75 = 1.5

Required time for desired thickness:

i.e. desired thickness =8 µm

Volume (mm^3) = Length (mm) x width (mm) x height (mm)
= 50 x 75 x 0.008 = 30 (mm^3)
Both sides are plated = 60 (mm^3)
Mass (g) = volume (mm^3) x density (g/(mm^3)
= 60 x 0.00714
= 0.4284 g

Note: density of Zn is taken as 7.14 (g/cm^3)

Time (s) = $\frac{n(e) * F(C/mol)}{Current(A)}$

= 6.55×10^{-3} x 2 x 96500 / 2

= 843.08 s

= 14 min

Note: n(e) is the number of moles of electrons and F is the Faraday constant 96,500 $Cmole^{-1}$

2 Calibration curve for determination of Cr(VI)

A calibration curve was made by plotting absorbance intensity at 540 nm (A) versus the concentration of Cr(VI). The least-square fitting gives a correlation equation, C = 3.5171x + 0.0025 with coefficient of determination 0.99. Using this calibration curve, the concentration of Cr(VI) in mg/l was determined.

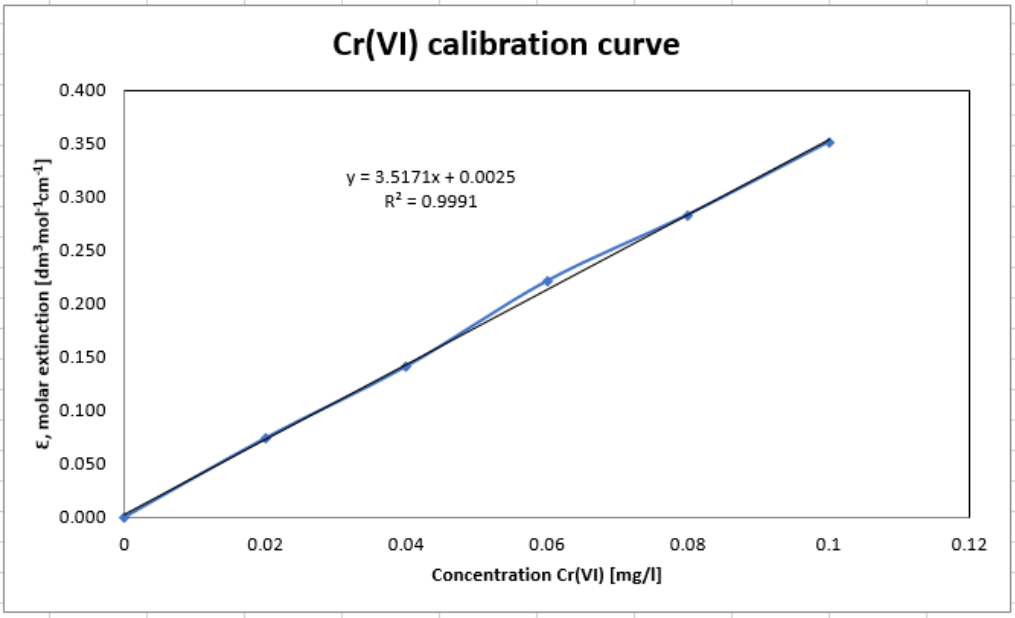

Figure A.1 A calibration curve showing the absorbance intensity at 540 nm vs Cr(VI) concentration

3 X-ray diffraction of the Cr(III)-based conversion coatings

Figures A.2 and A.3 show the XRD analysis of two selected TCC layers. Due to the fact that these TCC layers were thin and the Zn layer had a strong preferred orientation, no different XRD spectra were observed than the one from the alkaline Zn layer.

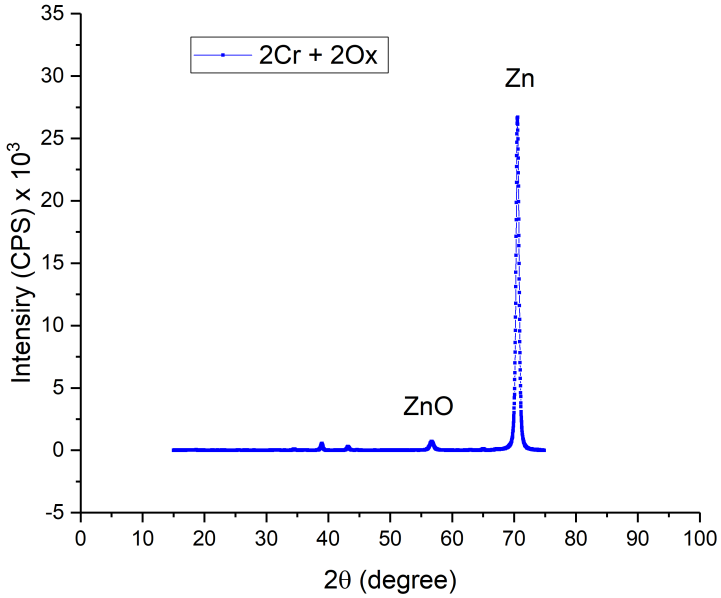

Figure A.2 XRD analysis of sample 2Cr + 2Ox

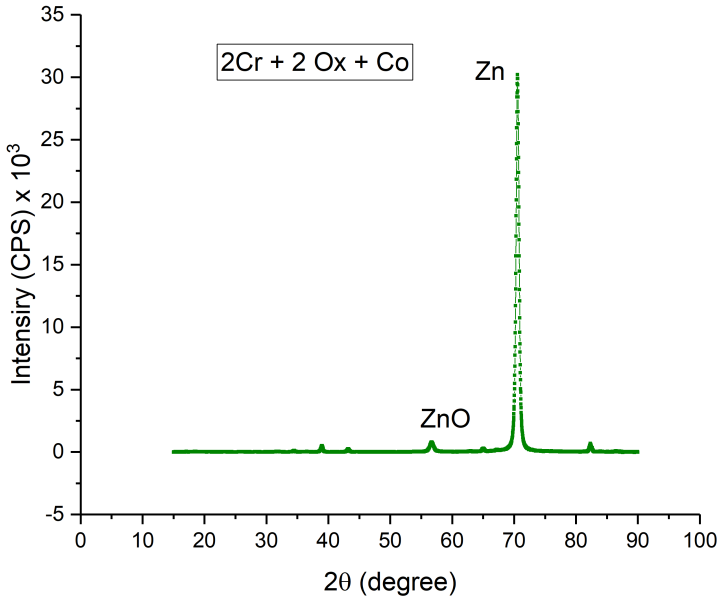

Figure A.3 XRD analysis of 2Cr + 2Ox + Co